Filamentous bacteriophage based application

Dissertation

zur Erlangung des Grades
des Doktors der Naturwissenschaften
der Naturwissenschaftlich-Technischen Fakultät
der Universität des Saarlandes

von

Baek, In-Hyuk

Saarbrücken

November 2024

Tag des Kolloquiums:	**25. Apr. 2025**
Dekan:	**Univ.-Prof. Dr.-Ing. Dirk Bähre**
Vorsitz:	**Prof. Dr. Tsing-Yong Dora Tang**
Berichterstatter:	**Prof. Dr. Volkhard Helms**
	Prof. Dr. Marc Schneider
Akademischer Mitarbeiter:	**Priv. -Doz. Dr. Jessica Hoppstädter**

Die vorliegende Arbeit wurde von Oktober 2014 bis November 2024 unter Anleitung von Prof. Dr. Volkhard Helms am Lehrstuhl für Computational Biology der Universität des Saarlandes angefertigt. Die in der Dissertation beschriebenen Experimente wurden von Oktober 2014 bis Februar 2020 am KIST Europe in der Abteilung für Bakteriophagen-Engineering und Umweltüberwachung mit Unterstützung von Dr. YoungJun Kim durchgeführt.

Table of Contents

Acknowledgements

Firstly, I would like to thank my supervisor Dr. Youngjun Kim, and Prof. Dr. Helms for helping me through this thesis. I would also like to thank all the people in the Environmental Safety Group who have helped me throughout my research. I would also like to thank my friends and family for their support over the last few years.

Completing my Ph.D. journey was incredibly challenging, and at times, I came close to not making it through. However, thanks to the unwavering support of my family and the guidance of my professors, I was able to complete my thesis. I feel deeply grateful to everyone who stood by me and believed in me throughout this journey.

I also have a special place in my heart for Saarbrücken, Germany, the city where my children were born. It will always feel like a second home, filled with unforgettable memories.

Most of all, I would love to thank my wife, KyungHa Lee, and my daughter and sons, Ye-Eun, YeJun, and YeChan, for all the love and support they have given me throughout my Ph.D.

SeJong, South Korea, October 2024

Baek, In-Hyuk

Zusammenfassung

Diese Studie untersucht die Entwicklung und Anwendung von virusbasierten molekular geprägten Polymeren (MIPs) und bioaktiven Gerüsten unter Verwendung von Bakteriophagen. Das Hauptziel besteht darin, ein System zu entwickeln, das saure pharmazeutische Verbindungen wie Clofibrinsäure durch phagenbasierte MIPs selektiv nachweisen kann. Dies wird die Spezifität und Sensitivität der derzeitigen Nachweismethoden verbessern und eine neuartige Strategie zur Überwachung und zum Management von pharmazeutischer Verschmutzung in sowohl umweltbezogenen als auch klinischen Kontexten bieten.

Darüber hinaus zielt diese Arbeit darauf ab, bioaktive Gerüste zu entwickeln, die biokompatible Bakteriophagen enthalten, um deren Potenzial zur Förderung der Angiogenese in der Gewebetechnik und der regenerativen Medizin zu erforschen. Diese bakteriophagenbasierten Gerüste werden auf ihre Fähigkeit untersucht, die Vaskularisation und Geweberegeneration zu unterstützen. Die Ergebnisse dieser Forschung könnten zur Entwicklung alternativer Plattformen für biomedizinische Studien beitragen, mit dem Potenzial, in zukünftigen Anwendungen die Abhängigkeit von Tierversuchen zu verringern.

Die Ergebnisse dieser Studie könnten zur Entwicklung umweltfreundlicher Überwachungstechnologien und innovativer Lösungen in der Gewebetechnik beitragen und neue Möglichkeiten sowohl in der Umweltwissenschaft als auch in der regenerativen Medizin schaffen.

Abstract

This study explores the development and application of virus-based molecularly imprinted polymers (MIPs) and bioactive scaffolds utilizing bacteriophages. The primary aim is to create a system that selectively detects acidic pharmaceutical compounds, which is clofibric acid through phage-based MIPs. This will enhance the specificity and sensitivity of current detection methods, providing a novel strategy for monitoring and managing pharmaceutical pollution in both environmental and clinical settings.

In addition, this thesis seeks to fabricate bioactive scaffolds incorporating biocompatible bacteriophages, with the aim of exploring their potential to promote angiogenesis in tissue engineering and regenerative medicine. These bacteriophage-based scaffolds are investigated for their ability to support vascularization and tissue regeneration. The findings from this research could contribute to the development of alternative platforms for biomedical studies, with the potential to reduce reliance on animal experiments in future applications.

The findings of this study could contribute to the development of environmentally friendly monitoring technologies and innovative tissue engineering solutions, creating new opportunities in both environmental science and regenerative medicine.

Sworn declaration

I declare under oath that I have prepared this thesis independently and without the help of others and that I have not used any other sources and resources than the ones stated. Parts that have been taken literally or correspondingly from published or unpublished texts or other sources have been labelled as such. This thesis has not been presented to any examination board in the same or similar form before.

Saarbrucken, In-Hyuk Baek

List of Abbreviations

AFM	- Atomic Force Microscopy
ATP	- Adenosine Triphosphate
AuNP	- Gold Nanoparticle
CA	- Clofibric Acid
CFU	- Colony Forming Units
CL	- Cross-linking
CRC	- Colorectal Cancer
CT	- Computed Tomography
DAPI	- 4′,6-Diamidino-2-Phenylindole (nuclear stain)
DLS	- Dynamic Light Scattering
DNA	- Deoxyribonucleic Acid
dsDNA	- Double-Stranded DNA
EDC	- 1-Ethyl-3-(3-dimethylaminopropyl) carbodiimide
EGFR	- Epidermal Growth Factor Receptor
ELISA	- Enzyme-Linked Immunosorbent Assay
FDA	- Food and Drug Administration
FACS	- Fluorescence-Activated Cell Sorting
FBS	- Fetal Bovine Serum
HER2	- Human Epidermal Growth Factor Receptor 2
HUVECs	- Human Umbilical Vein Endothelial Cells
ICTV	- International Committee on Taxonomy of Viruses
MALDI-TOF	- Matrix-Assisted Laser Desorption/Ionization - Time of Flight
MIP	- Molecularly Imprinted Polymer
MRI	- Magnetic Resonance Imaging
NHS	- N-Hydroxysuccinimide
NIP	- Non-Imprinted Polymer
NMR	- Nuclear Magnetic Resonance
pIII	- Minor Coat Protein III (of filamentous phage)

pVIII - Major Coat Protein VIII (of filamentous phage)

PBS - Phosphate Buffered Saline

PEG - Polyethylene Glycol

PD-L1 - Programmed Death-Ligand 1

pH - Potential of Hydrogen

QCM-D - Quartz Crystal Microbalance with Dissipation

RNA - Ribonucleic Acid

SEM - Scanning Electron Microscopy

siRNA - Small Interfering RNA

ssDNA - Single-Stranded DNA

SWNT - Single-Walled Carbon Nanotube

TCA - Tricarboxylic Acid Cycle (Krebs cycle)

TEM - Transmission Electron Microscopy

TGF-β1 - Transforming Growth Factor Beta 1

Trp - Tryptophan

TrxA - Thioredoxin

UV/Vis - Ultraviolet–Visible Spectroscopy

VEGF - Vascular Endothelial Growth Factor

Chapter 1

In order to present the theoretical background of the thesis, this chapter introduces filamentous bacteriophages and provides a biological, applicational and theoretical background for this thesis. Furthermore, it discusses additional methods that could have also been used to study molecular imprinted polymers, and lab-on-a-chips. The focus is placed on introducing the research fields addressed by the projects of this thesis. This chapter does not aim to comprehensively cover these topics.

1. Introduction

1-1. Filamentous bacteriophage

The bacteriophage is a virus that infects bacteria. Most bacteriophages are pathogens that kill their bacterial hosts, but there are also bacteriophages that coexist in cooperative relationships. Bacteriophages exist on the Earth in various forms and exhibit diversity (ex, infectious host, structure, genome, and sequence). According to the ICTV classification, a bacteriophage has about 49 families [1]. Filamentous bacteriophages belong to the family *Tubulavirales*. In order to have been reported to be infected with *Inovirus, Lineavirus, Infulavirus, Saetivirus, Versovirus, Villovirus, Coriovirus, Habenivirus,* and *Pahipatevirus*, etc (Table 1). With the main hosts of the viruses: *Clostridium Beijerinckii, Pseudomonas aeruginosa, Ralstonia solanacearum, Enterobacterium sp., Escherichia coli, Xanthomonas vesicatoria, Xanthomonas campestris, Xanthomonas oryzae, Vibrio parahaemolyticus, Vibrio alginolyticus,* and *Vibrio cholerae* have been reported [1-3]. The conserved gene, *pI* protein, of bacteriophages, is classified as phylogenetic clades [2, 4]. The filamentous bacteriophage used in this paper is *inovirus*, which consists of clade with Lineavirus, Infulavirus, and Setivirus, and has the characteristics of nonintegrative episomal phages (figure 1) [2]. The *Inovirus* belongs to the family *Inoviridae* in the order of *Tubulavirales*, and the bacteriophage has a long filamentous form, *M13, fd,* and *f1* are reported as representative species, and data such as genetic and biological characterization are accumulated [3, 5, 6]. The *Inovirus* consists of five capsid proteins. Major capsid *pVIII* consists of approximately 2000 – 3000 copies and major capsid *pVII, pIX, pVI,* and *pIII* each consisting of about 3-5 copies [6].

Table 1. Library of the filamentous phages in NCBI data base.

Phage	Host	Assession number	Reference
CAK1	*Clostridium Beijerinckii*	OX639564	unpublishsed
M13	*Enterobacterium sp.*	NC_003287	[7]
f1	*Enterobacterium sp.*	NC_025823	[8]
IKe	*Escherichia coli*	NC_002014	[9]
I2-2	*Escherichia coli*	NC_001332	[10]
If1	*Escherichia coli*	U02303	*
fd	*Escherichia coli*	NC_025824	[11]
fd-tet	*Escherichia coli (for cloning)*	AF217317	[12]
Pf3	*Pseudomonas aeruginosa*	NC_074763	[13]
Rs551	*Ralstonia solanacearum*	NC_047765	*
Rs603	*Ralstonia solanacearum*	NC_025454	[14]
PE226	*Ralstonia solanacearum*	NC_015297	[15]
RS611	*Ralstonia solanacearum*	AB931172	*
RS611	*Ralstonia solanacearum*	NC_055054	unpublishsed
Vaf1	*Vibrio alginolyticus*	OP297622	*
VP24-2_Ke	*Vibrio cholerae*	NC_073750	unpublishsed
VEJφ	*Vibrio cholerae*	NC_012757	[16]
VSKK	*Vibrio cholerae*	NC_003311	*
ND1-fs1	*Vibrio cholerae*	NC_055051	[17]
fs2	*Vibrio cholerae*	NC_001956	[18]
vB_Vipa36	*Vibrio parahaemolyticus*	MT188663	*
vB_Vipa26	*Vibrio parahaemolyticus*	MT188662	*
vB_Vipa10	*Vibrio parahaemolyticus*	MT188666	*
vB_Vipa4291	*Vibrio parahaemolyticus*	MT188665	*
vB_VipaK	*Vibrio parahaemolyticus*	MT188664	*
vB_Vipa71	*Vibrio parahaemolyticus*	MT193890	*

VfO4K68	*Vibrio parahaemolyticus*	NC_002363	[19]
Vf12	*Vibrio parahaemolyticus*	NC_005949	[20]
Vf33	*Vibrio parahaemolyticus*	NC_005948	[20]
VfO3K6	*Vibrio parahaemolyticus*	NC_002362	*
vB_VpI_FR1	*Vibrio parahaemolyticus*	OP628074	*
Cf1c	*Xanthomonas campestris*	NC_001396	[21]
Xf409	*Xanthomonas oryzae*	NC_055055	*
XaF13	*Xanthomonas vesicatoria*	NC_062737	unpublishsed

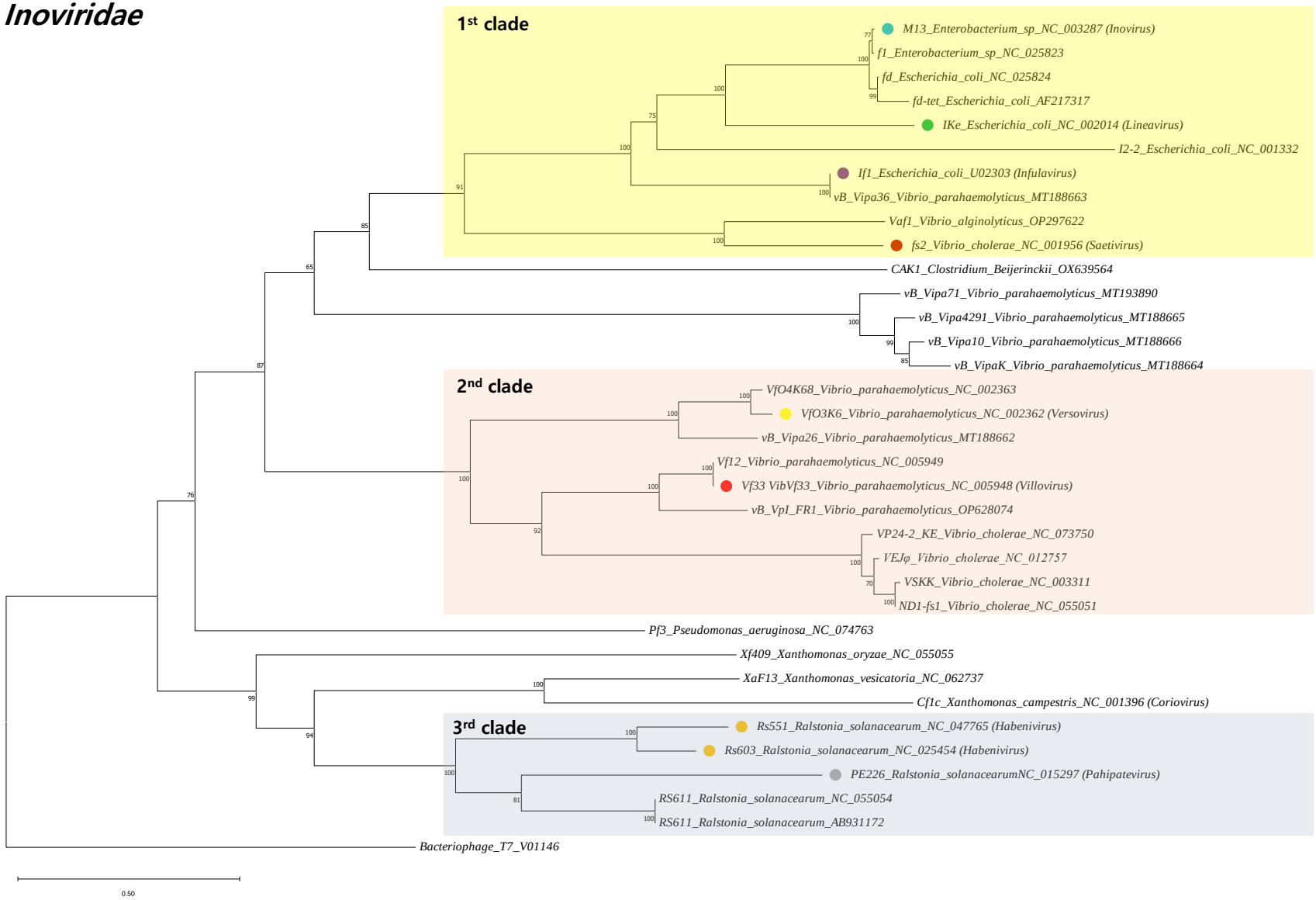
Inoviridae
1st clade
M13_Enterobacterium_sp_NC_003287 (Inovirus)
f1_Enterobacterium_sp_NC_025823
fd_Escherichia_coli_NC_025824
fd-tet_Escherichia_coli_AF217317
IKe_Escherichia_coli_NC_002014 (Lineavirus)
I2-2_Escherichia_coli_NC_001332
If1_Escherichia_coli_U02303 (Infulavirus)
vB_Vipa36_Vibrio_parahaemolyticus_MT188663
Vaf1_Vibrio_alginolyticus_OP297622
fs2_Vibrio_cholerae_NC_001956 (Saetivirus)
CAK1_Clostridium_Beijerinckii_OX639564
vB_Vipa71_Vibrio_parahaemolyticus_MT193890
vB_Vipa4291_Vibrio_parahaemolyticus_MT188665
vB_Vipa10_Vibrio_parahaemolyticus_MT188666
vB_VipaK_Vibrio_parahaemolyticus_MT188664
2nd clade
VfO4K68_Vibrio_parahaemolyticus_NC_002363
VfO3K6_Vibrio_parahaemolyticus_NC_002362 (Versovirus)
vB_Vipa26_Vibrio_parahaemolyticus_MT188662
Vf12_Vibrio_parahaemolyticus_NC_005949
Vf33 VibVf33_Vibrio_parahaemolyticus_NC_005948 (Villovirus)
vB_VpI_FR1_Vibrio_parahaemolyticus_OP628074
VP24-2_KE_Vibrio_cholerae_NC_073750
VEJφ_Vibrio_cholerae_NC_012757
VSKK_Vibrio_cholerae_NC_003311
ND1-fs1_Vibrio_cholerae_NC_055051
Pf3_Pseudomonas_aeruginosa_NC_074763
Xf409_Xanthomonas_oryzae_NC_055055
XaF13_Xanthomonas_vesicatoria_NC_062737
Cf1c_Xanthomonas_campestris_NC_001396 (Coriovirus)
3rd clade
Rs551_Ralstonia_solanacearum_NC_047765 (Habenivirus)
Rs603_Ralstonia_solanacearum_NC_025454 (Habenivirus)
PE226_Ralstonia_solanacearumNC_015297 (Pahipatevirus)
RS611_Ralstonia_solanacearum_NC_055054
RS611_Ralstonia_solanacearum_AB931172
Bacteriophage_T7_V01146
0.50

Figure 1. phylogenetic tree of filamentous phages. Phylogenetic tree built of the filamentous bacteriophages complete genes from NCBI nucleotide DB. The tree was evolutionary analysis by Maximum Likelihood method, bootstrap convergence test, and root on outgroup of *Autographiviridae T7 bacteriophage* by using MAGA11 program (Pennsylvania State, USA). Color circles are released on virus taxonomy from ICTV genera classification [1].

1-2. The filamentous bacteriophage genome of M13 strains

A full-sequence *M13* bacteriophage of 6407 nucleotide length was first reported in München in 1962, and the whole sequence was analyzed in 1980 [7, 22, 23]. The *M13* bacteriophage is circular (+) single strand DNA (ssDNA) and contains 11 genes. The filamentous bacteriophage genome contains genetic information for replication of phages and for constructing the capsid [5, 24, 25]. The 11 genes of phage are the same as in Figure 2 gene sequence information and translated protein roles. The *pII* and *pX* are required for (+) single strand DNA synthesis. The *pV* are performed the packing (+) single strand DNA before release the host. The *pVII,* and *pIX* are a protein at the viral end that comes out first when assembled from bacteria as a minor coat protein and released. The *pVIII* is a major coat protein, which is a small α-helical protein that wraps around the ssDNA phage genome with approximately 2000 – 3000 copies per virion and has a positive charge on the C-terminal. The *pIII*, which is involved in phage infection, is a minor coat protein that is located at the virion end and is involved in the completion of the phage assembly and the phage release from the bacterial cell membrane. The *pI* is promoted assembly by hydrolyzing ATP. The *pXI* is equal to one-third of the C-terminal end of the *pI*. The pI/pXI complex is an inner membrane channel which release the bacteriophage from cytoplasm. the *pIV* is a multilayer outer membrane channel which phages releasing from bacteria.

***Inovirus* (*M13* strain filamentous bacteriophage)**

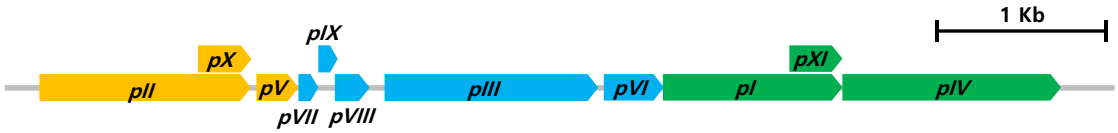

Gene	Protein Function	Number of bp	Number of aa	MW of proteins
pII	Phage DNA replication	1-831, 6006-6407	410	46,137
pX	Equal to the one-third of C-terminal of *pII*	496-831	111	12,672
pV	Dimers of *pV*, binding to ssDNA	843-1106	87	9,682
pVII	Minor coat protein	1108-1209	33	3,599
pIX	Minor coat protein	1206-1304	32	3,650
pVIII	Major coat protein	1301-1522	50	5,235
pIII	Minor coat protein	1579-2853	406	42,522
pVI	Minor coat protein	2856-3194	112	12,342
pI	The hydrolyze ATP to promote assembly	3196-4242	348	39,502
pXI	Equal to the one-third of C-terminal of *pI*	(3196-4242)	108	12,424
pIV	The outer membrane channel through which the phage exits the bacterium	4220-5500	405	43,476

Figure 2. Map of the M13 bacteriophage genome. The table lists the function of the proteins, the positions of the genes, and molecular weight of the proteins as below the map. The phage proteins are symbolized by the "p" as a prefix (e.g. *pVIII*).

1-3. Filamentous bacteriophage life cycle

As shown in Table 1. Most of the filamentous bacteriophages infect with gram-negative bacteria. In case of the *Fd* strain, it is sensitive to F sex/conjugation pilus of gram-negative bacteria. The bacteriophages are using the F sex/conjugation pilus, which penetrates the host membrane and enters the host cytoplasm [26]. Docking to the sex/conjugation pilus of bacteria has been experimentally demonstrated with the *pIII* protein of the bacteriophage [27]. The *pIII* has N1, N2 domains linked by Glycine linker. After the *N1* domain of the bacteriophage binds to the *TolA* protein of the sex/conjugation pilus, the phages are disassembled and the ssDNA are entered at the cytoplasm as the host (Figure 3a, 3b). The infectious phage genomes are called 'infective form' which is (+) ssDNA. Host RNA polymerase synthesis a short RNA. In a backtracks at short sequences, RNA were dissociated with a leaving the short RNA primer about 20 nt. After the complementary phage DNA is synthesized using DNA polymerase III to synthesize the 'replicative form' (Figure 3c). The replicative form of (+) ssDNA becomes a template which generates the DNA, mRNA, transcription of structural and non-structural proteins of filamentous bacteriophage in the infected host cell. At the early stage of infection, the concentration of *pV* is low, the newly synthesized DNA remain the replication form at the beginning of the infection. In this stage, the both phage DNA and proteins increase exponentially. As the concentration of *pV* increases, it binds to the newly generated (-) ssDNA strand. The binding of *pV* prevents DNA polymerase from converting to replication form of phage DNA. When the amount of dimer form of *pV* reaches to a critical point at the host, it goes to late infection stages. In late infection, phage (-) ssDNA is coated by the *pV*, and the structural protein required for bacteriophage assembly is transferred to the host inner membranes. The assembly of filamentous bacteriophages occurs during the process of phage secretion at the host cell inner membranes. The three types of non-virion proteins (*pI*/*pXI*, and *pIV*) and five types of structural proteins (*pIX, pIII, pVI*, and *pVIII*) act on the filamentous bacteriophage secretion process. Phage assembly begins when the *pI* protein recognizes the *pV*-ssDNA complex. As phage assembly process, it passes from *pI*/*pXI* in the inner membrane to *pIV* in the outer membrane. after then, phage is released. First, the *pVII* and *pIX* of 3-5 copies are first added to the phage DNA. During *pV* is removed from the phage DNA under the effects of thioredoxin (*TrxA*) and ATP hydrolysis, the *pVIII*, a major coat protein of approximately 2000 – 3000 copies, surrounds and coat the phage DNA. After (-) ssDNA coated on *pV* dimer, the (-) ssDNA-pV move to secreted channels of pI/pXI at inner membranes (Figure 3d). At the pI/pXI channel, the *pV* is removed and replaced by the *pVIII* of the major coating protein. The bacteriophage is released through the host outer membrane via the *pIV* channel.

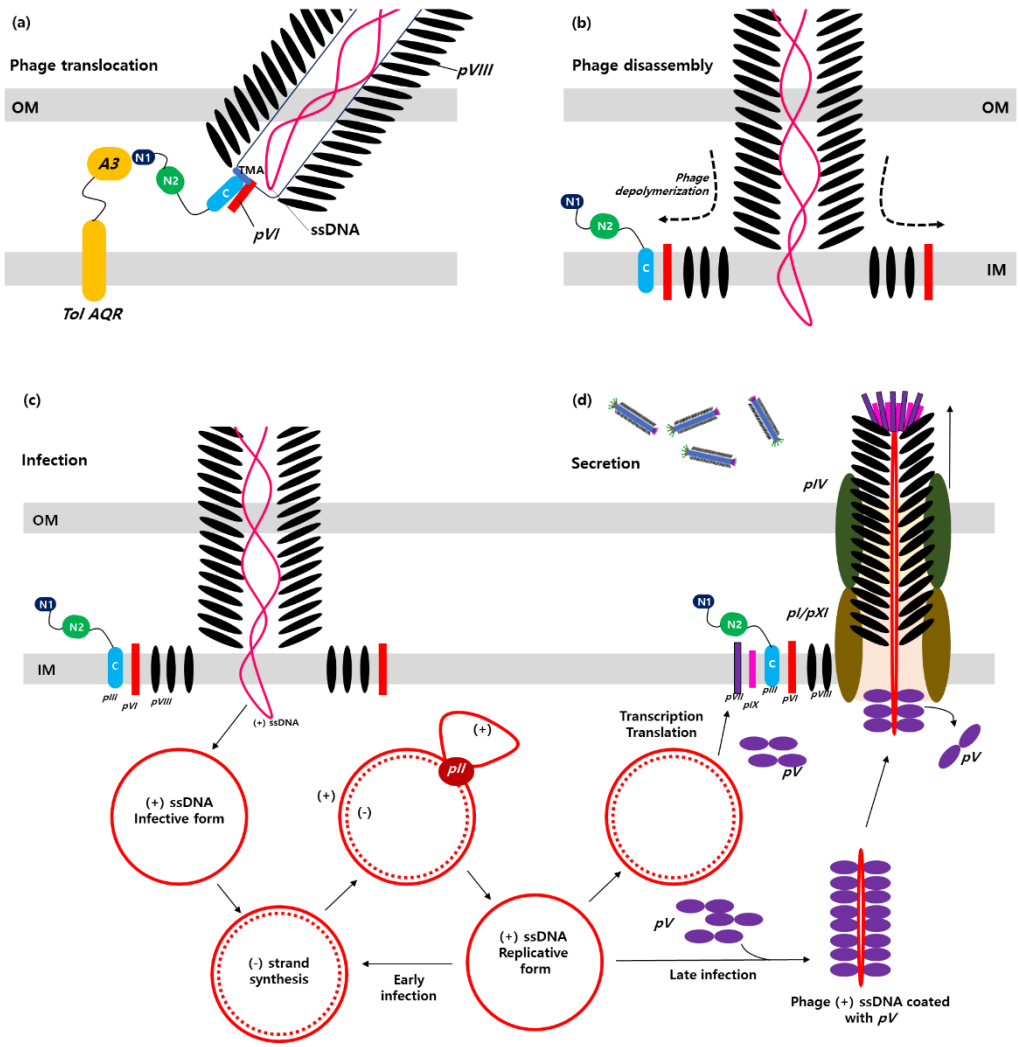

Figure 3. Overview of life cycle of filamentous bacteriophage. (a) In the initial stage of filamentous bacteriophage, the N2 domain of pIII binds to the F-pilus in *Escherichia coli*, after then, the N1 domain binds to *TolA* in the *TolQRA* complex in the inner membrane. (b) Phages are depolymerized in the inner membrane and (+) ssDNA is injected into cytoplasm. (c) The injected (+) ssDNA is generated for complementary phage DNA by host DNA polymerase III. The phage protein *pII* binds to the origin of DNA replication and makes the nicks of (+) DNA, and replicating by host DNA polymerase III to synthesis a double-stranded replication form. (d) In the stage of late infection, (+) ssDNA is coated by phage protein *pV*. The *pV*-ssDNA binds to minor coat proteins *pVII*, *pIX*, and is recognized by the pI/pXI protein in IM. As *pVII-pIX-pV*-ssDNA passes through *pI/pXI*, the *pV* coated on the ssDNA is replaced by phage protein of a major coat protein *pVIII*. After pVIII is added to emerging phage, it is moved outward through the *pIV*, and the terminal phage proteins *pIII*, *pVI*, are coated and released from the host cell.

1-4. Applications of filamentous bacteriophages

With the development of nanotechnology since 2000, bacteriophages have begun to play new roles in nanomedicine and bioengineering. In particular, the diagnosis of sensitive diseases and the treatment of target-specific therapies have been greatly improved through new research using phages. The advancement of panning technology using bacteriophages has enabled accurate targeting in the fields of drug and gene delivery. To date, the medical use of phages has not been approved by the FDA due to the lack of comprehensive research on their medical efficacy and safety. However, with the increasing need for treatment methods, vaccines, and precision medicine for antibiotic-resistant bacteria, phages are being studied extensively in the field of nanotechnology and show great potential.

1-4-1. Phage display

Filamentous bacteriophages, with their linear structures, have had their structural characteristics and genetic mapping fully elucidated, and the development of phage display technology has made them a powerful tool in nanomedicine. The external proteins of filamentous bacteriophages can simultaneously display multiple functions using display technology. There are five types of external proteins in filamentous bacteriophages: pIII, pIV, pVI, pVII, and pVIII. As shown in Figure 4, pIII, pVI, and pVIII can display specific peptides or proteins using genetic modification techniques, with one or more peptides being displayed on each coat protein.

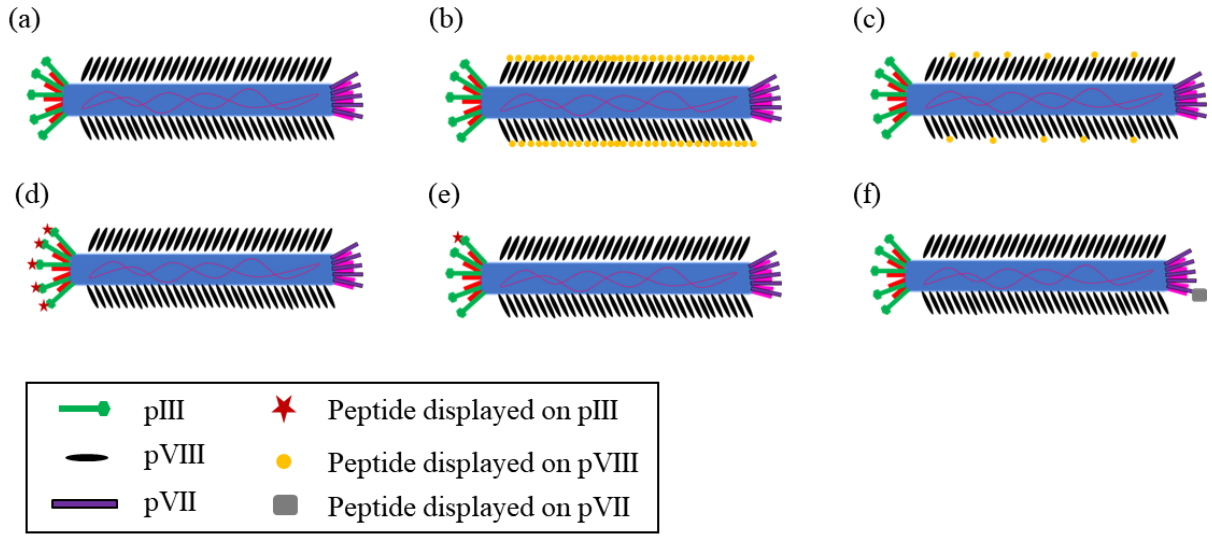

Figure 4. Commonly displayed sites of filamentous bacteriophages. (a) The natural structure of a filamentous bacteriophages. (b) The major coat protein pVIII is displayed with approximately 2000 – 3000 copies per phage. (c) The second pVIII gene is sparsely displayed with 10-100 copies along the phage. (d)

The minor coat protein pIII is displayed. (e, f) The monovalent phage display has been used to minor coat protein of the pIII and pVII.

pIII, the minor coat protein of filamentous bacteriophages, offers several advantages, including a domain linked with a glycine linker, ease of genetic modification, and the ability to accommodate large molecules. Currently, commercially available phage display systems such as M13 *Ph.D-12*, *Ph.D-7*, and *Ph.D-c7c* from New England Biolabs utilize a pIII random sequence library to generate protein libraries that are well-suited to antigen-targeted applications through biopanning. The production of target-specific libraries via biopanning does not require extensive prior research on the target materials, and these libraries can be generated with approximately 10^13 phage titers per milliliter. This method is used for producing antigen-specific monoclonal antibodies and developing peptide vaccines through epitope mapping [28, 29].

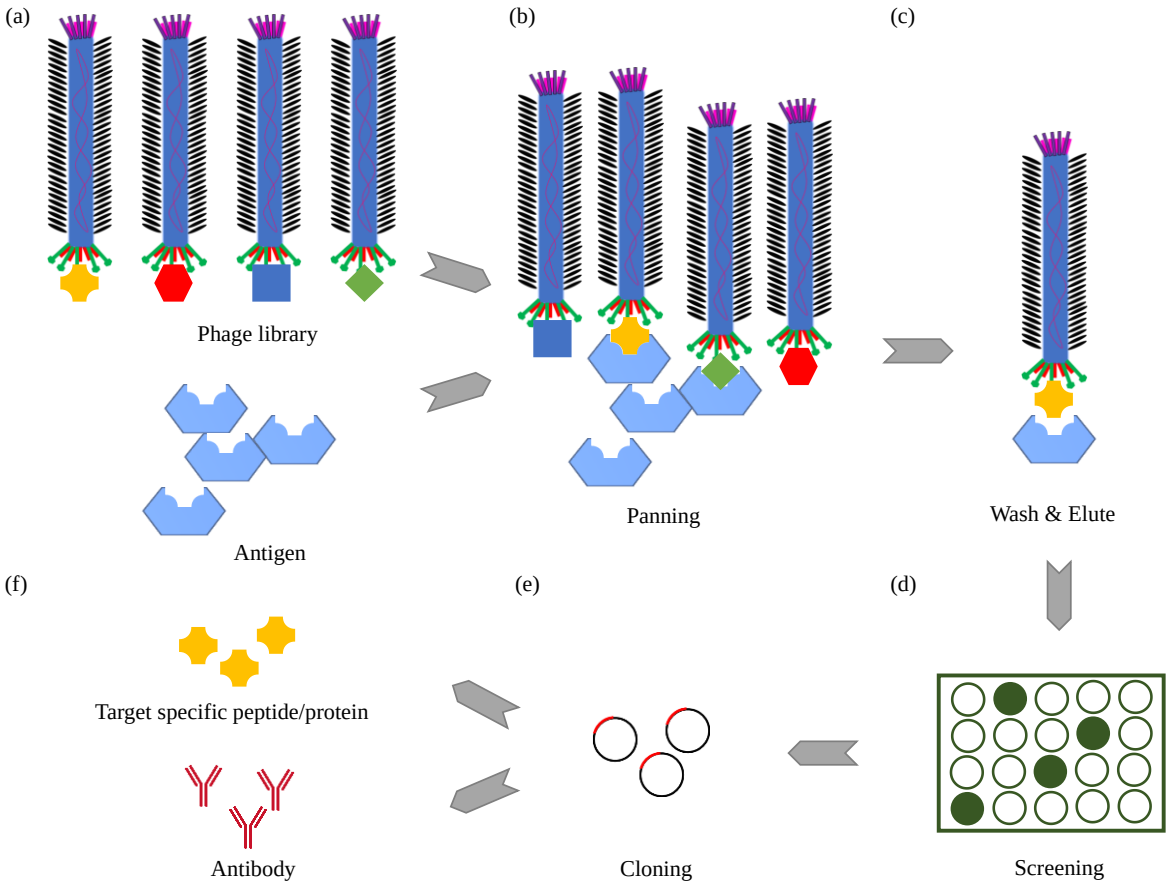

Figure 5. Overview of phage display technique. (a) The phage library is generated, with each filamentous bacteriophage displaying a random 12 or 7-peptide on pVIII major coat proteins (eg. M13 *Ph.D-12*, *Ph.D-7*, and *Ph.D-c7c*) . (b) Phages attached target ligands. (c) The unbound phages are washed, and bound phages

are eluted. (d) Screening the high-affinity phages are selected. (e) The selected peptide is induced at functional vector. (f) The selected peptide can be applied in the development of therapeutic antibodies, diagnostic tools, or targeted drug delivery systems.

The major coat protein, pVIII, has approximately 2000 to 3000 copies per bacteriophage, surrounding the phage DNA in a 54 amino acid, alpha-helix structure. This protein can be engineered to introduce small molecules, allowing for the modification of all 2000 to 3000 copies. In the f88 phage, there are two pVIII gene sites within a single bacteriophage genome. The first pVIII gene produces about 2700 overlapping copies, while the second pVIII gene produces 10 to 100 copies that are randomly displayed per f88 phage. Due to its location around the filamentous bacteriophage, pVIII is ideal for use in nanomaterials, where it can be functionalized to interact with specific molecules. Utilizing these characteristics, pVIII has been employed to display peptides that bind to CO_3O_4 and gold, which have been applied in various fields, including lithium-ion batteries [30], cancer imaging [31, 32], and electrodes [33].

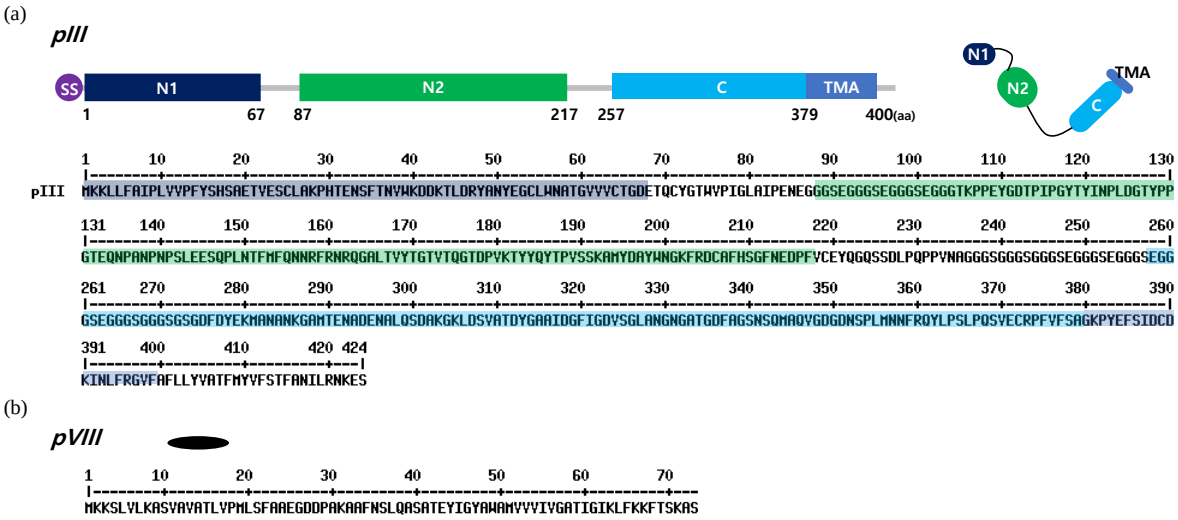

Figure 6. Illustration of the amino acid sequences of pIII and pVIII. (a) The pIII protein consists of several structural domains: signal sequence (SS), N1, N2, C, and transmembrane anchor (TMA) domains. These domains are connected by glycine linkers, allowing flexibility between each domain. Additionally, pIII can accommodate large protein sequences over 100 amino acids. (b) The pVIII protein is composed of 2000–3000 copies along the length of the filamentous bacteriophage, with each pVIII protein consisting of 73 amino acids. pVIII is typically used for the insertion of short peptides, about 6–8 amino acids, which are introduced at the C-terminus to enhance molecular affinity.

1-4-2. Nanomedicine

Bacterial infections have traditionally been treated using antibiotics, but the emergence of antibiotic resistance and the formation of biofilms have highlighted the need for new treatment methods. Research has shown that filamentous bacteriophages, when accumulating on the surface of bacteria in the early stages of infection, can promote biofilm formation by causing aggregation and altering hydrophobic properties [34]. This indicates that filamentous phages may contribute to biofilm formation in certain cases.

However, a study by Narancic et al. demonstrated that treating *Acinetobacter baumannii* infections using bacteriophages can increase sensitivity to antibiotics and reduce biofilm formation. This suggests that when used alongside antibiotics, bacteriophage therapy could serve as an effective clinical strategy in treating bacterial infections [35]. Thus, bacteriophage-based therapies are being explored as a strong alternative to addressing antibiotic-resistant bacteria and biofilm issues, enhancing the efficacy of traditional antibiotic treatments.

Filamentous bacteriophages possess a rod-like structure with a negatively charged surface, allowing for strong electrostatic interactions with positively charged materials. This characteristic is highly beneficial for the development of nanoscale drug and gene delivery systems [36, 37]. For example, by simply mixing M13 phages with polyethyleneimine (PEI), a phage-based vaccine platform can be created, which has been reported to show high stability and efficiency [37]. Furthermore, nanoparticles can bind to bacteriophages through specific peptide or hydrophobic interactions. This non-covalent binding method is very useful in designing nano-drug delivery carriers while maintaining the phage's inherent specificity. For instance, combining nanoparticles for targeted tumor detection with photothermal therapy is possible. This makes the phage-nanotechnology combination a highly promising tool not only for cancer treatment but also for the diagnosis and treatment of various diseases.

According to a study by Carrico et al., they successfully enhanced fluorescent imaging performance by modifying the amine group of the N-terminal of pVIII into ketones and conjugating PEG2k molecules. In addition, the selective binding ability of the phage was evaluated by targeting EGFR and HER2, confirming that the binding of PEG2k molecules did not significantly affect the phage's ability to bind to cancer cells. This suggests that the phage can maintain its target-binding ability while enhancing imaging performance [32].

M13 phages conjugated with silver nanoparticles (Au@Ag) can effectively kill bacteria, and this system can also contribute to suppressing colorectal cancer (CRC) by regulating the gut microbiota and reprogramming the tumor immune

microenvironment [36]. The combination of nanoparticles and phages offers the potential to selectively preserve beneficial gut bacteria while eliminating pathogenic bacteria.

A study by Liu et al. reported that genetically modified bacteriophages stimulated neural stem cells, inducing proliferation, infiltration, and differentiation, and promoting both angiogenesis and neurogenesis, leading to the restoration of certain brain functions. This highlights promising applications, particularly in stroke treatment [38].

In a study by Zhou et al., dual-display fd bacteriophages targeting vascular endothelial growth factor (VEGF) and programmed death-ligand 1 (PD-L1), biomarkers that predict the therapeutic response and prognosis of cervical cancer, were developed. This demonstrated the potential for more effective targeted diagnosis of cancer cells. By simultaneously detecting VEGF and PD-L1, this study suggests a new diagnostic strategy for cervical cancer [31]. Such studies indicate that various nanomedicine technologies based on bacteriophages could bring revolutionary advancements in disease treatment and prevention.

1-4-3. Nanomaterials

Filamentous bacteriophages can be conjugated with imaging agents like fluorescent dyes, radioactive isotopes, or magnetic nanoparticles to precisely detect disease biomarkers and bacteria. A recent study developed bacterial imaging technology using MRI in C57/BL6 mouse models. Borg et al. genetically engineered M13 and CTXΦ phages to bind to Mn^{2+}, successfully detecting *E. coli* and *V. cholerae* in mouse models and imaging them using MRI. This significantly expands the possibilities for bacterial detection and imaging [39].

The study by Szot-Karpińska et al. increased the affinity of carbon nanofibers through a pVII point mutation (A1142G, Q381R), confirming its potential as a biocompatible material through non-covalent π–π interactions [40].

In Korkmaz et al. study, M13 bacteriophages were genetically engineered to increase their binding affinity for AuNPs (gold nanoparticles), demonstrating their potential applications in nanoelectronics and biosensor development. This study successfully developed bacteriophages with enhanced gold-binding efficiency and metallization properties by introducing specific peptides (YYYYY, AYSSG, AYGDD) on the surface of M13 phages [41].

Moon et al. study demonstrated the potential to detect low concentrations of biomarkers using gold nanoparticles-encoded M13 bacteriophage (AuNPs_M13). This system significantly improves sensitivity in biosensor applications, offering

a new method for the rapid detection of low concentrations of disease biomarkers [42].

According to the study by Oh et al., genetic modification of the pVIII protein of the bacteriophage (DVYESALP) containing tyrosine (Y) was shown to interact with graphene and single-walled carbon nanotubes (SWNTs) through π-π interactions. This interaction allowed the virus to bind to graphene through hydrophobic-hydrophobic interactions, increasing the stability of graphene. This enabled the construction of an environmentally friendly graphene/virus nanotemplate. It was also confirmed that the specific capacity of bismuth oxyfluoride increased to 131 mAh g^{-1} at a current density of 300 mA g^{-1}, and the overvoltage in both charging and discharging cell reactions decreased. This technology can be applied to various material fields, including biosensors, supercapacitors, catalysts, and energy conversion [43].

These studies demonstrate the innovative potential of filamentous bacteriophages in medical imaging, nanotechnology, and biosensors. In particular, combining gold nanoparticles and MRI could significantly improve the precision of disease detection and treatment.

1-5. Additional molecularly imprinted polymer methods in Chapter 2

The methods described in the previous sections offer a brief overview of the preparation and functionalization of bacteriophage-integrated MIPs and their application for binding assays.

1-5-1. Chemicals and instrumentation in Chapter 2

Pyrrole was sourced from Sigma Aldrich, and stored in the dark at 4 °C to prevent oxidation. Nitrogen gas (Alphagaz) was obtained from Air Liquide. Ultrapure water was produced using a Millipore Milli-Q system for solution preparation. Before use, solutions intended for polymerization and binding were filtered with 0.2 μm polypropylene syringe filters. Stock solutions of clofibric acid (1 mM) were prepared in KNO_3 or phosphate buffer (pH 7.0) and refrigerated. Solutions of 2,4-D and CBZ (1 mM) were similarly prepared in phosphate buffer (pH 7.0) and refrigerated, with CBZ first dissolved in 2 mL DMSO and subsequently diluted to 100 mL with buffer solution. Voltammetric measurements were conducted using an Autolab PGSTAT 12 potentiostat (Metrohm/Eco Chemie, Utrecht, Netherlands) with GPES software. Certain coating experiments utilized a 10 mL beaker setup, comprising gold-coated glass wafers as working electrodes, a platinum wire as the counter electrode, and an $Ag/AgNO_3$ reference electrode. Quartz Crystal Microbalance (QCM)

measurements were performed with a Q-Sense E1 system (Q-Sense, Biolin Scientific AB, Stockholm, Sweden), incorporating an electrochemistry flow module (QEM 401) connected to the potentiostat. Sample solutions were introduced into the flow module using a peristaltic pump (IKA). In all QCM experiments, 4.95 MHz AT-cut quartz crystal gold sensors (exposed area 1.131 cm^2) served as working electrodes, with a platinum plate as the counter electrode and a Dri-REF Ag electrode (WPI, Sarasota, FL, USA) as the reference electrode. To ensure contamination-free conditions, the cell was thoroughly flushed with Milli-Q water, isopropanol, and Milli-Q water sequentially before each experiment to eliminate contaminants and trapped air bubbles. Wafers and quartz crystals were cleaned in a 2:1 (v/v) sulfuric acid and hydrogen peroxide solution for 10 minutes, then rinsed with Milli-Q water and dried under a nitrogen stream. The mass of deposited material on the sensor surface was determined using the Sauerbrey equation based on frequency changes, assuming a density of 1.48 $g \cdot cm^{-3}$ for calculating the thickness of the polypyrrole coating.

1-5-2. Synthesis and Characterization of Imprinted Polypyrrole Sensor in Chapter 2

Polypyrrole coatings were electrochemically deposited on gold-coated piezoelectric quartz crystals or wafers using cyclic voltammetry of the pyrrole monomer in aqueous KNO_3 solution or phosphate buffer (pH 7.0) containing clofibric acid. The potential was cycled between -200 and +800 mV. Following polymerization, sensors were rinsed with ethanol and water and either air-dried with nitrogen or subjected to vigorous washing (5 min–1 h) in 70% ethanol. In some cases, they underwent PAD washing for 15 minutes in an ethanol and potassium chloride/hydrochloric acid solution (70:30, pH 2.5). MIP-phage and Non-imprinted polymers (NIPs) were prepared using the same protocol, except that NIPs were prepared without clofibric acid.

1-6. Additional lab-on-a-chip methods in Chapter 3

The methods described in the previous sections offer a brief overview of the preparation and functionalization of bacteriophage-integrated MIPs and their application for binding assays.

1-6-1. Pre-trial experiments in Chapter 3

The initial testing utilized a custom-fabricated 2-channel wafer, provided by Prof. Seok Chung and Dr. Hojeong Jeon, to create poly-dimethylsiloxane (PDMS) devices using soft lithography. A plastic mold with channel patterns was prepared through injection molding, then Sylgard 184 silicone solution and

curing agent (weight ratio, 10:1, Dow Chemical, USA) were poured and cured on the mold at 80°C for 1 hour in a dry oven. Once cured, the PDMS plate was removed, and reservoirs for the medium and ECM channels were punched using biopsy punches (4 mm and 1 mm). The punched PDMS plate served as the top part of the macrofluidic device, with an unpunched PDMS plate as the bottom. After autoclaving, both PDMS parts were bonded through oxygen plasma treatment (CUTE, Femto Science, Korea). The ECM and medium channels measured 2 × 1 mm and 4 × 1.2 mm in width and height. Before filling with ECM and cells, channels were coated with a 2 mg/ml polydopamine solution for 2 hours at room temperature and then rinsed with MilliQ water. To achieve a hydrophobic surface, the device was dried for 5 hours in an 80°C dry chamber. Collagen type I solution (Corning, USA) was prepared at a concentration of 2 mg/ml in a mixture of 10 × PBS, 0.1 N NaOH, and MilliQ water, with pH adjusted to 7.4. This collagen solution was filled into the ECM channel and incubated at 37°C in a 5% CO_2 incubator to gel, while channel edges were secured to prevent overflow.

1-6-2. Transition to commercial microfluidics device in Chapter 3

Following the pre-trial experiment, the study transitioned to using the commercial DAX-1 device (AIM Biotech, Singapore), which features a comparable 2-channel PDMS setup as the custom-built modules. The DAX-1 device allowed for standardized experimentation with similar channel dimensions, providing consistent results for further testing and analysis.

1-6-3. cell culture in microfluidics device in Chapter 3

Endothelial cells were detached using a 0.25% trypsin/EDTA solution (Thermo Fisher Scientific, USA) and adjusted to a density of 5×10^5 cells/ml. The cell culture channels were filled with 100 μl of endothelial cell suspension, and the device was placed vertically in a 5% CO_2 incubator at 37°C for 1 hour to enable cell attachment to the collagen type I hydrogel. After cell attachment, the culture medium in all channels was refreshed. The endothelial cells were cultured over 3 days to form a confluent layer in the culture channels, with daily medium replacements.

1-7. Reference

1. Adams, M.J., et al., 50 years of the International Committee on Taxonomy of Viruses: progress and prospects. Arch Virol, 2017. 162(5): p. 1441-1446.
2. Lefkowitz, E.J., et al., Virus taxonomy: the database of the International Committee on Taxonomy of Viruses (ICTV). Nucleic Acids Res, 2018. 46(D1): p. D708-D717.
3. Knezevic, P., E.M. Adriaenssens, and C. Ictv Report, ICTV Virus Taxonomy Profile: Inoviridae. J Gen Virol, 2021. 102(7).
4. Roux, S., et al., Cryptic inoviruses revealed as pervasive in bacteria and archaea across Earth's biomes. Nat Microbiol, 2019. 4(11): p. 1895-1906.
5. Marvin, D.A., M.F. Symmons, and S.K. Straus, Structure and assembly of filamentous bacteriophages. Prog Biophys Mol Biol, 2014. 114(2): p. 80-122.
6. Wang, Y.A., et al., The structure of a filamentous bacteriophage. J Mol Biol, 2006. 361(2): p. 209-15.
7. van Wezenbeek, P.M., T.J. Hulsebos, and J.G. Schoenmakers, Nucleotide sequence of the filamentous bacteriophage M13 DNA genome: comparison with phage fd. Gene, 1980. 11(1-2): p. 129-48.
8. Hill, D.F. and G.B. Petersen, Nucleotide sequence of bacteriophage f1 DNA. J Virol, 1982. 44(1): p. 32-46.
9. Peeters, B.P., et al., Nucleotide sequence and genetic organization of the genome of the N-specific filamentous bacteriophage IKe. Comparison with the genome of the F-specific filamentous phages M13, fd and f1. J Mol Biol, 1985. 181(1): p. 27-39.
10. Stassen, A.P., et al., Nucleotide sequence of the genome of the filamentous bacteriophage I2-2: module evolution of the filamentous phage genome. J Mol Evol, 1992. 34(2): p. 141-52.
11. Horabin, J.I. and R.E. Webster, An amino acid sequence which directs membrane insertion causes loss of membrane potential. J Biol Chem, 1988. 263(23): p. 11575-83.
12. Zinder, N.D. and K. Horiuchi, Multiregulatory element of filamentous bacteriophages. Microbiol Rev, 1985. 49(2): p. 101-6.
13. Luiten, R.G., et al., Nucleotide sequence of the genome of Pf3, an IncP-1 plasmid-specific filamentous bacteriophage of Pseudomonas aeruginosa. J Virol, 1985. 56(1): p. 268-76.
14. Van, T.T., et al., Genomic characterization of varphiRS603, a filamentous bacteriophage that is infectious to the phytopathogen Ralstonia solanacearum. Microbiol Immunol, 2014. 58(12): p. 697-700.
15. Murugaiyan, S., et al., Characterization of filamentous bacteriophage PE226 infecting Ralstonia solanacearum strains. J Appl Microbiol, 2011. 110(1): p. 296-303.
16. Campos, J., et al., VEJphi, a novel filamentous phage of Vibrio cholerae able to transduce the cholera toxin genes. Microbiology (Reading), 2010. 156(Pt 1): p. 108-115.
17. Nguyen, D.T., et al., Characterization of Vibrio cholerae O139 of an Aquatic Isolate in Northern Vietnam. Open Microbiol J, 2012. 6: p. 14-21.
18. Ikema, M. and Y. Honma, A novel filamentous phage, fs-2, of Vibrio cholerae O139. Microbiology (Reading), 1998. 144 (Pt 7): p. 1901-1906.
19. Chan, B., et al., Isolation and genetic characterization of a novel filamentous bacteriophage, a deleted form of phage f237, from a pandemic Vibrio parahaemolyticus O4:K68 strain. Microbiol Immunol, 2002. 46(8): p. 565-9.

20. Chang, B., et al., Filamentous bacteriophages of Vibrio parahaemolyticus as a possible clue to genetic transmission. J Bacteriol, 1998. 180(19): p. 5094-101.
21. Kuo, T.T., et al., Complete nucleotide sequence of filamentous phage Cf1c from Xanthomonas campestris pv. citri. Nucleic Acids Res, 1991. 19(9): p. 2498.
22. Denhardt, D.T., The single-stranded DNA phages. CRC Crit Rev Microbiol, 1975. 4(2): p. 161-223.
23. Ray, D.S., A. Preuss, and P.H. Hofschneider, Replication of the single-stranded DNA of the male-specific bacteriophage M13: circular forms of the replicative DNA. J Mol Biol, 1966. 21(3): p. 485-91.
24. Haigh, N.G. and R.E. Webster, The pI and pXI assembly proteins serve separate and essential roles in filamentous phage assembly. J Mol Biol, 1999. 293(5): p. 1017-27.
25. Henry, T.J. and D. Pratt, The proteins of bacteriophage M13. Proc Natl Acad Sci U S A, 1969. 62(3): p. 800-7.
26. Deng, L.W., P. Malik, and R.N. Perham, Interaction of the globular domains of pIII protein of filamentous bacteriophage fd with the F-pilus of Escherichia coli. Virology, 1999. 253(2): p. 271-7.
27. Gutierrez-Rodarte, M., et al., The Vibrio cholerae minor pilin TcpB mediates uptake of the cholera toxin phage CTXphi. J Biol Chem, 2019. 294(43): p. 15698-15710.
28. Tesar, M., et al., Monoclonal antibody against pIII of filamentous phage: an immunological tool to study pIII fusion protein expression in phage display systems. Immunotechnology, 1995. 1(1): p. 53-64.
29. Li, Q., et al., Enhanced targeting: Production of filamentous bacteriophage monoclonal antibodies using the major coat protein pVIII as anchor. Biotechnol J, 2024. 19(3): p. e2300688.
30. Lee, Y.J., et al., Fabricating genetically engineered high-power lithium-ion batteries using multiple virus genes. Science, 2009. 324(5930): p. 1051-5.
31. Zhou, X., et al., Advanced detection of cervical cancer biomarkers using engineered filamentous phage nanofibers. Appl Microbiol Biotechnol, 2024. 108(1): p. 221.
32. Carrico, Z.M., et al., N-Terminal labeling of filamentous phage to create cancer marker imaging agents. ACS Nano, 2012. 6(8): p. 6675-80.
33. Kim, J.T., et al., Virus-templated redox nanowire network for enzyme electrode. Biosens Bioelectron, 2023. 237: p. 115518.
34. Gavric, D. and P. Knezevic, Filamentous Pseudomonas Phage Pf4 in the Context of Therapy-Inducibility, Infectivity, Lysogenic Conversion, and Potential Application. Viruses, 2022. 14(6).
35. Narancic, J., et al., First Characterization of Acinetobacter baumannii-Specific Filamentous Phages. Viruses, 2024. 16(6).
36. Wang, F., et al., Bio-mimetic nanostructure self-assembled from Au@Ag heterogeneous nanorods and phage fusion proteins for targeted tumor optical detection and photothermal therapy. Sci Rep, 2014. 4: p. 6808.
37. Dong, X., et al., Hybrid M13 bacteriophage-based vaccine platform for personalized cancer immunotherapy. Biomaterials, 2022. 289: p. 121763.
38. Liu, X., et al., Highly Effective Stroke Therapy Enabled by Genetically Engineered Viral Nanofibers. Adv Mater, 2022. 34(20): p. e2201210.
39. Borg, R.E., et al., Genetically engineered filamentous phage for bacterial detection using magnetic resonance imaging. Sens Diagn, 2023. 2(4): p. 948-955.

40. Szot-Karpinska, K., et al., Modified Filamentous Bacteriophage as a Scaffold for Carbon Nanofiber. Bioconjug Chem, 2016. 27(12): p. 2900-2910.
41. Korkmaz Zirpel, N., T. Arslan, and H. Lee, Engineering filamentous bacteriophages for enhanced gold binding and metallization properties. J Colloid Interface Sci, 2015. 454: p. 80-8.
42. Joung-Il Moon, E.J.C., Younju Joung, Jin-Woo Oh, Sang-Woo Joo, Jaebum Choo, Development of highly sensitive plasmonic biosensors encoded with gold nanoparticles on M13 bacteriophage networks. Sensors and Actuators B: Chemical, 2024. 400(Part B): p. 1.
43. Oh, D., et al., Graphene sheets stabilized on genetically engineered M13 viral templates as conducting frameworks for hybrid energy-storage materials. Small, 2012. 8(7): p. 1006-11.

2. Aim of this thesis

The main goal of this thesis was to understand the structure of bacteriophages and develop novel biomaterials by using phage display techniques.

The research aimed at identifying binding peptides through phage display technology and apply them for surface functionalization via phage-based scaffold fabrication. A key objective was to develop virus-based molecularly imprinted polymers (MIPs) designed to selectively detect and quantify acidic pharmaceutical compounds. This novel approach is intended to enhance the monitoring and management of pharmaceutical contamination in environmental and clinical area.

Additionally, another goal was to produce and evaluate bioactive scaffolds that promote angiogenesis within the fields of tissue engineering and regenerative medicine. By designing scaffolds incorporating bio-compatible bacteriophages, this research aimed to promote angiogenesis and tissue regeneration, developing a platform that could serve as an alternative to animal experiments at the lab-on-a-chip platform.

Chapter 2

Publication 1 – Molecularly imprinted polymers

Title: Detection of acidic pharmaceutical compounds using virus based molecularly imprinted polymers

This chapter introduces our approach to understand the development of a novel molecularly imprinted polymer (MIP) integrated with filamentous bacteriophages, designed to specifically bind the target substrate, clofibric acid (CA), through selective noncovalent interactions. It was published in the journal Polymers [44]. My contributions were to perform all experiments, and writing the first draft of the manuscript. The following sections are identical to the preprint version of the manuscript.

Detection of acidic pharmaceutical compounds using virus based molecularly imprinted polymers

In-Hyuk Baek[a,b], Hyung-Seop Han[c], Seungyun Baik[a], Volkhard Helms[b] and Youngjun Kim[a*]

[a] Environmental Safety Group, Korea Institute of Science & Technology Europe GmbH, Saarbrücken, Germany

[b] Center for Bioinformatics, Saarland University, Saarbrücken, Germany

[c] Nuffield Department of Orthopaedics, Rheumatology and Musculoskeletal Sciences, University of Oxford, Oxford, U.K

*Corresponding author: Youngjun Kim

Email: youngjunkim@kist-europe.de

Abstract

Molecularly imprinted molecules have proven to be particularly effective chemical probes for the molecular recognition of proteins, DNA and viruses. Here, we started from a filamentous bacteriophage to synthesize a multi-functionalized molecularly imprinted polymer (MIP) for detecting the acidic pharmaceutic clofibric acid (CA) as a chemical pollutant. Adsorption and QCM-D experiments showed that the phage-functionalized MIP had a good binding affinity and specificity for CA compared with the non-imprinted polymer and MIP. In addition, reusability of the phage-functionalized MIP was demonstrated for at least five repeated cycles without significant loss in binding activity. The results indicate that the exposed amino acids of the phage, together with the polymer matrix, create functional binding cavities that provide good affinity to acidic pharmaceutical compounds.

Keywords: Molecularly imprinted polymer (MIP), polypyrrole, filamentous bacteriophage, clofibric acid, self-assembly

1. Introduction

The fast increase in human lifespan and advancements in pharmaceutical technology have significantly improved the quality of human life in modern society. However, in parallel to this, uncontrolled usage and excretion of pharmaceutical compounds have become one of the biggest environmental concerns, as these compounds are widely detected in the sea [45], surface water [46, 47], ground water [48], and soils [49]. The clofibric acid (CA) is one of the metabolite forms of prescribed fibrate drugs (e.g., etofylline clofibrate, etofibrate and clofibrate). These are commonly used in prescription drugs to treat diseases related to the lipid-lowering symptom in the blood of both human and domestic animals [50]. Following digestion, CA and bioactive metabolite products are excreted from the body through urine and feces. Considering their effects in the mammalian lipid metabolism, these pharmaceutical metabolites might interfere with lipid homeostasis and growth of non-target exposed animals such as fish, as recently shown by the regulation of the genes that code for fatty acid-binding proteins and the enzyme fatty acyl-coenzyme-A oxidase, which is involved in fatty acid oxidation [51].

Molecularly imprinted polymer (MIP) is a central part of chemical removals or biosensors that depend on functionalized noncovalent recognition cavities. They fulfil new demands, particularly in the environmental monitoring of endocrine disruptors, heavy metals, chemicals and other emerging pollutants in the environment. MIP can also be used as antibody and receptor mimics, e.g. in materials obtained by imprinting with theophylline and diazepam for enzymatic catalysis [52] by mimicking the active center of the digestive enzyme chymotrypsin [53], and as biosensors. The recognition elements in biosensors usually consist of antibodies, enzymes or other biological receptors that are immobilized on the sensor surface. Conducting polymers show metal-like behavior due to conjugated double bonds, e.g., polyacetylene [54], polypyrrole [55], polythiophene [56], and polyaniline [57]. The polymerization can be conducted at room temperature in organic solvents or aqueous solutions. This is advantageous for the imprinting of biomolecules because denaturation and conformational changes can be avoided [58]. Polypyrrole belongs to the first routinely electrochemically synthesized polymers [59]. Biocomposites of conductive polymers and virus particles have been prepared with M13 [60] and tobacco mosaic virus (TMV) [61] and conductive polymers have been prepared by chemical polymerization [62]. Donavan et al showed that composites of poly(3,4-ethylenedioxythiophene) and filamentous bacteriophage M13 can be prepared by electrodeposition [63]. Also, the development of bacteriophage-based biosensors has been described. These were used for the recognition of

specific target molecules as well as biomarkers [64], including the detection of bacterial pathogens in food [65], processed wastewater [66], human or animal blood, urine, or sputum for clinical diagnostics [67].

The bacteriophage-driven hybrid biocomposites fabricated by electrochemical polymerization include PEDOT-M13 [63], polyaniline-M13 [60], and polypyrrole-T7 [68]. Upon exposure to solutions containing a target molecule that binds to the virus particles, films of the virus-PEDOT biocomposite showed increased electrical impedance while nanowires showed an increased DC resistance [63]. Filamentous bacteriophages (M13, f1, f88 and fd) have been used for various applications in material science [69], drug delivery [70], imaging [32], tissue engineering [71], energy storage [72], and as biosensors [63].

It has been demonstrated in many cases that MIP adsorption is an effective and economical method to sense and treat many pollutants in wastewater [73]. In contrast to this, the CA separation using MIP [74] or the MIP adsorbent drew little attention. Furthermore, the MIP mentioned above was prepared using a single template and thus these MIPs could not exhibit high selectivity for most compounds especially those belonging to different groups.

In this work, the pyrrole based MIP were co-polymerized with filamentous bacteriophages and cross-linked by cyclic voltammetry to form a polypyrrole-phage complex. Thus, we can hypothesize that the bacteriophage derived MIPs provide functional binding cavities to acidic pharmaceutical compounds. Acidic, aromatic and nucleophilic amino acids were electrochemically polymerized with pyrrole polymers. The MIPs were tested by QCM-D (Quartz Crystal Microbalance and Dissipation), SEM (Scanning Electron Microscopy) with UV/Vis spectroscopy in order to evaluate their binding properties and morphological changes.

2. Materials and methods

2-1. Reagents and materials

CA (purity, 97 %) and Pyrrole (reagent grade, 98 %) were purchased from Sigma-Aldrich (St. Louis, MO, USA). A 10 mM pyrrole solution was prepared in phosphate buffer (0.1 M NaH_2PO_4 and 0.1M Na_2HPO_4) containing 0.1 M KNO_3 and stored at 4 ºC to prevent oxidation. Solutions for polymerization and binding were filtered before use with 0.2 μm polypropylene syringe filters.

2-2. Amplification and purification of phage

Escherichia coli K91BluKan (K91BK) strain (kindly provided by Prof. Dr. Georg P Smith, University of Missouri, USA) was used as host for the amplification of phage particles [54]. Isolation of phages from the host cells was performed by the polyethylenglycol/sodium chloride (PEG/NaCl) precipitation method as previously described [75] after growing the transformed K91BK cells in Luria Broth (LB) supplemented with tetracycline (20 μg/ml) and Kanamycin (100 μg/ml) at 37 °C with vigorous shaking (260 rpm) overnight. The phage supernatants were dialyzed in distilled water to remove the remaining PEG. Samples were dialyzed with Mw 100 kD cut off membrane at 120 rpm stirring overnight at 4 °C (Biotech CE tubing, USA). The concentration (colony-forming unit per milliliter, CFU/ml) was measured in the dialyzed samples by UV/vis. The concentration of filamentous bacteriophages was determined by phage titration as previously described [76]. Phage suspensions were stored at 4 °C.

2-3. Electrochemical polymerization of polypyrrole-phage matrix

Cyclic voltammetry (CV) was performed using an electrochemical flow module of Quartz Crystal Microbalance with Dissipation monitoring (QCM-D, Q-sense, Sweden). This consists of a working electrode, a counter electrode and an Ag/AgCl reference electrode. Film deposition were used by the QCM 401 module which was a drop casting electrochemistry system. Determination of polymer's surface and thickness was performed with FE-SEM (Field Emission Scanning Electron Microscopy, Inspect F50, FEI, USA). Cross sections were obtained my cutting the MIP and MIP with phage using a diamond cutter (6-539-05, Ogura, Japan) and sputtered with platinum (E-1045, Hitachi Co., Japan) for observation. For the polymerization, pyrrole solutions were mixed with CA and phage. Non-imprinted polymer (NIP) (10 mM pyrrole), MIP (10 mM pyrrole and 0.5 mM CA) and MIP-wt-phage (10 mM pyrrole, 0.5 mM CA and 1.1 x 10^{13} cfu/mL phage) were separately placed on a standard 5 MHz AT-cut Au coated quartz crystal. The configuration was operated using a potentiostat (Autolab PGSTAT 12, Metrohm/Eco Chemie, Netherland) controlled by the GPES software (Eco Chemie, Germany). Initially, phosphate buffer (0.1 M NaH_2PO_4 and 0.1M Na_2HPO_4) containing 0.1 M KNO_3 was pumped through the flow module to remove contaminations and air bubbles. Subsequently, the module was filled in with the sample solution and equilibrated for 5 minutes. Finally, MIP was prepared on the gold coated surface of quartz crystals through cyclic voltammetry of pyrrole monomer in the presence of CA or phage in aqueous phosphate buffer (0.1 M NaH_2PO_4 and 0.1M Na_2HPO_4) containing 0.1 M KNO_3

(pH 7). The potential was cycled between -200 and +800 mV with 40 cycles at a scan rate of 100 mV/s. Freshly synthesized polypyrrole-phage films were then rinsed with water and immediately analyzed. After electropolymerization, the CA was extracted with methanol/acetic acid (9:1, v/v) in a shaker (100 rpm) for 16 hours. A standard AT-cut Au-coated quartz crystal was used at the 4.9 MHz resonance frequency. Information about the absorption process is obtained from changes in resonance frequency (Δf) and the dissipation factor (ΔD, $1x10^{-6}$) at overtone 7 which represent the harmonic resonances of the base frequency (Figure S1). The CA extraction and rebinding procedure was monitored by QCM-D analysis during several repeated cycles.

2-4. Analysis of the viscoelastic properties and topography of the polypyrrole matrix

To monitor the immobilization of polypyrrole-phage films on the Au electrode, we measured the increase in mass and the viscoelastic properties of the polypyrrole and polypyrrole-phage films by QCM-D analysis. A standard 5 MHz Au coated quartz crystal was excited at the resonance frequency (Δf, Hz). Information about the adsorption process was obtained from the changes in the dissipation factor (Δ D, $1x10^{-6}$) at overtone number 7 for the crystals. Measurements were performed at a flow rate of 100 μl/min at 25 °C. The resultant Δ f and Δ D were analyzed by the Voigt model in the Qtools software (Q-sense, Sweden) to extract information on the density, viscosity, shear, and binding mass. To analyze the parallel topography of the polypyrrole surface, electrodeposited films were visualized by SEM (FEI Quanta FEG 250, Netherland).

2-5. UV/Vis spectroscopy measurement

Ultraviolet-Visible (UV/Vis) analysis was performed on the solution of 1mM pyrrole, 1mM CA and $1x10^{12}$ cfu/ml bacteriophage by UV/Vis spectroscopy (Ultrospec 3300 pro, Amersham, UK). All prepared samples in distilled water were recorded between 200 nm and 350 nm of wavelength. The mixture prior to electropolymerization was characterized by UV/Vis spectrophotometry at different intervals to monitor the reaction.

2-6. Liquid Chromatography-Tandem Mass Spectrometry Analysis

CA was quantified in the samples with a HPLC system (Agilent 1290, Agilent Technologies, CA, USA) connected to a triple quadrupole mass spectrometry

(MS/MS) model 6460 Agilent (Agilent Technologies, CA, USA) equipped with electrospray Jet Stream technology operating a negative ion mode. The operating parameters of MS were as follows: capillary voltage of 3500 V, nebulizer pressure of 45 psi, drying gas flow of 10 L/min, gas temperature of 300 ºC, sheath gas flow of 11 L/min, sheath gas temperature of 350 ºC, and nozzle voltage of 1000 V. Separation of the target compound and its internal standard (4-chlorophenylacetic acid, Sigma Aldrich, St. Louis, MO, USA) was performed on a Zorbax Rapid Resolution High Definition column (2.1 mm × 50 mm, 1.8 μm particle size, Agilent, Stuttgart, Germany) maintained at 30° C. To protect the chromatographic column, a C18 guard column (Zorbax Eclipse Plus 2.1 mm × 5 mm, 1.8 μm, Agilent, Stuttgart, Germany) was connected to the column. We used a gradient method with three mobile phases, MilliQ-Q water containing 0.1 % formic acid and 50 mM ammonium acetate (mobile phase A), LC/MS grade acetonitrile (mobile phase B), and LC/MS grade methanol (mobile phase C), respectively. The initial conditions were 85 % A, 9 % B, and 6 % C, and this ratio was kept constant for 1.5 minutes. Both B and C were then increased to 59 % and 39 %, respectively, over 4.5 minutes and then kept constant for another 1.5 minutes. All the conditions of the mobile phases were set back to the initial conditions within 0.5 minutes. The total running time, including an additional 4 minutes of a post-run protocol, was 12 minutes. The flowrate was kept at 0.4 ml/min and the sample injection volume was set to 20 μl. The MS analysis in multiple reactions monitoring (MRM) mode for both CA and its internal standard was carried out using the instrument settings described in Table 1. We monitored the accurate mass of precursor ions and the transitions to two product ions. The most abundant transition was used for quantification, whereas the second one was used to confirm the target analyte. These source and fragmentation parameters were optimized for each analyte using 1 mg/L of a single standard dissolved in methanol by passing the same column explained above. A calibration curve for CA was established at five levels ranging from 0.02 μM to 10.0 μM with a correlation coefficient R^2>0.99. Values for the instrumental limit of detection (ILOD) and for the instrumental limit of quantification (ILOQ) were estimated from the low concentration calibration standard giving signal-to-noise ratios of 3:1 and 10:1, respectively. ILOD values of 0.001 μM and 0.005 μM for this analyte were obtained. Agilent Mass Hunter Qualitative Analysis and Quantitative Analysis software (v.B.06.00) were used for data processing.

Table 1. Negative mode multiple reactions monitoring (MRM) transitions selected for target analyte, CA, and its internal standard, 4-chlorophenylacetic acid, with fragment voltage (FV) and collision energy (CE)

Compound	Mass transition (m/z)	Fragmentor, eV	CE, eV	Usage
Clofibric acid (CA)	213 → 127	68	9	Quantitation
	213 → 85	68	5	Confirmation
4-chlorophenylacetic acid	169 → 125	56	5	Quantitation
	169 → 35	56	13	Confirmation

2-7. Reusability

1 mM CA was adsorbed onto the MIPs in KNO_3 (100 mM) buffer for 5 min, and subsequently washed with methanol:acetic acid (9:1, v:v) followed by stabilization in KNO_3 (100 mM) buffer. After stabilization, the adsorption of CA and rebinding procedure was repeated during several experiments.

3. Results and Discussion

3-1. Electropolymerization of polypyrrole-phage biocomposites

Figure 1 shows a schematic diagram for the construction of the polypyrrole-phage-based biocomposite. In the mixture, complexes form between a filamentous phage and CA that possess functional amino groups complementary to those on the CA template. Cross-linking polypyrrole monomers are added and the mixture is kept in electropolymerizing conditions in order to permanently and rigidly fix the spatial arrangement of the functional monomers. Following co-polymerization, CA is extracted from the polymer matrix, leaving behind cavities whose size, shape and chemical functionality complement that of the template. These empty cavities can selectively and reversibly rebind molecules similar to the original template. When the pyrrole is mixed with phage, Major pVIII coated amino acids might be bound to CA due to eleven variable amino acid residues of the C-terminal cytoplasmic domain [77].

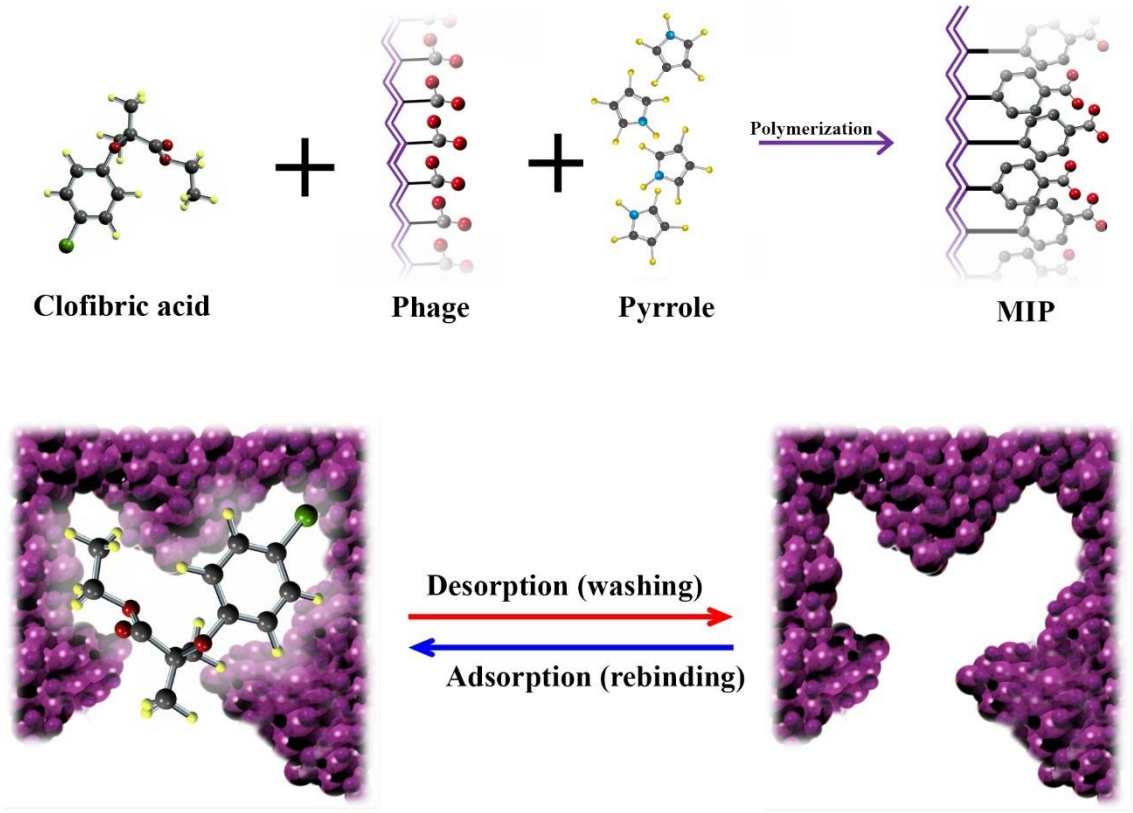

Figure1. Schematic drawing of the polymerization of MIP (molecularly imprinted polymers) and of the reusability process.

Cyclic voltammograms (CVs) combined with QCM-D were used to monitor the polypyrrole-phage electropolymerization. Figure 2 shows the accumulated curve obtained after 40 independent measurements. The CV of the redox reaction yielded an estimated stepwise-decreasing plot in the electrochemical module of QCM-D. On the plateau-shaped cyclic voltammograms between -0.2 V and 0.8 V was shown in Figure 2a, the peaks due to the oxidation and reduction of the film increase in intensity as the polypyrrole film formation. A broad oxidation peak was observed at the peak potential of 0.2 and reverse reduction peak was seen as a peak potential of 0.1 V. The deposition of the polymer was monitored by QCM-D, where the quartz crystal connected to a potentiostat is also the working electrode. There is no significant difference between the obtained CV curves of pyrrole and pyrrole-phage, indicating that phage in trapped pyrrole of the electron transfer abilities are similar to those of the polypyrrole composition (Figure 2b).

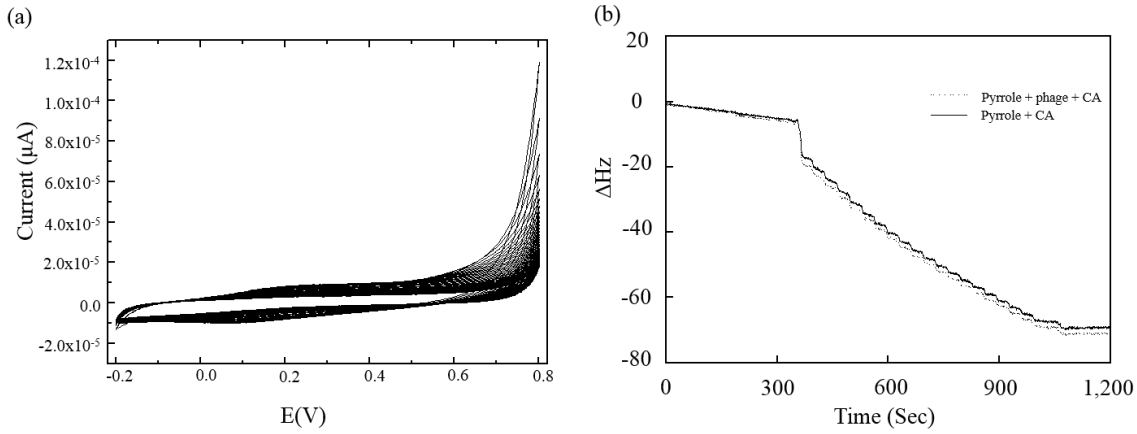

Figure 2. Cyclic voltammograms during the preparation of the polypyrrole film (a) and QCM-D analysis (b) during electropolymerization of 10 mM pyrrole containing 0.5 mM CA in phosphate buffer with 100 mM KNO_3 (solid line) and wt-bacteriophage (1.1 x 10^{13} cfu/mL, dashed line) with 40 cycles between -0.2 -0.8 V, scan rate 100 mVs^{-1}, respectively.

3-2. UV/Vis characterization of pyrrole, phage and CA complexes

Figure 3 shows the UV-vis absorption spectra for the mixture of bacteriophage, pyrrole, and CA prior to polymerization. The broad characteristic UV visible absorption between 200 and 350 nm contains maximum absorption bands at wavelengths 224, 269, and 275 nm. The filamentous bacteriophages have a characteristic peak at 269 nm [78]. The characteristic peak of the amide NH band showed up at 224 nm as previously described [79]. These correspond to wt-phage (figure 3a), pyrrole (figure 3b) and CA (figure 3c) solution, respectively. Their characteristic absorption shoulders are clearly noticeable in the curves for all mixtures (figure 3f). Only the mixture of phage and pyrrole, in comparison to the phage solution, exhibited a slightly decreased absorbance peak at 224 nm in contrast to an increased absorption peak at 269 nm (figure 3d). It seems that the mixture of phage and pyrrole forms only weak interactions with amino acid residues of the phage in the form of ionic interactions. Based on computer simulations, Rahim Ghadari reported that the aromatic amino acids Phe, Trp, and Tyr have the most favorable binding affinities toward pyrrole-like moieties due to stabilization by π–π stacking interactions and hydrogen bonding. Among the three amino acids, Trp appears to be the most effective π–hydrogen bond acceptor in proteins [80]. As described in table S1, filamentous bacteriophage presents not only filamentous folded structures on its surface but also an aromatic ring of amino acids (e.g. pVIII Phe (F) 4 amino acid (aa), Tyr (Y) 2 aa,

Trp (W) 1 aa; pIII F 22 aa, Y 21 aa, W 4 aa; pVI F 10 aa, Y 4 aa, W 1 aa; pIX F 3 aa, Y 2 aa, W 1 aa; pVIII F 2 aa, Y 1 aa). Thus, we speculate that a small amount of change in the λ_{max} is due to conformational changes in Phe, Trp and Try in the presence of the benzene ring of pyrrole.

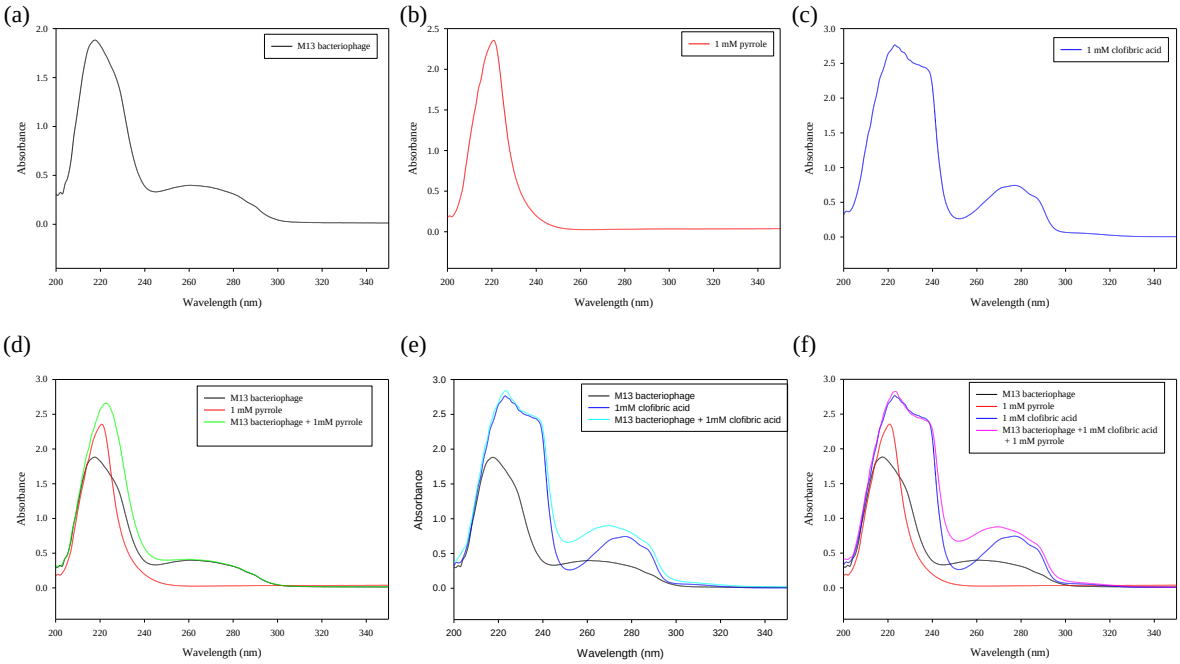

Figure 3. UV/vis spectra of wt-phage, pyrrole and CA. All samples were prepared in DI water at wt-phage (1×10^{12} cfu/ml), pyrrole (1 mM) and CA (1 mM) mixing ratio. wt-phage (black, a); 1 mM pyrrole (red, b); 1 mM CA (blue, c), wt-phage mixed with pyrrole (green, d), wt-phage mixed with CA (cyan, e); wt-phage and pyrrole mixed with CA (pink, f).

3-3. SEM analysis of polypyrrole matrix topography

SEM analyses shown in Figure 4 characterize the polypyrrole and polypyrrole-phage film on an Au surface. The typical sparse grains of a cauliflower-like polypyrrole matrix usually range from 60 nm to 150 nm [81]. Figure 4a demonstrates that the matrix was successfully prepared using the electro-polymerization method. In contrast to this, the surface morphology of MIP wt-phage showed cross-linked structures in the patch-like surfaces as shown in figure 4b. In this figure, large agglomerates of phage bundles, smaller clusters of phages, and individual phages in the polypyrrole layer were observed. The characteristic features of filamentous bacteriophages were approximately 6.6 nm wide and 100 nm long [82]. However, conjugation of pyrrole and wt-phages

resulted in encapsulation of wt-phages and showed a thickness of approximately 100 nm, indicating that the phages were successfully incorporated into the polypyrrole biocomposites. The MIP with filamentous bacteriophage complex may allow the further modification of structures and roughness following polymerization. After the desorption process of the CA, we measured the average thickness values using FE-SEM as the results are shown in Figure S3. From this figure, thicknesses of MIP (a) and MIP with wt-phase (b) were calculated as 0.94 and 1.23 μm on the Au coated electrode, respectively. This result, along with Figure 4, revealed that the thickness was not influenced by biochemical properties, but the different structure and roughness can be generated by filamentous bacteriophage. This new morphology could lead to a significant increase in the size of repeating structure and binding cavities of the polymer networks since the cross-linked structures provide a larger number of porosity sites for CA.

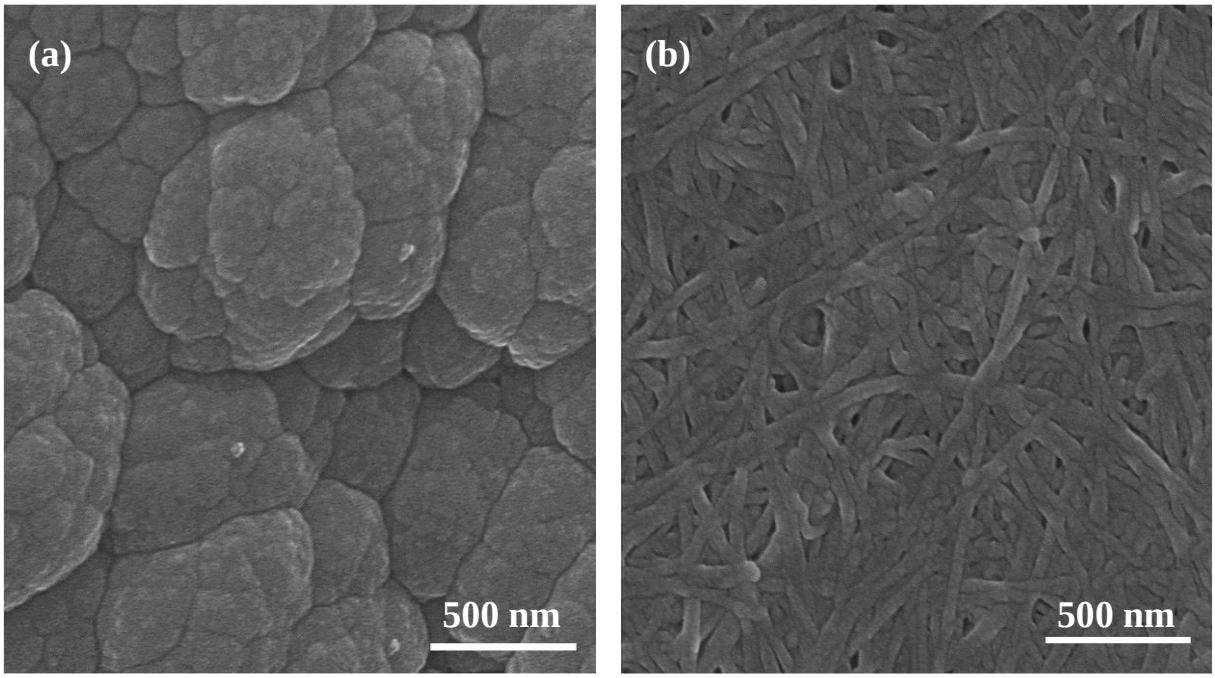

Figure 4. SEM images illustrating the polymerization of pyrrole (polypyrrole) (a) and of polypyrrole with wild type bacteriophages (polypyrrole wt-phage) (b).

3-4. Interaction of CA with the polypyrrole matrix on a microbalance sensor

QCM-D experiments were performed to investigate the binding affinity between CA and different types of MIPs in more detail. The frequency shift (figure 5a) showed a similar pattern of the dissipation shift (figure 5b) in the

QCM-D analysis. The black (bare electrode) and blue (NIP) lines represent a control experiment for CA adsorption. Injecting 1 mM CA solution into the flow channel led to strong increases of frequency and dissipation signals. The MIP and NIP showed an initial frequency increase of ~ -20.84 Hz (Δf), ~ 8.13 × 10^{-6} (ΔD) upon the injection of CA during 200 sec. All the lines were saturated after 400 sec. NIP especially closely reached the bare electrode frequency levels and, then, all MIPs were saturated at different levels. These results indicate that CA was initially non-specifically bound to the MIP and NIP surfaces. The resulting Δf / ΔD values for MIP wt-phage (Δf (-22.65) Hz / ΔD 5.36 × 10^{-6}) are much higher than those for MIP alone (Δf (-16.35) Hz / ΔD 3.20 × 10^{-6}). This suggests that the MIP wt-phage is more effective and has a higher affinity to CA than MIP alone. This result also indicates that the binding sites of the MIP wt-phage provide a number of effective binding arms, not only for NH_3^+ and COO^-, but also for aromatic rings of the wt-phage. Thus, high affinity for CA may be due to hydrophobic contacts and π-π stacking between the aromatic ring of CA and the binding pocket [83]. We included the QCM adsorption analysis graph of all overtones (Figures S1 and S2). Fig. S1 below shows that all overtones have a similar pattern. From the comparison of all overtones, we found that the frequency shift were tended to be high sensitive at the low overtone numbers. The low overtones (n= 1, 3, 5) needed more time for stabilization than higher overtones. Even though all overtones showed a similar pattern, high overtones showed more noise (n=9, 11, 13) (Figure S2). Similar trends were reported previously [84, 85]. Thus, we selected overtone number 7.

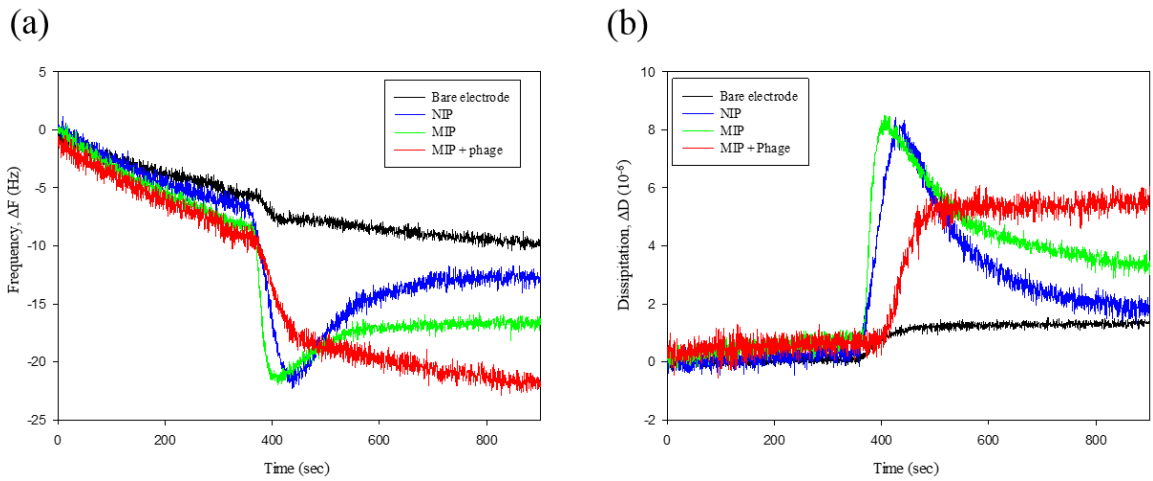

Figure 5. QCM adsorption analyses of bare electrode (black line), NIPs (blue line), MIP (green line), and MIP wt-phages (4×10^{12} cfu/ml, red line); frequency (a) and dissipation shift (b).

3-5. Binding efficiency and capacity of CA to polypyrrole matrix on microbalance sensor

In order to confirm specific interactions of the NIP and different types of MIP, a concentration based frequency change and a recovery experiment were conducted. The surface was washed using MilliQ water after adsorption of CA (1 mM). For the evaluation of the recovery on CA-imprinted polymer, the recovery potential of the polymers was tested by LC-MS/MS with quantification of CA from the flow through (PBS), washing of (MilliQ water), and elution of (MeOH, acetic acid 9:1, v:v) media samples. The results for the CA recovery (%) are shown in figure 6a; NIP (1.53 %), MIP (0.65 %) and MIP wt-phage (0.91 %) in flow through sample, NIP (94.65 %), MIP (81.13 %), and MIP wt-phage (10.15 %) in washing sample, and NIP (3.82 %), MIP (18.21 %) and MIP wt-phage (88.94 %) in elution sample. Figure 6b shows frequency responses for different concentrations of CA ranging from 50 μm to 1 mM. At a CA concentration of 50 μM, we detected no significant changes of the frequency. However, the reactive frequency can be clearly distinguished from binding signals above 50 μM of CA. In the environment, CA is mostly found in concentrations below 100 μM. Previously, Towuanse S et al showed that after doses of 500 – 1500 mg CA human urine contained the following concentrations of CA: 46.5 – 223.6 μM at 0-24 hours and 11.6 – 28.0 μM at 24-48 hours [81]. In waste water, CA exists in a wide range from pM to nM concentration [86, 87]. Thus, we assumed that MIP wt-phage can probably be used to diagnosis CA during the early stage (0-24 hours after doses of CA) in urine samples. These systems can't be adapted to the environmental diagnosis field because of low concentration of pharmaceutic residue. However, these systems can be applied in the water purification field, because our results show that MIPs are selective and reusable. Furthermore, previous research showed that MIP were stable over a wide range of temperature, pH and humidity [88]. The interaction of CA with the MIP wt-phage biocomposite further confirmed that CA has a higher affinity for MIP wt-phage than for MIP and NIP composites. This observation suggests that the components of the wt-phage, such as NH_3^+, COO^- and aromatic rings, could form complexes with CA in the polymer matrix. This may yield a higher CA binding affinity and sensitivity in contrast to polypyrrole composites. In particular, we previously reported that selective adsorption of CA compared to caffeine was achieved [89]. Similar to our finding for CA absorption to MIP, we hypothesize that phages decorated with amino acids can improve the binding affinity to CA. Based on our study, it appears as if the MIP and wt-phage complex provide patch-like structures which can provide different thickness and roughness compared to MIP and NIP. Thus we assumed that multiple interactions contributed to the absorption of CA that were based on

the different physicochemical properties of the functional amino acids in binding cavities.

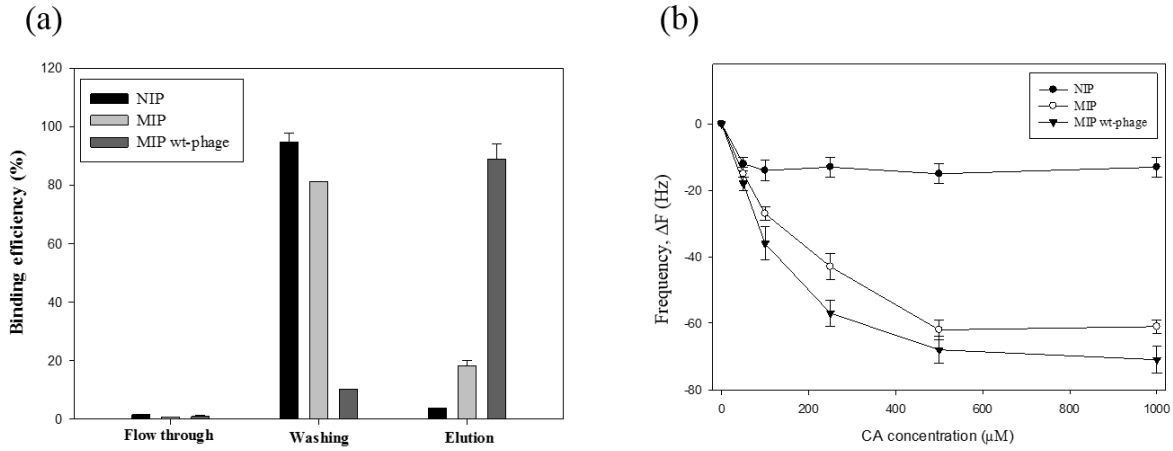

Figure 6. Adsorption and binding capacity of MIPs. The CA binding affinity from flow through, washing and elution of the samples by LC-MS/MS analysis (a). CA removal from MIPs was carried out in buffer with 10% acetic acid in the elution step. The changes of frequency from 0 to 1mM concentration of CA (b). Data were analyzed statistically by ANOVA at a $P < 0.05$ confidence interval (n= 3).

3-6. Reproducibility of CA sensing activity on phage-pyrrole matrix

The reusability of MIP was tested by five sequential adsorption and desorption of regeneration cycles (figure 7). Captured CA on MIP wt-phage was elutriated and washed using methanol:acetic acid (9:1, v:v) mixture. As there was no obvious decrease in the adsorption efficiency for CA, this proves that the MIP can be used in at least five cycles and it has a certain regeneration adsorption efficiency. All of these are signs of good reusability. Moreover, five rebinding cycles of CA onto the polypyrrole-phage composites did not influence the sensitivity of the QCM analysis. This suggests that detecting the acidic pharmaceutic compounds on a microbalance sensor is a highly effective methodology with sufficiently high sensitivity, affinity and long-term stability. The sensitivity of the imprinted polymer and its imprinting specificity were tested with MIP, NIP, and MIP wt-phage. The MIP wt-phage showed a higher response to CA than NIP and MIP. This high binding affinity might have resulted from the structure and functionality changes of MIP wt-phage. Filamentous bacteriophages are decorated with polar and non-polar amino acid side chains which may explain the effective adsorption ability. In future, further experiments are warranted with various waste water chemical compounds in complex matrices.

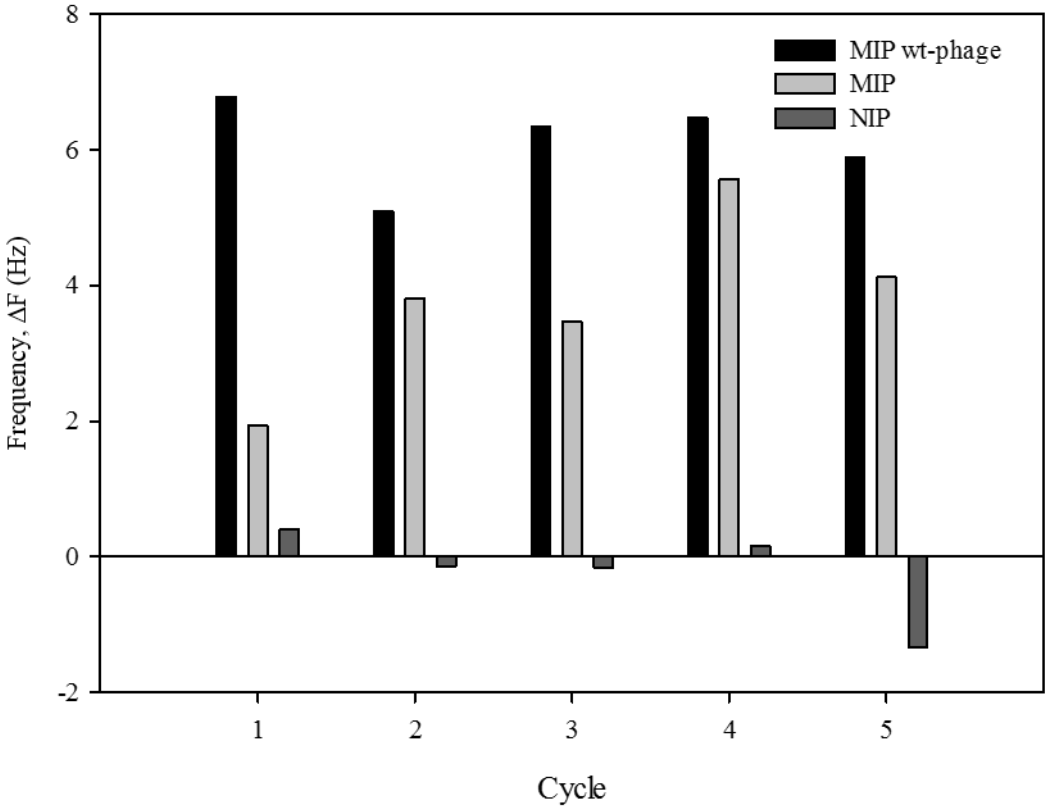

Figure 7. MIP regeneration and reusability. Frequency changes in five repeated runs indicate adsorption and desorption of CA on MIP wt-phage, MIP and NIP, respectively.

4. Conclusion

A novel MIP combined with filamentous bacteriophages was shown to bind specifically to the substrate CA due to specific noncovalent interactions. Also, we described the use of functionalized-phage pyrrole MIP for the real time monitoring of CA. Thus, the functionalized-phage conductive polymer can be used for efficient on/off sensing of targets. The new method appears to be a promising, unique and versatile method with high and efficient reproducibility that should have many applications in the field of sensors, electronics and biomedical engineering.

5. Acknowledgements

We thank Michael Müller for help with experimental setup and guidance for electropolymerization. We also thank Dr. Jaeho Lee, Dr. Jungtae Kim and Dr.

Sangwon Kim for electrochemistry analysis, Dr. Nuriye Korkmarz for helpful discussions about bacteriophage and Ms Hyunseon Seo for measuring the thickness. This study was supported by Korea Institute of Science and Technology Europe (KIST-Europe) joint program (Project no. 11805).

6. Author Contributions

Conceived and designed the experiments: YJ Kim and I-H Baek, Performed the experiments: I-H Baek, Analyzed the data: SY Baik, Drew schematic diagram: HS Han. Contributed reagents/materials/analysis tools: I-H Baek. Wrote the paper: I-H, Baek and YJ Kim. Proofread: V Helms and HS Han.

7. References

1. Halling-Sorensen B, Nors Nielsen S, Lanzky PF, Ingerslev F, Holten Lutzhoft HC, and Jorgensen SE. Chemosphere 1998;36(2):357-393.

2. Sacher F, Ehmann M, Gabriel S, Graf C, and Brauch HJ. J Environ Monit 2008;10(5):664-670.

3. Jux U, Baginski RM, Arnold HG, Kronke M, and Seng PN. Int J Hyg Environ Health 2002;205(5):393-398.

4. Stan THH-J. International Journal of Environmental Analytical Chemistry 1997;67:113-124

5. Hans-Rudolf Buser MDM. Environ. Sci. Technol. 1998;32 ((1)):188–192.

6. Pagano RE, Puri V, Dominguez M, and Marks DL. Traffic 2000;1(11):807-815.

7. Esplugas S, Bila DM, Krause LG, and Dezotti M. J Hazard Mater 2007;149(3):631-642.

8. Yilmaz E, Mosbach K, and Haupt K. Analytical Communications 1999;36(5):167-170.

9. Lele BS, Kulkarni MG, and Mashelkar RA. Reactive & Functional Polymers 1999;39(1):37-52.

10. Korkmaz N, Kim YJ, and Nam CH. Macromol Biosci 2013;13(3):376-387.

11. Nezhadali A, Es'haghi Z, and Khatibi A. Analytical Methods 2016;8(8):1813-1827.

12. Lindqvist N, Tuhkanen T, and Kronberg L. Water Res 2005;39(11):2219-2228.

13. Loos R, Gawlik BM, Locoro G, Rimaviciute E, Contini S, and Bidoglio G. Environ Pollut 2009;157(2):561-568.

14. Tan CJ and Tong YW. Langmuir 2007;23(5):2722-2730.

15. Kanazawa KK, Diaz AF, Geiss RH, Gill WD, Kwak JF, Logan JA, Rabolt JF, and Street GB. Journal of the Chemical Society-Chemical Communications 1979(19):854-855.

16. Niu ZW, Bruckman MA, Harp B, Mello CM, and Wang Q. Nano Research 2008;1(3):235-241.

17. Tseng RJ, Tsai CL, Ma LP, and Ouyang JY. Nature Nanotechnology 2006;1(1):72-77.

18. Arter JA, Taggart DK, McIntire TM, Penner RM, and Weiss GA. Nano Lett 2010;10(12):4858-4862.

19. Arter JA, Taggart DK, McIntire TM, Penner RM, and Weiss GA. Nano Letters 2010;10(12):4858-4862.

20. Lee JW, Song J, Hwang MP, and Lee KH. International Journal of Nanomedicine 2013;8:3917-3925.

21. Singh A, Arutyunov D, Szymanski CM, and Evoy S. Analyst 2012;137(15):3405-3421.

22. Chen JH, Alcaine SD, Jiang ZW, Rotello VM, and Nugen SR. Analytical Chemistry 2015;87(17):8977-8984.

23. Sorokulova I, Olsen E, and Vodyanoy V. Expert Review of Medical Devices 2014;11(2):175-186.

24. Shirale DJ, Bangar MA, Park M, Yates MV, Chen W, Myung NV, and Mulchandani A. Environmental Science & Technology 2010;44(23):9030-9035.

25. Lee SK, Yun DS, and Belcher AM. Biomacromolecules 2006;7(1):14-17.

26. Yacoby I, Shamis M, Bar H, Shabat D, and Benhar I. Antimicrobial Agents and Chemotherapy 2006;50(6):2087-2097.

27. Carrico ZM, Farkas ME, Zhou Y, Hsiao SC, Marks JD, Chokhawala H, Clark DS, and Francis MB. Acs Nano 2012;6(8):6675-6680.

28. Merzlyak A, Indrakanti S, and Lee SW. Nano Letters 2009;9(2):846-852.

29. Oh DY, Dang XN, Yi HJ, Allen MA, Xu K, Lee YJ, and Belcher AM. Small 2012;8(7):1006-1011.

30. Huang DL, Wang RZ, Liu YG, Zeng GM, Lai C, Xu P, Lu BA, Xu JJ, Wang C, and Huang C. Environmental Science and Pollution Research 2015;22(2):963-977.

31. Dai CM, Zhang J, Zhang YL, Zhou XF, and Liu SG. PLoS One 2013;8(10).

32. Korkmaz N, Kim YJ, and Nam CH. Macromolecular Bioscience 2013;13(3):376-387.

33. Warner CM, Barker N, Lee SW, and Perkins EJ. Bioprocess and Biosystems Engineering 2014;37(10):2067-2072.

34. Wang L, Ying GG, Zhao JL, Yang XB, Chen F, Tao R, Liu S, and Zhou LJ. Sci Total Environ 2010;408(16):3139-3147.

35. Warner CM, Barker N, Lee SW, and Perkins EJ. Bioprocess Biosyst Eng 2014;37(10):2067-2072.

36. D.J. Abraham RDR. Tetrahedron Letters 1972;13(10):909-912.

37. Ghadari R. Phys Chem Chem Phys 2016;18(6):4352-4361.

38. Emudianughe TS, Caldwell J, Sinclair KA, and Smith RL. Drug Metab Dispos 1983;11(2):97-102.

39. Bhattacharjee S, Glucksman MJ, and Makowski L. Biophysical Journal 1992;61(3):725-735.

40. Hunter CA, Lawson KR, Perkins J, and Urch CJ. Journal of the Chemical Society-Perkin Transactions 2 2001(5):651-669.

41. Modin C, Stranne AL, Foss M, Duch M, Justesen J, Chevallier J, Andersen LK, Hemmersam AG, Pedersen FS, and Besenbacher F. Biomaterials 2006;27(8):1346-1354.

42. Duner G, Thormann E, and Dedinaite A. J Colloid Interface Sci 2013;408:229-234.

43. Weigel S, Kuhlmann J, and Huhnerfuss H. Sci Total Environ 2002;295(1-3):131-141.

44. Heberer T, Schmidt-Baumler K, and Stan HJ. Acta Hydrochimica Et Hydrobiologica 1998;26(5):272-278.

45. Svenson J, Andersson HS, Piletsky SA, and Nicholls IA. J Mol Recognit 1998;11(1-6):83-86.

46. Schweiger B, Kim J, Kim YJ, and Ulbricht M. Sensors (Basel) 2015;15(3):4870-4889.

Supplementary figures and tables for:

Detection of acidic pharmaceutical compounds using virus based molecularly imprinted polymers

In-Hyuk Baek[a,b], Hyung-Seop Han[c], Seungyun Baik[a], Volkhard Helms[b], Youngjun Kim[a*]

[a] Environmental Safety Group, Korea Institute of Science & Technology Europe GmbH, Saarbrücken, Germany

[b] Center for Bioinformatics, Saarland University, Saarbrücken, Germany

[c] Nuffield Department of Orthopaedics, Rheumatology and Musculoskeletal Sciences, University of Oxford, Oxford, U.K

*Corresponding author: Youngjun Kim

Email: youngjunkim@kist-europe.de

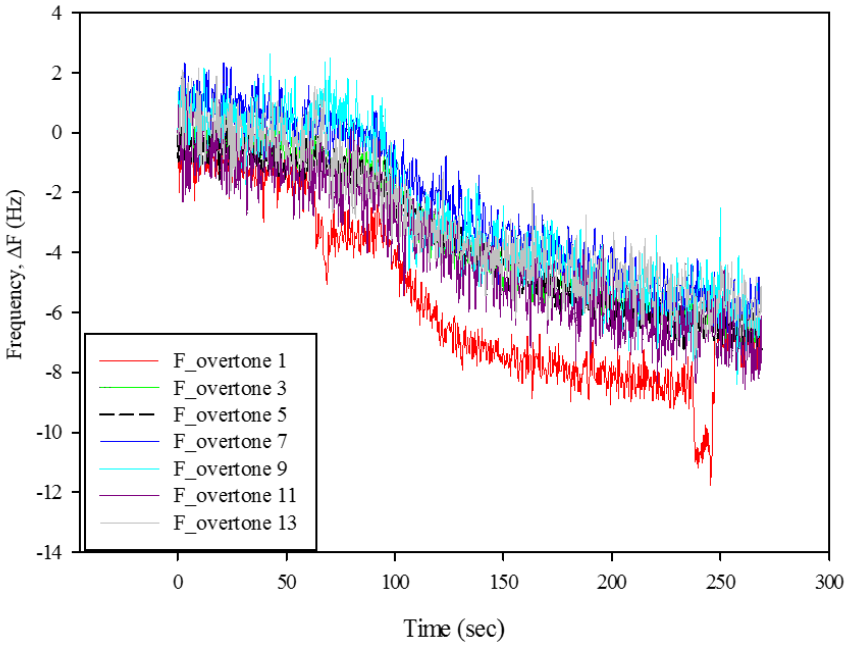

Figure S1. QCM adsorption analysis of seven overtones (1, 3, 5, 7, 9, 11, 13) based on MIP with bacteriophage. The arrow indicates the initial loading of 100 μM CA.

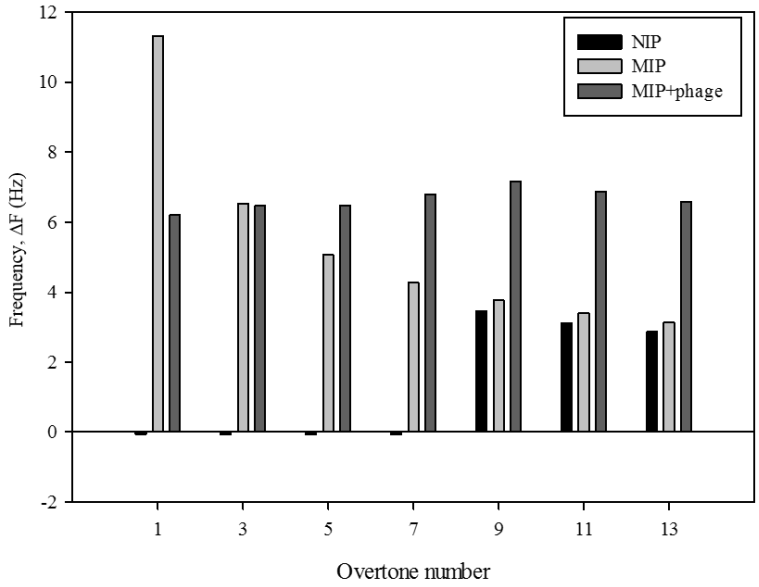

Figure S2. Frequency changes of MIP, NIP and MIP with phage at seven overtones

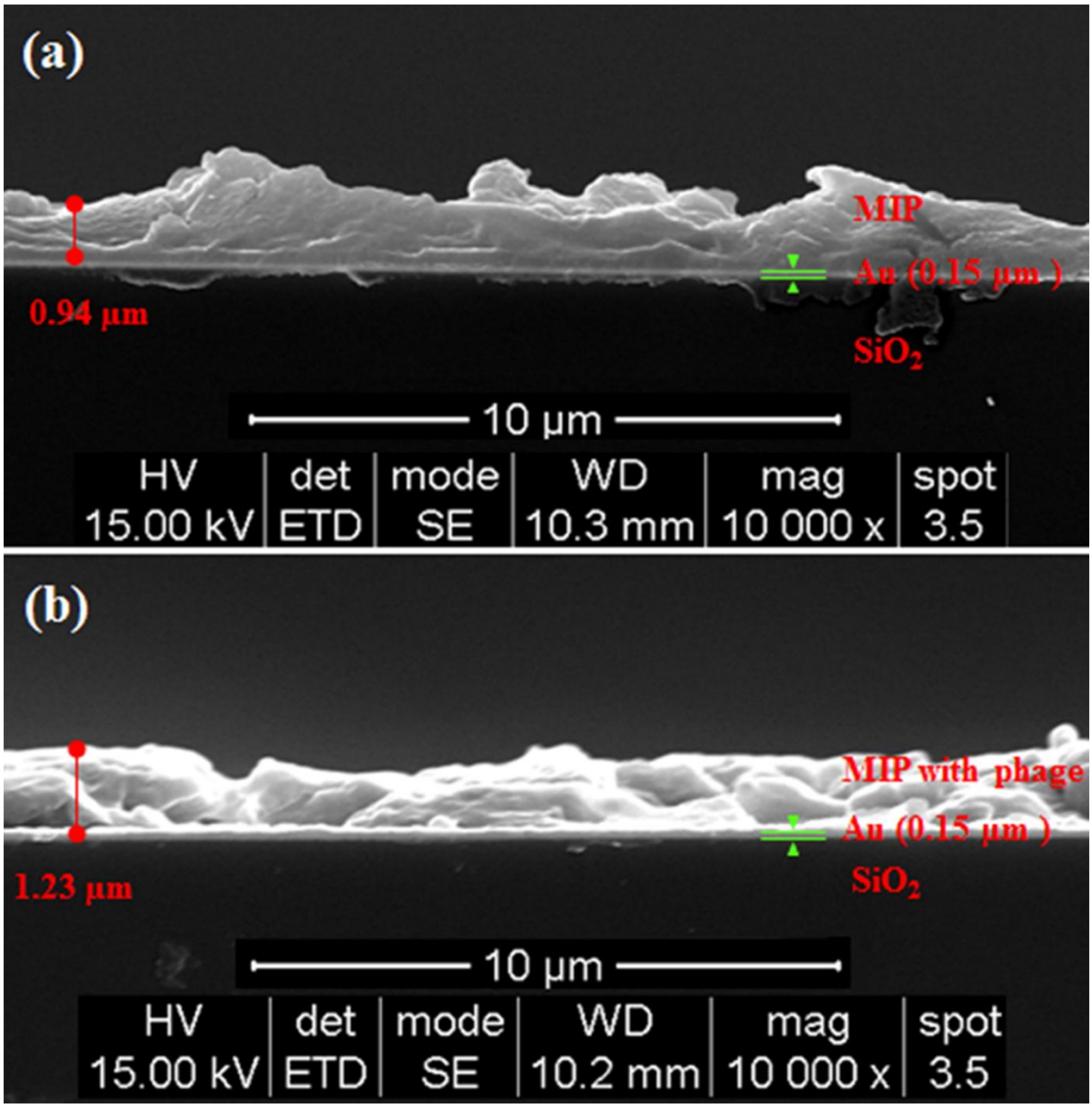

Figure S3. Comparison of thickness and roughness from MIP (a) and MIP wt-phage (b) by using FE-SEM.

Table S1. M13 filamentous bacteriophage protein information (accession number **NC_003287** from NCBI)

- Major coat protein (pVIII) – 1301 – 1522

MKKSLVLKASVAVATLVPMLSFAAEGDDPAKAAFNSLQASATEYIGYAW
AMVVVIVGATIGIKLFKKFTSKAS

- Minor coat protein (pIII) 1579–2853

MKKLLFAIPLVVPFYSHSAETVESCLAKPHTENSFTNVWKDDKTLDRYAN
YEGCLWNATGVVVCTGDETQCYGTWVPIGLAIPENEGGGSEGGGSEGGG
SEGGGTKPPEYGDPIPGYTYINPLDGTYPPGTEQNPANPNPSLEESQPLNTF
MFQNNRFRNRQGALTVYTGTVTQGTDPVKTYYQYTPVSSKAMYDAYWN
GKFDCAFHSGFNEDPFVCEYQGQSSDLPQPPVNAGGGSGGGSGGGSEGG
GSEGGGSEGGGSEGGGSGGGSGSGDFDYEKMANANKGAMTENADENAL
QSDAKKLDSVATDYGAAIDGFIGDVSGLANGNGATGDFAGSNSQMAQVG
DGDNSPLMNNFRQYLPSLPQSVECRPFVFSAGKPYEFSIDCDKINLFRGVF
AFLLYVAFMYVFSTFANILRNKES

- Minor coat protein (pVI) 2856 – 3194

MPVLLGIPLLLRFLGFLLVTLFGYLLTFLKKGFGKIAIAISLFLALIIGLNSIL
VGYLSDISAQLPSDFVQGVQLILPSNALPCFYVILSVKAAIFIFDVKQKIVS
YLDWDK

- Minor coat protein (pIX) 1206 – 1304

MSVLVYSFASFVLGWCLRSGITYFTRLMETSS

- Minor coat protein (pVII) 1108 – 1209

MEQVADFDTIYQAMIQISVVLCFALGIIAGGQR

Chapter 3

Publication 2 – Biomaterials

Title: Genetically Engineered Filamentous Bacteriophages Displaying TGF-β1 Promote Angiogenesis in 3D Microenvironments

This chapter introduces our approach to understanding the use of an angiogenic matrix utilizing bacteriophages as a potential alternative to traditional in vitro models. It was published in the Journal of Functional Biomaterials [90]. My contributions were to perform all experiments, analysis, visualization, and writing the first draft of the manuscript. The following sections are identical to the preprint version of the manuscript.

Genetically Engineered Filamentous Bacteriophages Displaying TGF-β1 Promote Angiogenesis in 3D Microenvironments

In-Hyuk Baek[1, 2], **Volkhard Helms**[2], **Youngjun Kim**[1,*]

[1] Environmental Safety Group, Korea Institute of Science & Technology Europe GmbH, Campus E71. 66123, Saarbrücken, Germany; baekja85@gmail.com
[2] Center for Bioinformatics, Saarland University, 66123, Saarbrücken, Germany; volkhard.helms@bioinformatik.uni-saarland.de
* Correspondence: youngjunkim@kist-europe.de; Tel.: +49-(0)681-9382-327

Abstract

Combined 3D cell culture in vitro assays with microenvironment-mimicking systems are effective for cell-based screening tests of drug and chemical toxicity. Filamentous bacteriophages have diverse applications in material science, drug delivery, tissue engineering, energy, and biosensor development. Specifically, genetically modified bacteriophages have the potential to deliver therapeutic molecules or genes to targeted tumor tissues. The engineered bacteriophages in this study significantly enhanced endothelial cell migration and tube formation within the extracellular matrix (ECM). Compared to TGF-β1 alone and non-modified phages, the presence of TGF-β1 on the bacteriophages demonstrated superior performance as a continuous stimulant in the microenvironment, effectively promoting these angiogenic processes. Assays, including RT-qPCR, ELISA, and fluorescence microscopy, confirmed the expression of angiogenic markers such as CD31, validating the formation of 3D angiogenic structures. Our findings indicate that the TGF-β1 displayed by bacteriophages likely acted as a chemotactic factor, promoting the migration, proliferation, and tube formation of endothelial cells (ECs) within the ECM. Although direct contact between ECs and bacteriophages was not explicitly confirmed, the observed effects strongly suggest that TGF-β1-RGD bacteriophages contributed to the stimulation of angiogenic processes. The formation of angiogenic structures by ECs in the ECM was confirmed as three-dimensional and regulated by the surface treatment of microfluidic channels. These results suggest that biocompatible TGF-β1-displaying bacteriophages could continuously stimulate the microenvironment in vitro for angiogenesis models. Furthermore, we demonstrated that these functionalized bacteriophages have the potential to be utilized as versatile

biomaterials in the field of biomedical engineering. Similar strategies could be applied to develop angiogenic matrices for tissue engineering in in vitro assays.

Keywords: filamentous bacteriophage; angiogenesis; HUVECs; bacteriophage display; lab-on-a-chip; ECM

1. Introduction

Vascular systems ensure a constant circulation of oxygen, nutrients, blood, and lymphocytes as the basis for the survival and homeostasis of the body [91]. They are composed of an intricate network of capillaries, veins, and vessels, all lined with a single layer of squamous endothelial cells (ECs).

These ECs exhibit a thick layer in a heterogeneous mixture of vessels [92]. Capillaries surrounding organs account for 95% of the adult blood vessels and must be considered when simulating the actual characteristics of human tissue in three-dimensional (3D) microenvironments [93]. In such circumstances, it is crucial to account for factors that induce cell morphogenesis, migration, angiogenesis, metastasis and differentiation [94].

In vitro microvessel environmental systems are mainly applied by an extracellular matrix (ECM) and ECs. Pre-clinical trial models based on animals and two-dimensional (2D) in vitro models have been dominant in the field of translational research despite their limitations. Unfortunately, the differences between human taxonomy and inaccurate simulations of 3D physiologies often lead to results vastly different from actual clinical trials. However, in recent years, significant efforts have been exerted to develop artificial chip-based 3D models using microsystem technology with microfluidic devices to overcome the abovementioned flaws and to closely mimic the physical environment [94, 95]. Recently, scaffolds with biological activity, such as bone morphogenic proteins (BMPs), have been utilized in tissue engineering. Additionally, various materials, including polymers, hydrogels, metals, ceramics, and bio-glass, are being explored for their potential applications in this field [96]. Microenvironmental systems mimicking functional tissue are recognized as 3D cell culture models, providing considerable advantages over well plate 2D cell culture approaches. Combining 3D cell culture in vitro assays with microenvironment-mimicking systems is effective for cell-based drug screening and the toxicity screening of chemicals to check for cell migration, angiogenesis, metastasis, and morphogenesis. The microfluidic platform has been used in many kinds of applications of 3D cell culture including 3D microvascular networks and the physiology of human lungs. The angiogenic structure of networks of ECs in hydrogel was confirmed as 3D and as regulated by the surface treatment of

microfluidic channels [95]. Angiogenesis plays a crucial role in wound healing and tumorigenesis [97, 98]. Tumorigenesis is mediated by TGF-β/Smads signaling, which involves vascular endothelial growth factor (VEGF), fibroblast growth factor-1 (FGF-1), platelet-derived growth factor (PDGF), and TGF-β1 [99]. TGF-β1 signaling has been shown to regulate angiogenic factors. TGF-β1 binds to TGF type I receptors and is activated by activin receptor-like kinase (ALK1) and/or activin receptor-like kinase 5 (ALK5). TGF-β1/ALK5 signaling regulates the expression of tumor promoting, suppressing, and angiogenesis genes via Smad2/3, Smad4, and FOXO1 [100, 101].

Filamentous bacteriophages (M13, F1, f88, and fd) are members of the Inoviridae family. Filamentous bacteriophages consist of five coat proteins, approximately 2700 copies of the major coat protein pVIII, and about 3–5 copies each of the minor coat proteins pVII, pIX, pVI, and pIII per phage [102]. The f88 phage consists of two pVIII genes in one bacteriophage genome [103]. The first major coat protein pVIII gene comprises about 2700 overlapping copies, while the second pVIII gene is randomly displayed on 10–100 copies per f88 phage [103]. Bacteriophages are being rapidly developed and utilized as functional biomaterials across various fields, including SARS-CoV-2 vaccines [104], molecularly imprinted polymers [44], lithium-ion batteries [105], SPR electrochemical biosensors [106], polyethyleneimine drug carriers , monoclonal antibody production (phage display libraries) [107], TLR9 signal pathway cancer therapy [108], and carbon nanofibers [40].

The advantages of bacteriophages are their ease of genetic engineering, resistance to environmental changes (temperature, pH), and biosafety for human use, as they exclusively infect bacteria. Clinical trials are currently exploring their potential in vaccines and immunotherapy [109-111]. The filamentous bacteriophage has a diameter of about 6.6 nm and a length of 100 nm [112], and is thereby larger than hydrogel pores which have a size of about 1–38 nm [113].

Our hypothesis is that, if the genetically modified filamentous bacteriophage encodes a growth factor and cell adhesion motif, this would not only support the ECM structure for the building block, but may also induce cell growth. In this study, we displayed TGF-β1 and the integrin-binding motif, RGD peptide, on the f88 bacteriophage. We confirmed the use of phages as an in vitro material to induce the migration and stability of ECs on a DAX-1 microfluidic chip.

2. *Materials and Methods*

2-1. Amplification and purification of phage

The f88 phage vector (kindly provided by Prof. Dr. Georg P Smith, University of Missouri, USA) was engineered to display a cyclic RGD peptide (CRGDGRC; Cys-Arg-Gly-Asp-Gly-Arg-Cys) on its pVIII major coat protein [102, 103]. To insert the cyclic RGD gene sequence into the phage genome, oligonucleotide hybridization was performed whereby oligonucleotide was mixed and complementary pairs were incubated for 10 min at 100 °C. Thereafter, the chamber was slowly cooled to 50 °Cover 90 min. AP-treated hybridization products were inserted into the f88 vector by *HindIII* and *KpnI* enzyme digestion followed by ligation. Active TGF-β1 (NCBI accession number: NM_000660, human TGF-β1 gene cDNA clone, Sino biological, Beijing, China) was displayed on the minor coat protein p3. TGF-β1 was cloned. The ligated vector was transferred into MC1061 *E. coli*-competent cells by electroporation (voltage: 2.5 kW; capacity: 25 μF; resistance: 200 Ω, Biorad Feldkirchen, Germany). Subsequent to confirming the DNA sequence by sequencing analyses (Eurofin MWG operon, Ebersberg, Germany), the genetically modified phage vector was transformed into K91BK *E. coli*-competent cells to amplify the phage particles. Phage purification was performed in 20% Polyethyleneglycol (mw 8000)/2.5 M sodium chloride solution after growing the transformed K91BK cells as previously described [75]. To induce overexpression of the second recombinant pVIII genes, we added 0.5 mM of IPTG 0.5 mL to the bacterial culture medium where a cyclic RGD peptide phage was produced as in previous research [114]. To ensure minimal PEG contamination, the final soluble phage solutions were dialyzed against MilliQ water overnight at 4 °C using D-Tube Dialyzer Maxi (Millipore, Massachusetts, USA) with a 6–8 kDa molecular weight cutoff [115].The final soluble phage supernatant was dialyzed against MilliQ water overnight to remove the remaining PEG. The concentration (colony-forming unit per milliliter, CFU/mL) of filamentous bacteriophages was determined by phage titration as previously described [44, 78]. Phage suspensions were stored at 4 °C. The primer sequences used are listed in Table A1.

2-2. Enzyme-linked immunosorbant assay (ELISA)

The concentration of TGF-β1-displaying phage was investigated with ELISA. We serially diluted with phage (10^{12}–10^{8} cfu mL^{-1}) or TGF-β1 (10^{1}–10^{-3} ng ml^{-1}) solutions in a coating buffer (0.1 M Na_2CO_3, 0.1 M $NaHCO_3$, pH 9.4) and coated in a 96-well ELISA plate (Thermo Scientific, Massachusetts, USA) overnight at 4 °C. Afterward, the solution was washed three times with 200 μL of PBS containing 0.05% Tween20 (PBS-T). The plates were blocked in 2% (*w*/*v*) bovine serum albumin (BSA) (Sigma Aldrich, Baden-Württemberg, Germany) in PBS-T for 2 h at room temperature. The anti-TGF-β1 rabbit monoclonal antibody (diluted 1:1000, Abcam, Cambridge, UK) was incubated with 1% BSA in PBS-T

for 1 h at 37 °C. After washing three times with PBS-T, the secondary antibody of 100 μL of peroxidase-conjugated (HRP) goat anti-rabbit IgG (diluted 1:20,000 in PBS-T containing 1% BSA, Abcam, Cambridge, UK) was added to each well and incubated for 1 h at 37 °C. After three rounds of washing, the plates were developed in ortho-phenylenediamine (Sigma Aldrich, St. Louis, MO, USA) for 5 min. The reaction was stopped by adding 50 μL of 1M H_2SO_4 per well. We measured the HRP substrate on a microplate reader (SPECTRA Rainbow, Tecan, Männedorf, Switzerland) at OD_{492} nm. As a negative control, we used non-genetically modified f88 bacteriophage.

2-3. Fluorescence assay

To test the release of growth factor, we prepared a collagen type I gel (5 mg/mL, Ibidi, Gräfelfing, Germany). The collagen was diluted with DI water, endothelial cell growth medium (Promocell, Heidelberg, Germany), 1N NaOH, $NaHCO_3$, bacteriophage (10^{11} cfu ml^{-1}), and/or TGF-β1 (1 ng ml^{-1}) to achieve a final concentration of 2 mg/mL with a pH of 7.4. The gel was filled (100 μL into each well) into the wells of a black 96-well microplate (Greiner Bio-One, Frickenhausen, Germany). Then, it was incubated in a humid chamber at 37 °C for 30 min. After gelation, we added 100 μL of growth-factor-free HUVEC growth media into each well. All media were changed daily. After 4 days, the collagen type I gels with TGF-β1-displaying phages and/or TGF-β1 were fixed with 4% paraformaldehyde (PFA, Sigma Aldrich) for 15 min at room temperature. Then, we blocked these with 2% BSA in PBS overnight at 4 °C. The fixed hydrogels were treated with anti-TGF-β1 rabbit monoclonal antibody (diluted 1:500) for 1 h. After washing three times with PBS, 100 μL of Alexa Fluor® 488 conjugated goat anti-rabbit IgG (Abcam, Cambridge, UK) diluted 1:200 in PBS-T containing 1% BSA (Sigma Aldrich, Baden-Württemberg, Germany) was added to each well and incubated for 1 h at 37 °C. We measured fluorescence intensity on a modulus microplate multimode reader (Promega, Mannheim, Germany) at room temperature and an excitation wavelength of 490 nm and emission wavelengths of 510–570 nm, respectively.

2-4. Cell culture

Human umbilical vein endothelial cells (HUVECs, Promocell, Heidelberg, Germany) were grown in endothelial cell growth medium containing 2% fetal calf serum (FCS; Promocell, Heidelberg, Germany) at 37 °C in the presence of 5% CO_2. The cellular density and viability of HUVECs were maintained by microscopic observations and using a hemocytometer after trypan blue staining. The HUVECs were used in passages 4–6.

2-5. Biocompatibility test

To identify biocompatibility, we measured cell viability by using WST-1 assays which detected the residual mitochondrial activities of HUVECs at 24 h, 48 h, 72 h, and 96 h. Briefly, 1×10^4 of HUVECs were seeded in a 96-microwell plate (Thermo Scientific, Massachusetts, USA). After attaching the HUVECs, 10^{11} cfu ml^{-1} of TGF-β1-displaying bacteriophages or 10^{11} cfu ml^{-1} of f88 bacteriophages or 1 ng ml^{-1} of TGF-β1 were added to the wells of a 96-well microwell plate (Thermo Scientific, Massachusetts, USA) at 37 °C in the presence of 5% CO_2. An amount of 10 μL of the WST-1 reagent was added to each well and monitored over 1 h on a microplate reader at OD_{440} nm. After measuring the HUVECs, we washed them three times with endothelial cell growth medium and continued the culture until the 96 h point.

2-6. Tube formation assay

To identify the cell and growth factor effects, we tested tube formation in the cells cultured on a matrigel matrix (Corning, New York, USA). Briefly, 50 μL of matrigel per well was added to the FC black 96-well imaging plate (Mobitec, Goettingen, Germany). Then, the imaging plate was incubated in a humid chamber at 37 °C for 30 min. After gelation, we added 100 μL of 15,000 HUVECs with TGF-β1-displaying bacteriophages (10^{11} cfu ml^{-1}) or bacteriophages (10^{11} cfu ml^{-1}) or TGF-β1 (1 ng ml^{-1}) to each well. The plate was incubated for 16 h. Next, the matrigel and cells were fixed with 4% paraformaldehyde for 15 min at room temperature. After fixation, we blocked them with 2% BSA in PBS overnight at 4 °C. For immunofluorescence analysis, the cell nuclei were stained with 4′,6-diamidino-2-phenylindole (DAPI; Sigma-Aldrich Baden-Württemberg, Germany) and then observed under a confocal microscope (LSM 900, Carl Zeiss, Oberkochen, Germany).

2-7. Lap-on-a-chip migration assay

The cell migration was studied in a Lap-on-a-chip (DAX-1, 3D cell culture chip, Singapore). The hydrogel channels of a collagen type I gel were loaded either with 10^{11} cfu ml^{-1} of TGF-β1-displaying bacteriophages or the 10^{11} cfu ml^{-1} of f88 bacteriophages or 1 ng ml^{-1} of TGF-β1. The 3D cell culture chip was incubated at 37 °C in the presence of 5% CO_2 for 30 min. After gelation, all channels were activated by adding endothelial cell growth medium for 30 min. Subsequently, one channel was seeded with 2×10^6 HUVECs. The media were changed every 12 h. For immunostaining, we used the three dyes DAPI, CD 31 mouse monoclonal antibody (1:1600, Cell Signaling Technology, Massachusetts, USA), and VE-Cadherin (1:400, Cell signaling Technology) and observed them under a confocal microscope.

2-8. RT-qPCR

To identify gene expression patterns, HUVECs were cultured with 10^{11} cfu ml^{-1} of TGF-β1-displaying bacteriophages or 10^{11} cfu ml^{-1} of f88 bacteriophages or 1 ng ml^{-1} of TGF-β1 for 4 days. The phage-free media were changed every 12 h. After 4 days, the cells were harvested by using trypsin-EDTA (0.25%, Thermo Fisher scientific, Maryland, USA). Total RNA extraction from the harvested cells was performed by using Trizol (Gibco BRL, Grand Island, NY, USA) according to the manufacturer's instructions. The concentration of total RNA was measured by the Nano drop (Thermo Fisher scientific). cDNA synthesis was performed by a high-capacity RNA to cDNA kit (applied biosystems, Thermoscientific). Primer- and fluorescent dye-labeled TaqMan MGB probes were designed based on gene bank sequences for CD31 (accession number M37780), VE-cadherin (accession number U84722), and GAPDH (accession number NM_002046) by using the PRIMER EXPRESS 3.0 program (Applied Biosystems, Foster City, CA, USA). The real-time PCR was carried out with one cycle of pre-denaturation at 94 °C for 5 min, followed by 40 cycles of amplification with denaturation for 30 s at 94 °C, annealing for 30 s at 60 °C, extension for 30 s at 72 °C, and a final 10 min extension at 72 °C in a 7500 fast real-time PCR system (Applied Biosystems, Foster City, CA, USA).

2-9. Statistical analysis

All the data were analyzed using the software SigmaPlot 12.0 (SigmaPlot Software, La Jolla, CA, USA). The quantitative data are expressed as mean ± standard error of the mean (SEM). From Figure 1 to Figure 5, statistical significance was analyzed by using the Kruskal–Wallis and Mann–Whitney tests, where differences were considered statistically significant at a p-value < 0.05. While all experiments were performed in triplicate, only the data presented in Figure 6 yielded statistically significant results. Statistical analyses were conducted for the other figures and tables; however, the results did not pass the significance threshold (p-value ≥ 0.05). Consequently, these data are presented as trends, reflecting the experimental outcomes as observed without statistical significance.

3. Results

As shown in Figure 1, we confirmed the induction of an invasion of ECs due to genetically engineered bacteriophages using a DAX-1 microfluidics chip. We constructed filamentous bacteriophages based on f88 phages that express

recombinant human TGF-β1 cloned into the major coat protein pIII and the cell adhesion motif (cysteine mediate RGD peptide) cloned into the major coat protein pVIII (Figure 1a). The f88 phages sparsely displayed the major coat protein which carried 10 to 100 copies of recombinant pVIII proteins. The filamentous bacteriophage vectors were provided by the Smith group (Prof. Dr. Georg P Smith, University of Missouri, USA). We used the DAX-1 microfluidic chips which commercialized 3D multicellular cell culture. DAX-1 comprises three multichannels which provide one polymerizable gel and two of medium channels (Figure 1b). As shown in Figure 1c–e, we seeded the hydrogel, bacteriophages, and HUVECs in the channels. After seeding, we monitored the HUVEC invasion of microfluidic chips (Figure 1f).

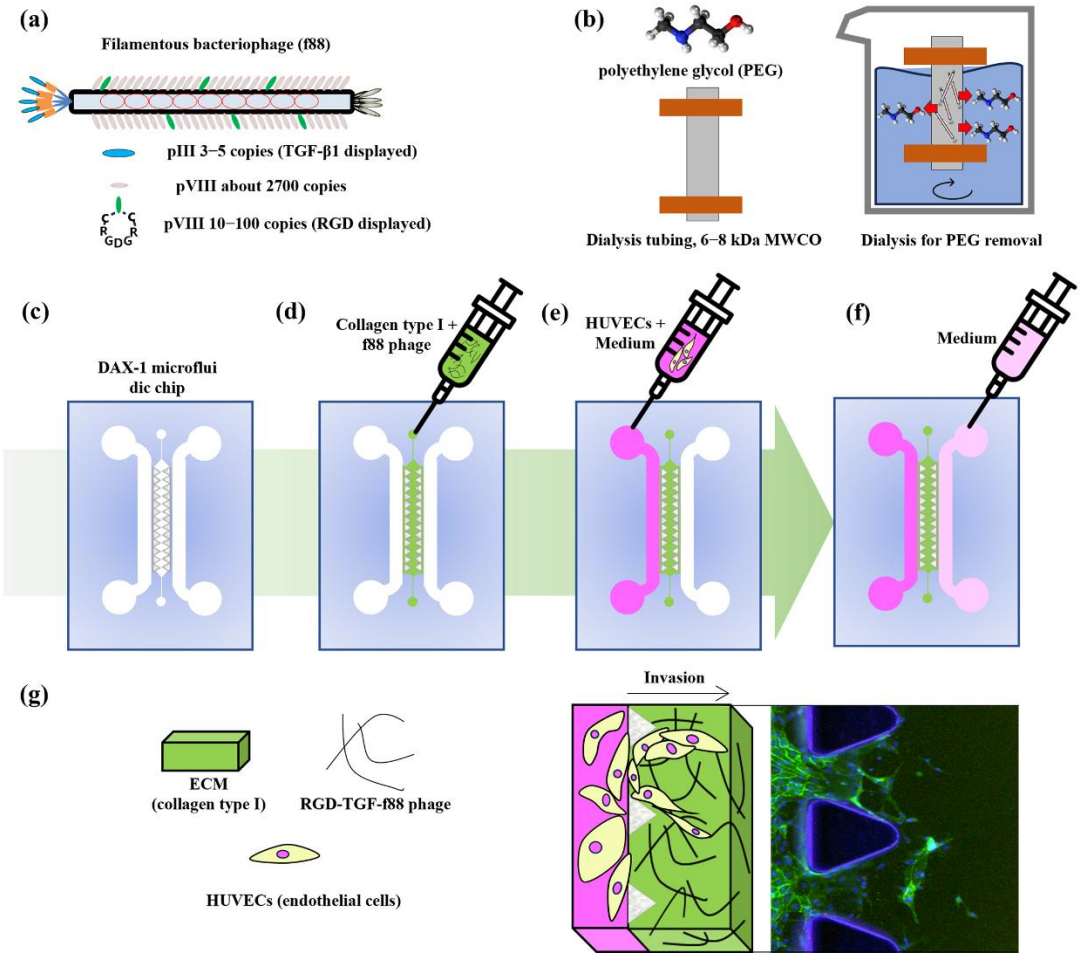

Figure 1. Schematic illustration of the construction of the functional filamentous bacteriophages and cell seeding and cell culturing in microfluidic chips. (**a**) The structure of the functionalized genetically engineered site of the filamentous bacteriophages. (**b**) Dialysis for removal of contaminants and unbound PEG from the bacteriophage elution solution. (**c**) The microfluidics chip of DAX-1. (**d**) The polymerization of the type I hydrogel and bacteriophages at the gel channel. (**e**)

The seeding of cells with medium at the left medium channel. (**f**) The filling of the medium at the right medium channel. (**g**) The monitoring of the HUVEC invasion during TGF-b1 interaction with cells in a microfluidics chip.

3-1. ELISA results

To test the relative amount of the TGF-β1 recombinant at the pIII minor coat proteins, we performed the enzyme-linked immunosorbent assay (ELISA). In Figure 2, absorbance intensity represents the TGF-β1 proteins that validate the quantification of the protein on 96-well plate surfaces. We calculated the relative amount of TGF-β1 between the displayed phages and proteins by setting the wild-type f88 filamentous bacteriophage as the control. In order to optimize the relative concentration of RGD-TGF-β1 bacteriophages, we plotted the logistic regression model in Table 1. As shown in Figure 2 and Table 1, the fitted ELISA curves had high regression coefficients (r2) which ranged from 0.9974 to 0.999, and their ANOVA p-values were smaller than 0.0026.

Logistic (L): Ai (absorbance intensity) = $\alpha/1 + (c/\gamma)\hat{}\beta$

As shown in Figure 2, regression curves between TGF-β1 and the RGD-TGF-β1 phage had one crossing point at a 0.25 absorbance intensity. TGF-β1 exhibited an absorbance intensity of 0.2482 ± 0.0347 at a concentration of 1 ng ml−1. The RGD-TGF-β1 phage had a concentration of 0.2407 ± 0.0306 at a 1011 pfu/mL concentration.

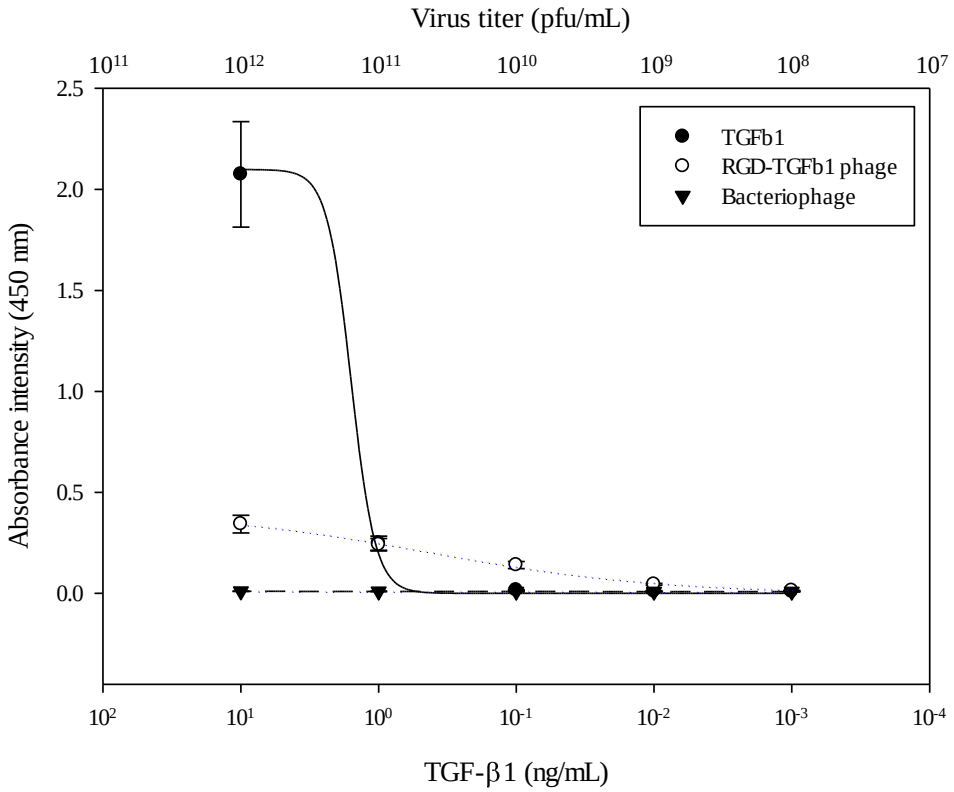

Figure 2. The evaluation of the TGF-β1 proteins on genetically modified bacteriophages by ELISA. Data are presented as mean ± SEM.

Table 1. Parameters of the logistic models for TGF-β1, RGD-TGFβ1 phage, and bacteriophage.

Materials	r2	Logistic model parameters		
		Height	slope	Slop at max 50%
TGF β1	0.9987	2.0984	-4.9648	1.5817
RGD-TGFβ1 phage	0.9974	0.4074	-0.5181	0.4317
Bacteriophage	0.9999	0.0166	-0.0395	0.0012

3-2. Fluorescence results

As shown in Figure 3, a collagen type I gel with embedded growth factors was confirmed by immunostaining the fluorescence-labeled TGF-β1 proteins. We hypothesized that macromolecules of the RGD-TGF-β1 are displayed on the bacteriophages. The TGF-β1-sensitive fluorescence intensities were measured on day 0 as being $2.9 \times 10^3 \pm 3.2 \times 10^1$ of 1 ng of TGF-β1 and $3.4 \times 10^3 \pm 2.8 \times 10^2$ of 1011 pfu mL^{-1} of RGD-TGF-β1 phages, and on day 4 as being $2.5 \times 10^3 \pm 3.1 \times 10^2$ of TGF-β1 and $3.4 \times 10^3 \pm 1.5 \times 10^2$ of RGD-TGF-β1 phages. The results show that the macromolecules of the filamentous bacteriophages remained in a collagen matrix. However, the native TGF-β1 proteins were transferred into the medium. In general, the cell culture medium was replaced every 2–3 days. Some of the cells require a growth factor when cultivated. In particular, if we create a 3D microenvironment with hydrogels, we validate that the growth factors have integrated into the hydrogels and track the mode of action to the effects on the cells. However, suppose the RGD-TGF-β1 filamentous bacteriophages existed in the collagen matrix. In that case, the displayed growth factor can affect cellular growth for a long-term cell culture because the RGD-TGF-β1 bacteriophages are larger in size than the hydrogel pores [112, 113]. This observation suggests that bacteriophages can probably be used in long-term cell culture systems.

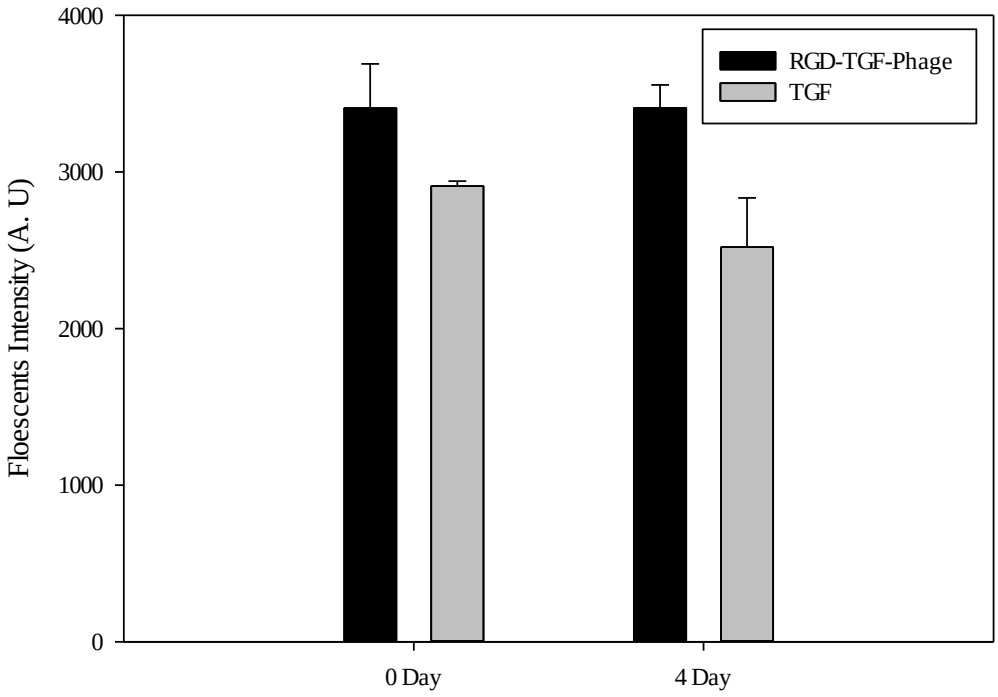

Figure 3. The fluorescence intensity profiles of phages and growth factor in the type I collagen (Days 0 and 4). Data are presented as mean ± SEM.

3-3. Viability test

Next, we characterized the cell viability against genetically modified filamentous bacteriophages. HUVECs were seeded onto a 96-well plate at concentrations of 2×10^4 cells.cm^{-3}. After 24 h, we assessed the presence of growth factors and/or bacteriophages on a culturing plate. After 72 h of culture, we evaluated mitochondrial activities by WST-1 assay. For comparison of cell growth properties, we selected FBS including growth medium as the positive control and FBS without additional growth reagents as a negative control. As shown in Figure 4, the resulting viabilities are 140% for the TGF-β1-treated positive controls, 169% for the TGF-β1-displaying bacteriophages, 103% for the natural bacteriophages, and 4% for the negative control after 72 h of culture. This experiment confirmed that ECs grew faster when TGF-β1 was added than without TGF-β1 in the medium. Additionally, this shows that filamentous bacteriophages did not exhibit an adverse effect on the cell viabilities. Therefore, this observation suggests that endothelial cell cultures could be co-cultivated with filamentous bacteriophages over 4 days of culture.

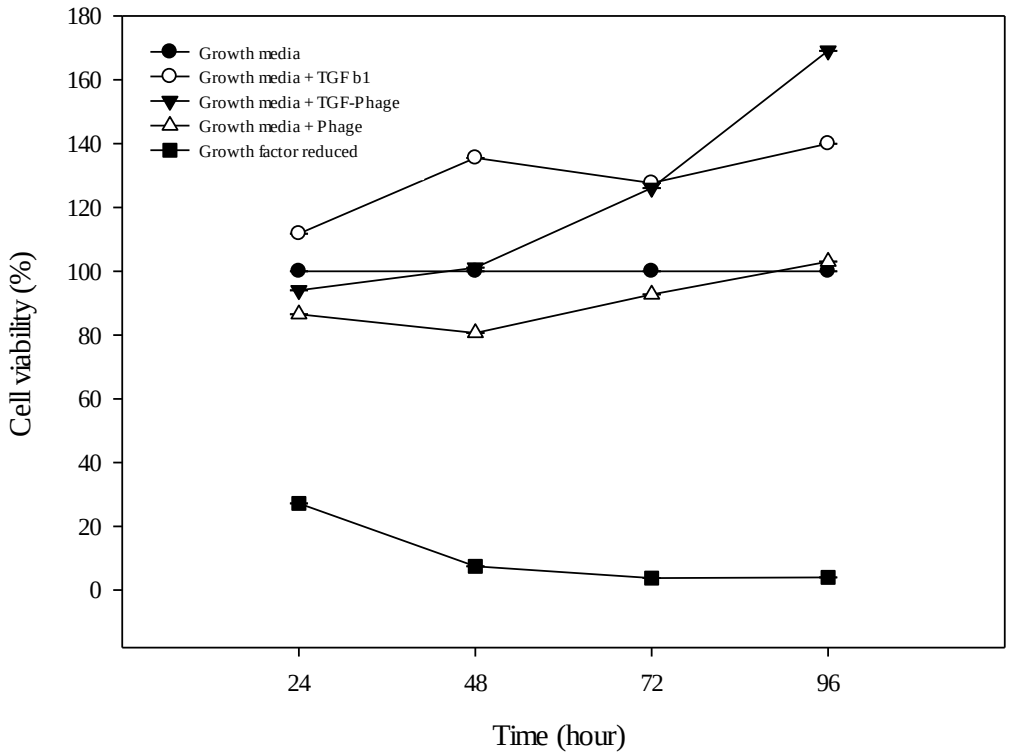

Figure 4. The proliferation of HUVECs, cultured with bacteriophages (Days 0, 1, 3, and 4), was determined by a CCK-8 cell proliferation assay. Data are presented as mean ± SEM.

3-4. Tube Formation of ECs

To define the network pattern of competitive ECs, we performed a tube formation assay on matrigel. Figure 5 shows that, according to growth factor and/or bacteriophage treatment conditions, either pseudo-capillary growth and/or branched points were observed. The pseudo-capillary growth and branched points in Figure 5e,f were evaluated by using the software ImageJ version 1.54 [7]. The RGD-TGF-β1 bacteriophages generated 5.40 ± 0.29 mm of total capillary extension and 14.7 ± 0.58 branch points (Figure 5d). In comparison, the positive control of TGF-β1 growth factor generated 5.14 ± 0.31 mm of total capillary extension and 13.67 ± 1.53 branch points (Figure 5b), whereas the negative control of the growth factor had a reduced total length of 4.05 ± 0.54 mm with 9.0 ± 1.73 branch points. Hence, this analysis showed that TGF-β1 growth factor induced an enhanced extension of pseudo-capillary ECs. Interestingly, non-displaying bacteriophages were weakly stimulated and induced tube formation with a total length of 4.96 ± 0.33 mm, and 11.33 ± 1.53 branch points in

comparison with the negative control of Figure 5a. As shown in Figure 4, the RGD-TGF-β1 bacteriophage was found to be safe and growth-supporting. Furthermore, Figure 5 shows the efficacy of the bacteriophage in tube formation. In summary, these data confirm that RGD-TGF-β1 bacteriophages can be used as a biomaterial to induce a microvessel formation model using ECs during the construction of a microenvironment.

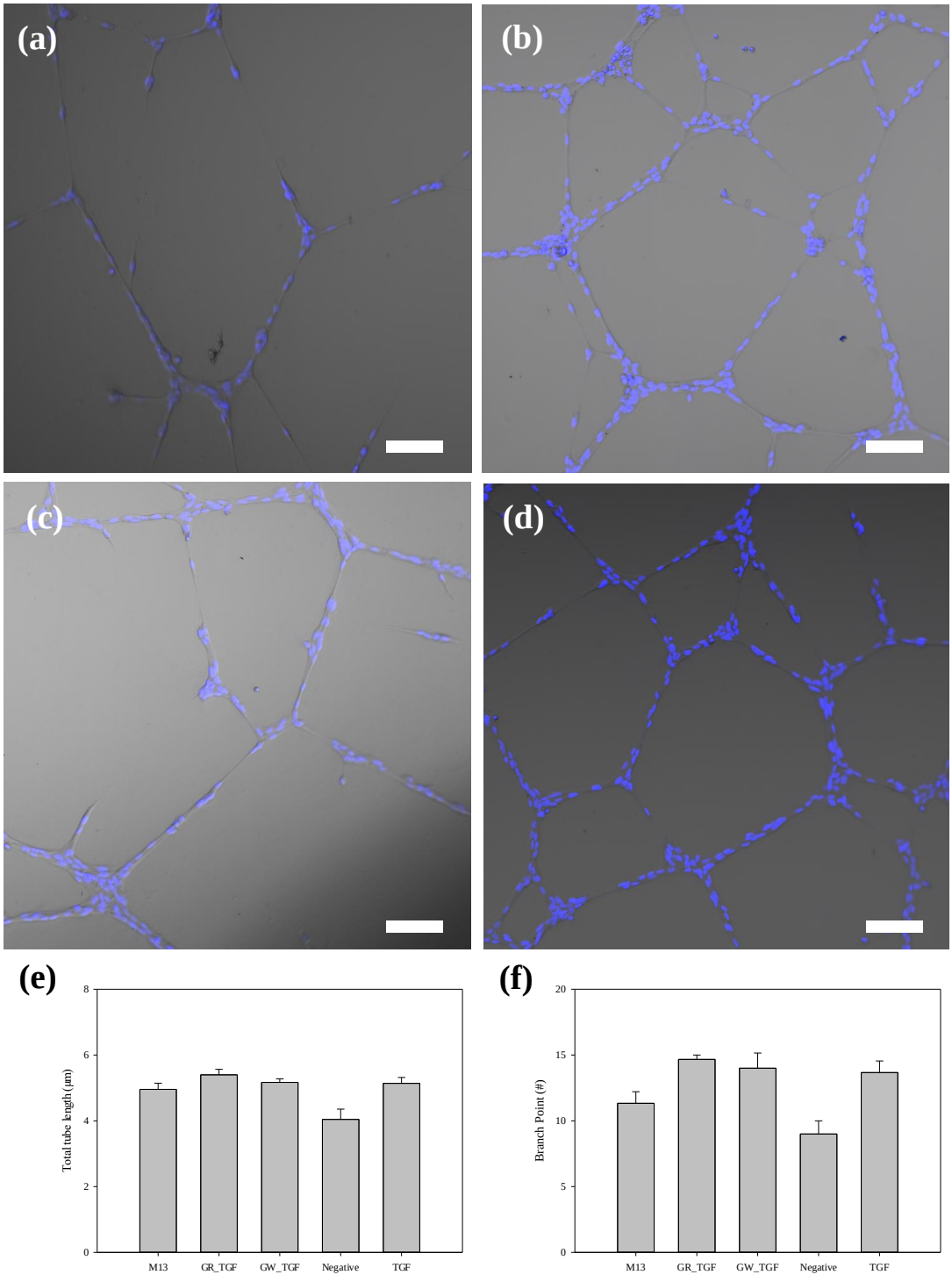

Figure 5. Tube formation of HUVECs on matrigel after 24 h of seeding; (**a**) negative control; (**b**) TGF-β1, 1 ng ml^{-1}; (**c**) f88, 1 × 10^{11} cfu ml^{-1}; (**d**) RGD-TGF phage, 1 × 10^{11} cfu ml^{-1}. The image analysis was carried out with the angiogenesis analyzer module of ImageJ; (**e**,**f**) show the total tube length (**e**) and the number of branch points (**f**). The scale bar in (**a**–**d**) is 100 μm (40× magnification). Data are presented as mean ± SEM.

3-5. Migration test on a microfluidics chip

We used the DAX-1 microfluidics chip designed by AIM biotech to generate a migration microenvironment. It has three channels in total, two channels for cell and/or media and one central gel channel. We generated the hydrogel of collagen type I in a gel channel and seeded the ECs in a media channel. As shown in Figure 6, the ECs showed migration effects into the hydrogel. The average migration length was determined as 200.84 ± 76.29 μm for the group treated with RGD-TGF bacteriophages and 149.98 ± 75.82 μm for the group directly induced by TGF-β1 growth factor. In comparison, the native filamentous bacteriophages used as a negative control showed only a 74.61 μm migration length. We stained two endothelial cell biomarkers and the nucleus with CD31 (green), VE-cadherin (red), and DAPI (blue; nucleus). The results showed a strong CD31 expression. However, the cell-to-cell adhesion junction of VE-cadherin (CD144) was not detected in ECs in Figure 6a–d. To quantify expression, we tested the mRNA levels of CD31, VE-cadherin, and the housekeeping gene GAPDH by TaqMan qRT-PCR. As shown in Figure 6f, the CD31 mRNA levels increased five-fold when TGF-β1 growth factor was induced. However, VE-cadherin expression was not detected at the mRNA level when induced by TGF-β1 growth factor. These results show that the mRNA level of CD31 from qPCR was correlated with the results from the confocal microscope. In general, while HUVECs upregulated VE-cadherin, Ando et al. and Kocherova et al. showed that shearing stress and/or medium condition can reduce the level of VE-cadherin [116, 117]. Interestingly, the tube formation and the number of branch points tended to increase compared to the negative control in the natural f88 page used as the control of the bacteriophage, and similar results were obtained in the fluidics chip as shown in Figures 5c and 6c. This proves that the linear structural characteristics of bacteriophage affected endothelial cell migration.

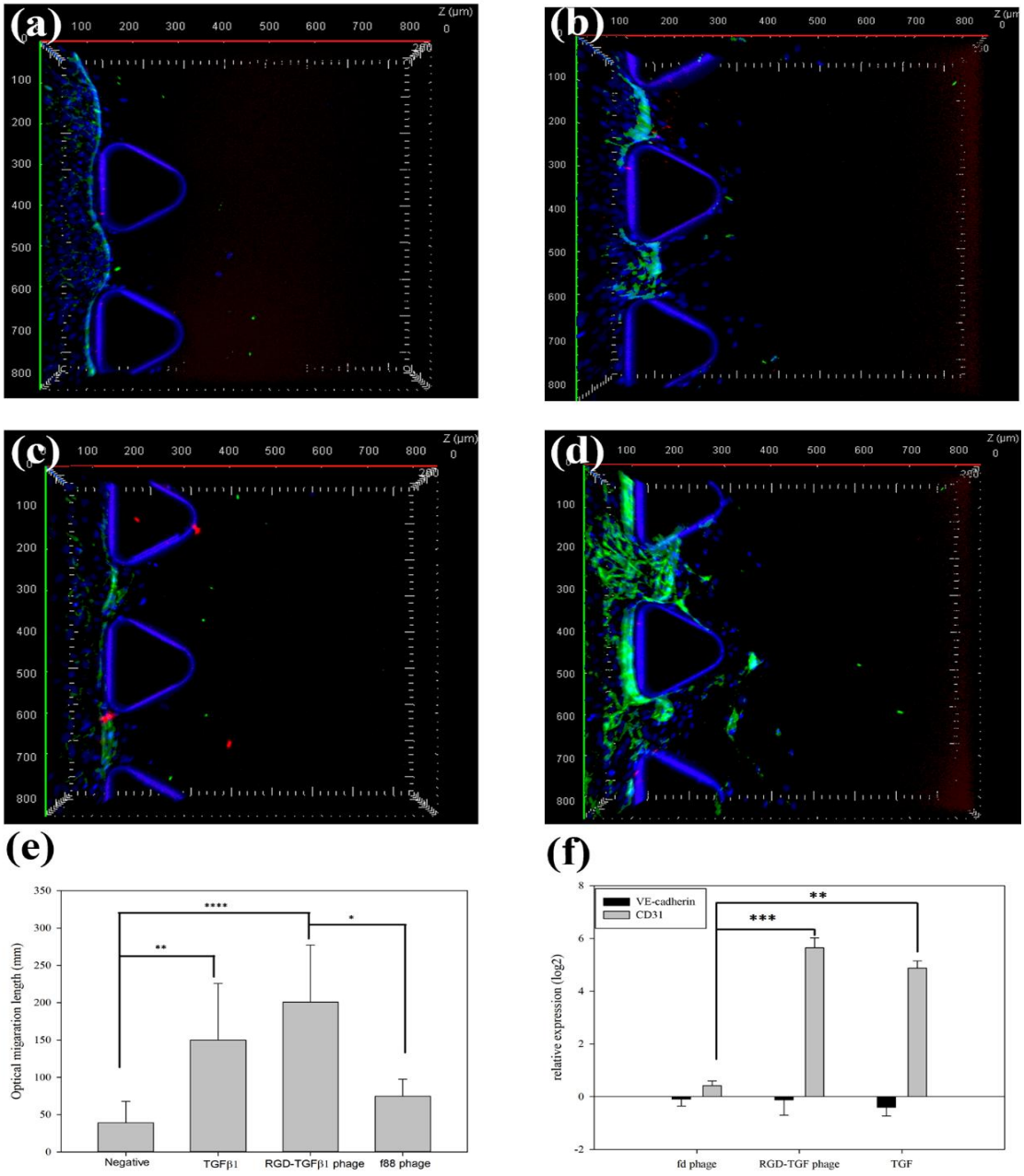

Figure 6. The observation of angiogenesis on a vascular-on-a-chip after 4 days of treatment. The conditions are as follows: (**a**) growth media control, (**b**) TGF-β1 (1 ng/mL), (**c**) f88 phage (1×10^{11} cfu/mL), and (**d**) RGD-TGF phage (1×10^{11} cfu/mL). (**e**) The quantification of the optical migration length (mm) and (**f**) mRNA expression levels of CD31 and VE-cadherin, measured by real-time PCR. Data are presented as mean ± SEM. Statistical analysis was performed using the Kruskal–Wallis test with a confidence interval of $p < 0.04$ ($n = 6$). Significant differences are indicated by p-values of <0.05 (*), <0.01 (**), <0.001 (***), <0.0001 (****), respectively.

4. Discussion

According to the 3R principles (replacement, reduction, and improvement), it is generally desirable to replace animal testing by alternative non-animal testing methods. As alternative testing methods, 3D cell culture, organoid, and lab-on-a-chip methods are being developed. In this study, we verified the function and effectiveness of genetically modified filamentous bacteriophages as safe in vitro models in tissue engineering. We showed that the genetically manipulated phages can sustainably support the growth of cells in a long-term culture. Three-dimensional cell culture is a technology used to mimic organ and tissue culture. During long-term 3D cell culture, there is often a lack of proper circulation of nutrients and oxygen, so that the inner cells may turn necrotic. Thus, we utilized a lab-on-a-chip platform that facilitates convenient media exchange, allowing for better control of oxygen levels [118]. To overcome this problem, previous studies modifying the ECM, cells, and media have been reported [119, 120]. Furthermore, our results suggest that TGF-β1 displayed by bacteriophages functions as a chemotactic factor, promoting endothelial cell migration and angiogenesis. Although we did not directly observe a physical interaction between the ECs and the bacteriophages, the increase in cell migration and tube formation observed is consistent with the known roles of TGF-β1 in stimulating chemotactic responses, as evidenced by CD31 expression in ECs. This effect may further enhance cell adhesion and migration in the presence of RGD. We believe that our study is closely related to concepts modifying the ECM, and provides additional functionality as a support for cell culture. This study confirmed the safety and long-term effectiveness of the potential materials. We did not observe abnormalities in the cells. Bacteriophage is a material that proves biosafety and is currently undergoing phase 2 clinical trials [121]. Using bacteriophages emphasizes safety when used as materials; although, the simple, functional increases are also substantial. Additionally, we employed bacteriophages ranging from 6.6 nm to 100 nm in size, which are larger than the hydrogel pore sizes (1–38 nm), to enhance interaction with the ECM. Our study demonstrated that TGF-β1 displayed by the bacteriophages promoted angiogenesis and endothelial cell (EC) tube formation, validating their role in enhancing vascular formation. However, further research is needed to fully understand the potential of bacteriophages as ECM biomaterials and their long-term effects on angiogenesis. Moreover, our results suggest that TGF-β1 displayed by bacteriophages serves as a chemotactic factor, enhancing endothelial cell migration and promoting angiogenesis. Although we did not directly observe a physical interaction between ECs and the bacteriophages, the increase in cell migration and tube formation aligns with TGF-β1's role in stimulating chemotactic responses, as evidenced by CD31 expression in ECs as previously

described [122]. This effect could potentially enhance cell adhesion and migration, particularly in the presence of RGD. One of the greatest challenges in tissue engineering is achieving long-term cell culture viability by mimicking the oxygen and nutrient delivery systems found in vivo [118]. By utilizing genetically modified filamentous bacteriophages, we demonstrate a promising alternative that not only supports cell migration but also supports growth factor in long-term cultures of 3D cell culture systems. The growth factor-displaying bacteriophages enhance angiogenesis and endothelial cell migration, key components of vascularization. Compared to traditional cell culture, bacteriophages offer a level of biosafety and adjustability that makes them ideal for use in scaffolds [123]. Despite these findings, the risk of endotoxin contamination must be carefully addressed in future studies, as highlighted by previous research [124, 125]. Effective control of endotoxin mechanisms will be crucial to ensure the safety and reproducibility of bacteriophage-based biomedical applications.

One key step in cancer metastasis is that tumor cells penetrate into tissues and induce angiogenesis. Both stages are regulated by the interaction between the tumor microenvironment and cell-to-cell interaction [126, 127]. When trying to mimic this microenvironment in an in vitro system, it is important to supply nutrients and growth factors. We would like to reduce the gap to in vivo cancer metastasis conditions by using a microfluidic platform to mimic the tumor microenvironment and cell-to-cell interaction in vitro. In fact, microfluidics platforms have been developed previously to mimic angiogenesis and organ-on-chip implementation [128-130]. Three essential components are required for the implementation of 3D cell culture. One needs the cells to be implemented, the supports to support them, and the necessary nutrients so that the cells grow and function properly. Many studies are ongoing and attempts are being made to create an organ-like environment. In line with these studies, we propose a new material that can provide a continuous inflow of nutrients using genetically modified filamentous bacteriophages that display growth factors and increase the permeability of ECM to help with long-term incubation. We advocate the possibility of using bacteriophage displays as a safe material to independently monitor biochemistry and components to study cell-to-cell interactions. In our previous work, we reported on the use of VEGF-A bacteriophages in microfluidic chips [123]. With the continuous supply of VEGF-A and TGF-b1 growth factors and induction of vascular production, an organ-on-a-chip will be constructed by building a cancer metastasis model on the microfluidics chip through co-culture with the organ-specific cells. Additionally, Doub et al. have reported that the use of bacteriophages can lead to endotoxin contamination and the formation of bacterial biofilms [124, 125]. Despite these findings, the risk of endotoxin

contamination must be carefully addressed in future studies, as highlighted by previous research [124, 125]. Effective control of endotoxin mechanisms will be crucial to ensure the safety and reproducibility of bacteriophage-based biomedical applications. Thus, to better understand the efficacy of bacteriophages, it is crucial to implement controls for endotoxin and bacterial enzyme contamination in future studies. In the future, we plan to implement a platform that can assess the effectiveness of in vitro drugs, which has only been found in animals through our research.

5. Conclusions

This study investigated the potential use of an angiogenic matrix in tissue engineering as an alternative to conventional in vitro models. The researchers observed that ECs established connections with biocompatible bacteriophages, which were able to migrate and sprout into the ECM. The findings indicated that bacteriophages displaying biocompatible TGF-β1 could contribute to the continuous stimulation of the microenvironment, promoting angiogenesis in in vitro models. Furthermore, the researchers suggested that these functionalized bacteriophages could serve as a viable biomaterial in biomedical engineering. The study demonstrated that growth factor-displaying filamentous bacteriophages could be utilized not only for long-term cell culture, providing biocompatible and continuously effective materials, but also in other biomedical engineering applications such as 3D cell culture and organoid culture. Our results propose that similar strategies could be employed in the future to enhance angiogenic matrixes in tissue engineering assays.

6. Author Contributions:

Baek, I.-H.: Formal analysis, Visualization, Writing –original draft. Helms, V.: Writing- review and editing. Baek, I..: Investigation, Software, Writing – review and editing. Kim, Y: Conceptualization, Validation, Writing – review & editing. All authors have read and agreed to the published version of the manuscript.

7. Acknowledgments

We gratefully thank Dr. Choi Soo choel (a dispatch employee from Jeonbuk state) for his assistance in the laboratory and with the revised manuscript. This

research was supported by the Bio-cluster Industry Capacity Enhancement Project of Jeonbuk Technopark (JBTP).

Suppl. table 1 Primer sequences used.

Primer sequence (5′ – 3′)	
HindIII_RGDGR_KpnI_F#	AGC TTT TGT AGG GGT GAC GGT AGG TGC GGT AC
HindIII_RGDGR_KpnI_R#	CGC ACC TAC CGT CAC CCC TAC AAA
SfiI_TGFbeta1 F#	GGC CCA GCC GGC CAT GGC CCT GGA CAC
TGFbeta1_Not I R#	TGC GGC CGC GCT GCA CTT GCA GGA G
VE cadherin F#	TGT GGG CTC TCT GTT TGT TGA G
VE cadherin R#	CTT CAT CGT CGA GGC CAC A
VE cadherin Probe	CGA GGG CAT CAT CA
CD31 F#	AAC AGT GTT GAC ATG AAG AGC CTG
CD31 R#	AAG GAT GAC GTG CTG TTT TAC AAC
CD31 Probe	CGG ATG TCA GCA CCA C
GAPDH F#	CGA GCC ACA TCG CTC AGA C
GAPDH R#	CGT ATT GGG CGC CTG GT
GAPDH Probe	CGG AGT CAA CGG ATT T

8. References

1. Abbott, A. 2003. 'Cell culture: biology's new dimension', *Nature*, 424: 870-2.
2. Alfaleh, M. A., H. O. Alsaab, A. B. Mahmoud, A. A. Alkayyal, M. L. Jones, S. M. Mahler, and A. M. Hashem. 2020. 'Phage Display Derived Monoclonal Antibodies: From Bench to Bedside', *Front Immunol*, 11: 1986.
3. Ando, J., and K. Yamamoto. 2011. 'Effects of shear stress and stretch on endothelial function', *Antioxid Redox Signal*, 15: 1389-403.
4. Annan, D. A., H. Kikuchi, N. Maishi, Y. Hida, and K. Hida. 2020. 'Tumor Endothelial Cell-A Biological Tool for Translational Cancer Research', *Int J Mol Sci*, 21.
5. Baek, I. H., H. S. Han, S. Baik, V. Helms, and Y. Kim. 2018. 'Detection of Acidic Pharmaceutical Compounds Using Virus-Based Molecularly Imprinted Polymers', *Polymers (Basel)*, 10.
6. Barbu, E. M., K. C. Cady, and B. Hubby. 2016. 'Phage Therapy in the Era of Synthetic Biology', *Cold Spring Harb Perspect Biol*, 8.
7. Bhattacharjee, S., M. J. Glucksman, and L. Makowski. 1992. 'Structural polymorphism correlated to surface charge in filamentous bacteriophages', *Biophys J*, 61: 725-35.
8. Bohle, A. S., and H. Kalthoff. 1999. 'Molecular mechanisms of tumor metastasis and angiogenesis', *Langenbecks Arch Surg*, 384: 133-40.
9. Caballero, D., S. M. Blackburn, M. de Pablo, J. Samitier, and L. Albertazzi. 2017. 'Tumour-vessel-on-a-chip models for drug delivery', *Lab Chip*, 17: 3760-71.
10. Choi, D. H., H. W. Liu, Y. H. Jung, J. Ahn, J. A. Kim, D. Oh, Y. Jeong, M. Kim, H. Yoon, B. Kang, E. Hong, E. Song, and S. Chung. 2023. 'Analyzing angiogenesis on a chip using deep learning-based image processing', *Lab Chip*, 23: 475-84.
11. Choi, D. S., H. E. Jin, S. Y. Yoo, and S. W. Lee. 2014. 'Cyclic RGD peptide incorporation on phage major coat proteins for improved internalization by HeLa cells', *Bioconjug Chem*, 25: 216-23.
12. Chung, J. Y., M. K. Chan, J. S. Li, A. S. Chan, P. C. Tang, K. T. Leung, K. F. To, H. Y. Lan, and P. M. Tang. 2021. 'TGF-beta Signaling: From Tissue Fibrosis to Tumor Microenvironment', *Int J Mol Sci*, 22.

13. Cuccia, N. L., S. Pothineni, B. Wu, J. Mendez Harper, and J. C. Burton. 2020. 'Pore-size dependence and slow relaxation of hydrogel friction on smooth surfaces', *Proc Natl Acad Sci U S A*, 117: 11247-56.

14. Dvorak, H. F. 1986. 'Tumors: wounds that do not heal. Similarities between tumor stroma generation and wound healing', *N Engl J Med*, 315: 1650-9.

15. Enshell-Seijffers, D., L. Smelyanski, and J. M. Gershoni. 2001. 'The rational design of a 'type 88' genetically stable peptide display vector in the filamentous bacteriophage fd', *Nucleic Acids Res*, 29: E50-0.

16. Gupta, S., C. Konradt, A. Corken, J. Ware, B. Nieswandt, J. Di Paola, M. Yu, D. Wang, M. T. Nieman, S. W. Whiteheart, and L. F. Brass. 2020. 'Hemostasis vs. homeostasis: Platelets are essential for preserving vascular barrier function in the absence of injury or inflammation', *Proc Natl Acad Sci U S A*, 117: 24316-25.

17. Hussey, G. S., M. C. Cramer, and S. F. Badylak. 2018. 'Extracellular Matrix Bioscaffolds for Building Gastrointestinal Tissue', *Cell Mol Gastroenterol Hepatol*, 5: 1-13.

18. Karimi, M., H. Mirshekari, S. M. Moosavi Basri, S. Bahrami, M. Moghoofei, and M. R. Hamblin. 2016. 'Bacteriophages and phage-inspired nanocarriers for targeted delivery of therapeutic cargos', *Adv Drug Deliv Rev*, 106: 45-62.

19. Kim, S., W. Kim, S. Lim, and J. S. Jeon. 2017. 'Vasculature-On-A-Chip for In Vitro Disease Models', *Bioengineering (Basel)*, 4.

20. Ko, J., J. Ahn, S. Kim, Y. Lee, J. Lee, D. Park, and N. L. Jeon. 2019. 'Tumor spheroid-on-a-chip: a standardized microfluidic culture platform for investigating tumor angiogenesis', *Lab Chip*, 19: 2822-33.

21. Kocherova, I., A. Bryja, P. Mozdziak, A. Angelova Volponi, M. Dyszkiewicz-Konwinska, H. Piotrowska-Kempisty, P. Antosik, D. Bukowska, M. Bruska, D. Izycki, M. Zabel, M. Nowicki, and B. Kempisty. 2019. 'Human Umbilical Vein Endothelial Cells (HUVECs) Co-Culture with Osteogenic Cells: From Molecular Communication to Engineering Prevascularised Bone Grafts', *J Clin Med*, 8.

22. Korkmaz, N., Y. J. Kim, and C. H. Nam. 2013. 'Bacteriophages as Templates for Manufacturing Supramolecular Structures', *Macromolecular Bioscience*, 13: 376-87.

23. Kurakazu, I., Y. Akasaki, H. Tsushima, T. Sueishi, M. Toya, M. Kuwahara, T. Uchida, M. K. Lotz, and Y. Nakashima. 2021. 'TGFbeta1 signaling protects

chondrocytes against oxidative stress via FOXO1-autophagy axis', *Osteoarthritis Cartilage*, 29: 1600-13.

24. Lee, Y. J., H. Yi, W. J. Kim, K. Kang, D. S. Yun, M. S. Strano, G. Ceder, and A. M. Belcher. 2009. 'Fabricating genetically engineered high-power lithium-ion batteries using multiple virus genes', *Science*, 324: 1051-5.
25. Meulmeester, E., and P. Ten Dijke. 2011. 'The dynamic roles of TGF-beta in cancer', *J Pathol*, 223: 205-18.
26. 'National Institute of Allergy and Infectious Diseases (NIAID) A Phase 1b/2 Trial of the Safety and Microbiological Activity of Bacteriophage Therapy in Cystic Fibrosis Subjects Colonized with Pseudomonas Aeruginosa. [(accessed on 28 February 2023)]; Available online: https://clinicaltrials.gov/ct2/show/NCT05453578'.
27. Ribatti, D., R. Tamma, S. Ruggieri, T. Annese, and E. Crivellato. 2020. 'Surface markers: An identity card of endothelial cells', *Microcirculation*, 27: e12587.
28. Rybinski, B., J. Franco-Barraza, and E. Cukierman. 2014. 'The wound healing, chronic fibrosis, and cancer progression triad', *Physiol Genomics*, 46: 223-44.
29. Safari, Z., S. Soudi, N. Jafarzadeh, A. Z. Hosseini, E. Vojoudi, and M. Sadeghizadeh. 2019. 'Promotion of angiogenesis by M13 phage and RGD peptide in vitro and in vivo', *Sci Rep*, 9: 11182.
30. Samoylova, T. I., T. D. Braden, J. A. Spencer, and F. F. Bartol. 2017. 'Immunocontraception: Filamentous Bacteriophage as a Platform for Vaccine Development', *Curr Med Chem*, 24: 3907-20.
31. Staquicini, D. I., F. H. F. Tang, C. Markosian, V. J. Yao, F. I. Staquicini, E. Dodero-Rojas, V. G. Contessoto, D. Davis, P. O'Brien, N. Habib, T. L. Smith, N. Bruiners, R. L. Sidman, M. L. Gennaro, E. C. Lattime, S. K. Libutti, P. C. Whitford, S. K. Burley, J. N. Onuchic, W. Arap, and R. Pasqualini. 2021. 'Design and proof of concept for targeted phage-based COVID-19 vaccination strategies with a streamlined cold-free supply chain', *Proc Natl Acad Sci U S A*, 118.
32. Vajkoczy, P., A. Ullrich, and M. D. Menger. 2000. 'Intravital fluorescence videomicroscopy to study tumor angiogenesis and microcirculation', *Neoplasia*, 2: 53-61.
33. van Houten, N. E., M. B. Zwick, A. Menendez, and J. K. Scott. 2006. 'Filamentous phage as an immunogenic carrier to elicit focused antibody responses against a synthetic peptide', *Vaccine*, 24: 4188-200.

34. Warner, C. M., N. Barker, S. W. Lee, and E. J. Perkins. 2014. 'M13 bacteriophage production for large-scale applications', *Bioprocess Biosyst Eng*, 37: 2067-72.

35. Xu, Ping, Subhadeep Ghosh, Anam Ran Gula, Jigna R. Bhamore, Jong Pil Park, and Tae Jung Park. 2021. 'Screening of specific binding peptides using phage-display techniques and their biosensing applications', *TrAC Trends in Analytical Chemistry*, 137.

36. Yoon, J., N. Korkmaz Zirpel, H. J. Park, S. Han, K. H. Hwang, J. Shin, S. W. Cho, C. H. Nam, and S. Chung. 2016. 'Angiogenic Type I Collagen Extracellular Matrix Integrated with Recombinant Bacteriophages Displaying Vascular Endothelial Growth Factors', *Adv Healthc Mater*, 5: 205-12.

37. Zacher, A. N., 3rd, C. A. Stock, J. W. Golden, 2nd, and G. P. Smith. 1980. 'A new filamentous phage cloning vector: fd-tet', *Gene*, 9: 127-40.

Chapter 4

Publication 3 – Mixture toxicity (KIST-Europe internal project)

Title: Investigation of the Synergistic Toxicity of Binary Mixtures of Pesticides and Pharmaceuticals on Aliivibrio fischeri in Major River Basins in South Korea

This chapter introduces our approach to understanding the synergistic, additive, and antagonistic toxicological interactions of binary mixtures of pesticides and pharmaceuticals commonly detected in major river basins in South Korea. It was published in the journal Environmental Research and Public Health [131]. My contributions were to prepare all materials, carrying out measurements, calculation of the single and mixture toxicity, and writing the first draft of the manuscript. The following sections are identical to the preprint version of the manuscript .

Research paper

Investigation of the Synergistic Toxicity of Binary Mixtures of Pesticides and Pharmaceuticals on Aliivibrio fischeri in Major River Basins in South Korea

In-hyuk Baek [1, 2], Youngjun Kim [1, 3], Seungyun Baik [1] and Jongwoon Kim [1, 3,†,*]

[1] Environmental Safety Group, Korea Institute of Science and Technology (KIST) Europe, Campus E 7.1, Saarbruecken, Germany; ih.baek@kist-europe.de @kist-europe.de (I-H.B.); youngjunkim@kist-europe.de (Y.K.); sbaik@kist-europe.de (S.B.); with.jwkim@gmail.com (J.K.)

[2] Center for Bioinformatics, Saarland University, Campus E 2.1, Saarbruecken, Germany

[3] Division of Energy and Environment Technology, KIST School, University of Science and Technology, Hwarang-ro 14-gil, Seoul, Republic of Korea

* Correspondence: with.jwkim@gmail.com

[†] Present address: Chemical Safety Research Center, Korea Research Institute of Chemical Technology (KRICT), 141 Gajeong-ro, Yuseong-gu, Daejeon 34114, Republic of Korea

Academic Editor: name
Received: date; Accepted: date; Published: date

Abstract

This work introduced the potential synergistic toxicity of binary mixtures of pesticides and pharmaceuticals, which have been substantially detected in major river basins in South Korea. Different dose-response curve functions were employed in each experimental toxicity dataset for *Aliivibrio fischeri*. We tested the toxicity of 30 binary mixtures at two effect concentrations: high effect concentration [EC_{50}] and low effect concentration [EC_{10}] ranges. Thus, the toxicological interactions were evaluated at 60 effected concentration data points in total and based on model deviation ratios (MDRs) between predicted and observed toxicity values (e.g., three types of combined effects: synergistic (MDR > 2), additive (0.5 ≤ MDR ≤ 2), and antagonistic (MDR < 0.5)). From the 60 data points, MDRs could not be applied to 17 points, since their toxicities could not be measured. The result showed 48 %-additive (n = 20), 40 %-antagonistic (n = 17), and 12 %-synergistic (n = 6) toxicity effects from 43 binaries (excluding the 17 combinations without MDRs). In this study, EC_{10} ratio mixtures at a low overall effect range showed a general tendency to have more synergistic effects than the EC_{50} ratio mixtures at a high effect range. We also found an inversion phenomenon, which detected three binaries of the combination of synergism at low concentrations and additive antagonism at high concentrations.

Keywords: Mixture toxicity; Concentration addition; Pesticide; Pharmaceuticals; *Aliivibrio fischeri*

1. Introduction

Conventional chemical risk assessments frequently focus on individual substances rather than mixtures even though previous studies have shown that the toxicity of mixtures can be provoked by combined effects among chemicals even at no observed effect concentrations [132, 133]. The types of the mixture toxicity are generally explained as additivity, synergism (greater than additivity), and antagonism (less than additivity) [134, 135]. Among these combined effects, additive and synergistic toxicity effects can be regarded as more significant than the antagonistic effect (from the aspect of the regulatory chemical risk assessment, which assumes the worst-case scenario as the default) [136]. In this context, the conventional regulatory risk assessment of chemical mixtures is mostly based on the concentration addition (CA) model as a default for estimating the mixture toxicity [137-140]. Although the worst-case scenario can be substantial synergistic toxicity, the CA model, which ignores the synergistic interaction, has been mainly employed since available predictive models for estimating the synergistic effect have been very limited for the purpose of regulatory risk assessment [136]. In addition, some studies have shown that the synergistic interaction could be a relatively rare occurrence, at least within pesticide mixtures and realistic mixtures having low concentrations in mammals (which are comprised of approximately 5 % of the tested mixtures) [141-144]. In contrast, a recently published review showed that less than 25 % of research and experiments on the toxicity of chemical mixtures investigated seven or more compounds [145, 146]. Some clinical researchers in human toxicology also showed that the probability of synergistic toxicity could be increased in proportion to the number of components, e.g., an 8 % toxicity effect was caused by pharmaceutical products with five to ten mixed components, and a 38 % toxicity effect was provoked by pharmaceuticals with fourteen or more mixture components [136, 147, 148]. This issue related to synergism is still controversial and difficult to conclude since most of the studies concerning mixture toxicity have been conducted with a specific binary mixture or simple mixtures having less than ten components [136]. Many studies have found that pesticides and pharmaceuticals were detected in the aquatic environment and thus they might lead to mixture toxicity for aquatic nontarget organisms [145, 149-152]. Thus, when considering environmental mixtures with complex matrices and different chemicals, any potential risk posed might have been underestimated by the CA model if the synergistic interaction occurred in such mixtures [145].

The objective of this study was to preliminarily investigate the potential synergistic interactions of pharmaceutical and pesticide residues that can be found in the aquatic environment. For this purpose, we tested and evaluated the toxicity of different binary mixtures of pesticides and pharmaceuticals, which had been substantially identified in major river basins in South Korea. To evaluate the toxicity of single and mixed chemicals, a bioassay with a luminescent bacterium, *Aliivibrio fischeri*, which is widely used in standard toxicity methods, was conducted [153, 154]. Based on the original best-fit approach [155], different dose-response curve (DRC) functions were employed to test data sets, and best-fit functions of single and mixed chemicals were used in the mixture toxicity modeling

2. Materials and Methods

2.1. Selection of target pesticides and pharmaceuticals

Through previously published studies *[156-162]* that investigated the environmental concentration level of 47 pharmaceuticals in four major river basins (Han River, Geum River, Bukhan River, and Yeongsan River) in South Korea, 29 pharmaceuticals could be identified *[163]*. In addition, based on a study by Lee et al. *[164]* monitoring 140 pesticide residues in six Korean river basins (Han River, Geum River, Bukhan River, Yeongsan River, Mankyeong River, and Seomjin River), eight pesticides (isoprothiolane >, butachlor >, prothiofos >, chlorpyrifos >, hexaconazole, molinate >, diazinon, and alachlor) could be found. From those 29 pharmaceuticals and eight pesticides, six chemicals, including four pharmaceuticals (tetracycline, trimethoprim, sulfamethoxazole, and chlortetracycline) and two pesticides (hexaconazole, and isoprothionlane), were finally selected as target mixutre components in this study (Table S1). The selction was made by considering their toxicities to A. fischeri, solubilities in water and carrier solvents, and detection frequencies in the aquatic environment. To our knowledge, this is the first study to investigate the toxicity of hexaconazole, isoprothiolane, and chlortetracycline and their binary mixtures to A. fischeri.

2.1. Test reagents, chemicals and sample preparation

Six target compounds were purchased from Sigma-Aldrich (Seelze, Germany). According to the physico-chemical properties of these compounds, stock solutions were prepared in either 99.9 % dimethyl sulfoxide (DMSO, Sigma-Aldrich, Seelze, Germany) for trimethoprim and chlortetracycline or 99.8 % ethanol (EtOH, Carl Roth GmbH, Karlsruhe, Germany) for tetracycline, hexaconazole, isoprothiolane and

sulfamethoxazole. All of the stock solutions were kept at -20 ℃ under dark conditions until the working solutions were prepared. For quality control and quality assurance, the concentrations of the stock solutions were quantified with an HPLC system (Agilent 1290, Agilent Technologies, CA, USA) connected to a triple quadrupole mass spectrometry (MS/MS) model 6460 Agilent (Agilent Technologies, CA, USA). Before the experiments, working solutions (1:25) were prepared by diluting the stock solutions in 2 % sodium chloride for a marine bacterium, *A. vibrio*, according to ISO 11348-3 [153]. The pH values of the working solutions were checked and adjusted to between 6.0 and 8.0 with 1 N NaOH and 1 N HCl.

2.2. Testing organism and culture

The bioluminescent bacteria *A. fischeri* (strain NRRL-B-11177 and formerly called *Vibrio fischeri*) were purchased from MicroTox® (Lot number 15C4025A, Modern Water, UK). The freeze-dried bacteria were activated with the reconstitution solution provided by the MicroTox® for 30 minutes at 15 ℃. The activated bacteria were transferred to a photobacteria medium (Sigma-Aldrich) for preculture at 20 ℃. For stock culturing, activated *A. fischeri* were estimated in a 250 ml main culture medium at an initial turbidity of a 1:10 dilution by UV-vis photometric (Ultraspec 3300, Amersham, UK) at OD_{578} was 0.02 (10 Formazine turbidity units, FNU). *A. fischeri* were cultured at 20 ℃ with shaking at 180 rpm/min until the turbidity of the OD_{578} was 1.74 (700 FNU to 1800 FNU). The amplified *A. fischeri* were purified twice with a 2 % sodium chloride solution at 4 ℃ and 20 minute at 7000 × g. The bacteria were slowly suspended in protective medium (66 g D(+)-Glucose monohydrate, 4 g sodium chloride, 2 g L-Histidine and 0.5 g BSA in 100 ml) at an ice cooled condition until the turbidity of the OD_{578} was 2.58 (2000 FNU to 3000 FNU). The suspended stock bacteria were stored at -80 ℃.

2.3. Single chemical toxicity test

Determination of an effective concentration of samples was performed [165] using the standardized methods of ISO 11348-3, 1998 by luminescent bacteria (*A. fischeri*) [153]. To activate, the frozen bacteria were suspended using a reconstituted solution (20 g sodium chloride, 0.3 g potassium chloride, HEPES 50 mM and glucose 50 mM for 1 liter) for 30 minutes at 15 ℃. The activated luminescence bacteria were mixed with 2 % sodium chloride at a 1:25 dilution. Six single compounds were serially diluted at a ratio of 1:1 (100 μl) on a flat-bottomed black 96-well plate (Greiner bio-one, Germany). The bacterial suspensions were exposed to the serially diluted sample at a ratio of 100 μl by 100 μl. Then, reactive samples were measured after 15 minutes of exposure at 15 ℃ by a luminescent reader (Tristar2, Berthold technologies, Germany). To assure the quality of the bacteria, a 100ppm zinc sulfate (Sigma-Aldrich, Germany) solution was measured every time.

2.4. Mixture toxicity test

An investigation of the synergistic toxicity of all binary mixtures that could be prepared from the six target compounds in Table S1 was conducted in a fixed ratio design based on the equitoxic mixture and the generation of dose-response curves from the mixtures employed in previous studies [166-170]. The advantages of the fixed ratio design are not only the ability to maximize the distribution of the effective dose range but also to minimize the number of experiments [168, 171-173]. With the same compounds in Table S1, two different equitoxic mixtures were prepared at a 50 % effective concentration for each compound as a high effective concentration ratio mixture (EC_{50} ratio mixture) to *A. fischeri* and at a 10 % effective concentration ratio mixture (EC_{10} ratio mixture) as a low effective concentration ratio mixture. As shown in Table 1, a total of 30 equitoxic binary mixtures of each combination were tested at high and low effective concentration levels. However, the total doses of the mixtures were systematically different.

Table 1. Binary mixture designs for target pesticides and pharmaceuticals

Mixture No.	Substance A	Substance B	Mixture design
1	Tetracycline	Sulfamethoxazole	$EC_{50} + EC_{50}$
2	Tetracycline	Sulfamethoxazole	$EC_{10} + EC_{10}$
3	Tetracycline	Hexaconazole	$EC_{50} + EC_{50}$
4	Tetracycline	Hexaconazole	$EC_{10} + EC_{10}$
5	Tetracycline	Chlortetracycline	$EC_{50} + EC_{50}$
6	Tetracycline	Chlortetracycline	$EC_{10} + EC_{10}$
7	Tetracycline	Isoprothiolane	$EC_{50} + EC_{50}$
8	Tetracycline	Isoprothiolane	$EC_{10} + EC_{10}$
9	Tetracycline	Trimethoprim	$EC_{50} + EC_{50}$
10	Tetracycline	Trimethoprim	$EC_{10} + EC_{10}$
11	Trimethoprim	Sulfamethoxazole	$EC_{50} + EC_{50}$
12	Trimethoprim	Sulfamethoxazole	$EC_{10} + EC_{10}$
13	Trimethoprim	Hexaconazole	$EC_{50} + EC_{50}$
14	Trimethoprim	Hexaconazole	$EC_{10} + EC_{10}$
15	Trimethoprim	Chlortetracycline	$EC_{50} + EC_{50}$
16	Trimethoprim	Chlortetracycline	$EC_{10} + EC_{10}$
17	Trimethoprim	Isoprothiolane	$EC_{50} + EC_{50}$

18	Trimethoprim	Isoprothiolane	EC_{10} + EC_{10}
19	Sulfamethoxazole	Hexaconazole	EC_{50} + EC_{50}
20	Sulfamethoxazole	Hexaconazole	EC_{10} + EC_{10}
21	Sulfamethoxazole	Chlortetracycline	EC_{50} + EC_{50}
22	Sulfamethoxazole	Chlortetracycline	EC_{10} + EC_{10}
23	Sulfamethoxazole	Isoprothiolane	EC_{50} + EC_{50}
24	Sulfamethoxazole	Isoprothiolane	EC_{10} + EC_{10}
25	Hexaconazole	Chlortetracycline	EC_{50} + EC_{50}
26	Hexaconazole	Chlortetracycline	EC_{10} + EC_{10}
27	Hexaconazole	Isoprothiolane	EC_{50} + EC_{50}
28	Hexaconazole	Isoprothiolane	EC_{10} + EC_{10}
29	Chlortetracycline	Isoprothiolane	EC_{50} + EC_{50}
30	Chlortetracycline	Isoprothiolane	EC_{10} + EC_{10}

2.5. Statistical analysis of the mixture toxicity

A "best-fit" approach [155, 174] was used to select the best model with the smallest sum of absolute residuals among the different sigmoidal functions because no single function could statistically describe all of the DRCs. Best-fit models with three-parameter sigmoidal equations were finally determined and applied to describe the experimental data of the mixture components tested in this study. The parameters in the sigmoidal regression equations and 95 % confidence intervals were estimated using SigmaPlot® (Ver. 12.5, Systat Software, Chicago, IL, USA). The ECx (e.g., EC_{10} and EC_{50}) of the test chemicals was derived from the regression models shown in Table 2 and S2. It was assumed that all of the models were confined to the effects range from 0 to 100 %. In order to compare between the highest and lowest toxicity without, we expressed the orders of magnitude which were determined as follows:

$$\text{Orders of magnitude} = \log\left(\frac{EC_{x-highest\ toxicity}}{EC_{x-lowest\ toxicity}}\right)$$

However, in case a test chemical showed low solubility in water, the model for that chemical was assumed to have a range between >0 % and <the maximum effect (%), where the chemicals were present at a maximum solubility in water under the test conditions in this study.

The ECx for mixtures was calculated by the CA model according to the Loewe equation [142, 175]:

$$ECx_{\text{mix}} = \left(\sum_{i=1}^{n} \frac{p_i}{ECx_i} \right)^{-1}$$

where ECx_{mix} is the predicted effective concentration of a mixture; Pi and ECx_i are the fraction and the individual effective concentration of the component with in the mixture, respectively.

MDR values (Belden et al., 2007) were used to quantify the interaction between the mixture components. The MDR values were frequently applied to determine the type of interactions of the mixture toxicity [144, 176, 177]. MDR is defined as

$$MDR = \frac{Predicted\ ECx\ of\ mixture}{Observed\ ECx\ of\ mixture}$$

where the predicted ECx indicates the effective concentration of a mixture based on the predictive model, and the observed ECx is the effective concentration of the mixture obtained from experimental toxicity testing. In this study, the CA model, which is recommended as a default approximation for mixtures, was used to predict mixture toxicity [136, 141, 176, 178, 179]. Based on the MDR value, the types of combined effects are divided into three groups: synergistic (MDR > 2), additive (0.5 ≤ MDR ≤ 2) and antagonistic (MDR < 0.5) [142, 144].

3. Results and Discussion

3.1. DRCs for single compounds

DRCs of all six compounds in Table S1 were empirically determined for *A. fischeri*, as illustrated in Figure 1. Table 2 summarizes the parameter values of all the best-fitting regression models for the DRCs of single compounds. Table S2 explains the regression models described in Table 2. The best-fitting curves for all of the compounds showed high regression coefficients (r^2) ranging from 0.969 to 0.995 and their ANOVA *p*-values were less than 0.0001. As presented in Table 2, the deviation between the steeper function of the highest slope values (65.25 for chlortetracycline) and the more gradual slope of the lowest (0.0034 for sulfamethoxazole) slope values was approximately 4.28 orders of magnitude. These considerable differences among the slopes of the DRCs of the compounds suggest that the compounds had highly different curve shapes for estimating the toxicity of each compound.

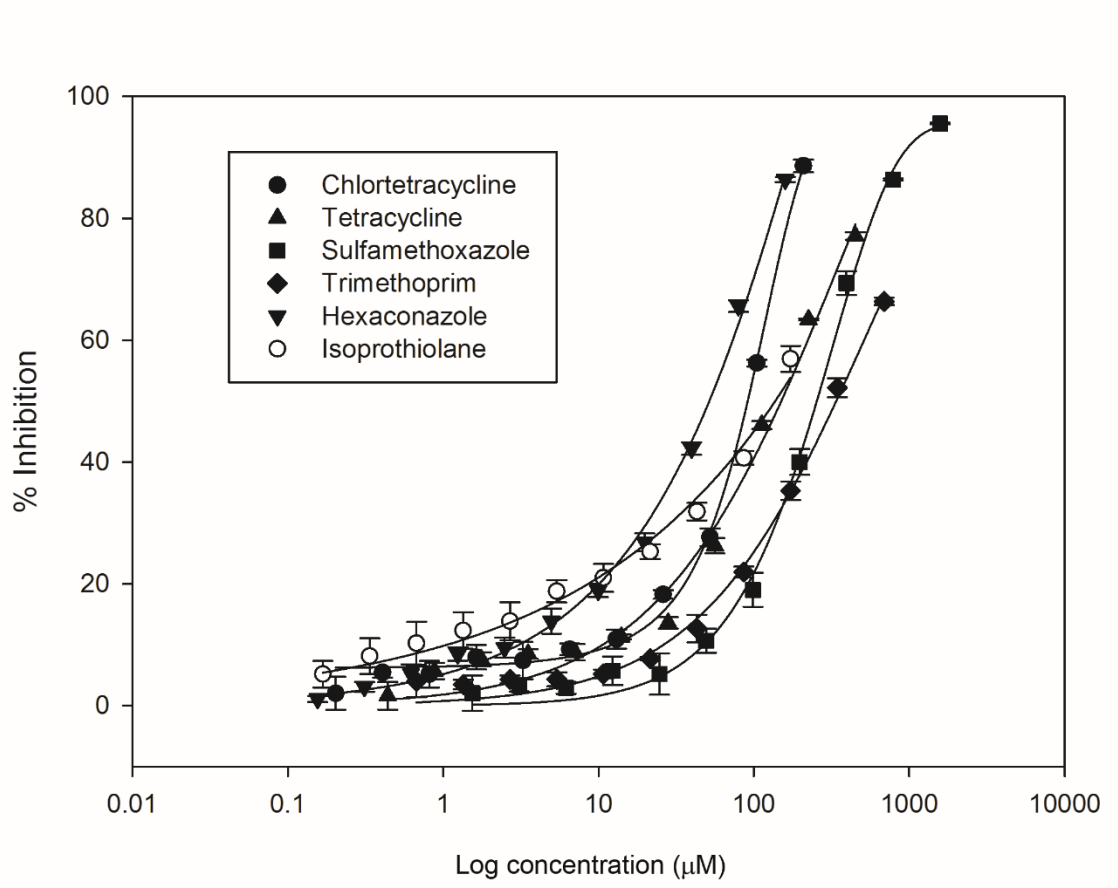

Figure 1. DRCs for the bioluminescent inhibition of *A. fischeri* for single compounds in Table 1 (the data points are geometric means ± standard deviation [SD] of the experimentally observed data and statistical best-fits [solid lines]).

The best-fitted DRCs for each compound had high regression coefficients (r^2) ranging from 0.971 to 0.995. The EC_{50} values of *A. fischeri* were up to 0.82 orders of magnitude and ranged from 51.65 μM for hexaconazole to 338.81 μM for trimethoprim. However, the EC_{10} values of *A. fischeri* were up to 1.66 orders of magnitude and ranged from 1.05 μM for isoprothiolane to 47.79 μM for sulfamethoxazole. That is, hexaconazole and isoprothiolane presented the lowest effective concentrations (or the highest toxicity) at the respective EC_{50} and EC_{10} values, whereas isoprothiolane and sulfamethoxazole showed the highest effective concentrations (or the lowest toxicity) at the corresponding EC_{50} and EC_{10} values. These results also show that the toxicological profiles of compounds can be varied according to a given effective concentration level. In the cases of isoprothione, tetracycline, haxaconazole and trimethoprim, more than 80 %-effect concentrations couldn't be obtained under the testing conditions because of their water solubility limits.

Table 2. Parameters of the regression models for dose-response curves of *A. fischeri* for pesticide and pharmaceutical single compounds in Table S1 (the 95 % confidence intervals are provided in the brackets).

Substance	EC_{50} (μM)	EC_{10} (μM)	RM[1)]	r^2	Model parameter		
					A[2)]	B[3)]	Γ[4)]
Hexaconazole	51.65 [50.97-52.33]	3.06 [2.38-3.74]	C	0.995	1.4335	0.0035	0.5869
Isoprothiolane	137.07 [136.14-138.0]	1.05 [0.12-1.85]	H	0.971	97.3866	0.3312	1.10E+09
Tetracycline	150.08 [148.85-151.30]	10.60 [9.38-11.83]	L	0.981	1.4806	-0.7364	374.5933
Trimethoprim	338.81 [338.05-339.56]	26.20 [25.45-26.95]	L	0.990	1.2286	-0.7997	542.4834
Sulfamethoxazole	254.20 [253.25-255.15]	47.79 [46.83-48.74]	C	0.994	0.9561	0.0034	1.1932
Chlortetracycline	91.32 [90.52-92.12]	12.32 [11.52-13.12]	G	0.993	0.9902	65.2541	66.4673

Notes. [1)]Regression models (C: Chapman, G: Gompertz, H: Hill, L: Logistic); [2)]Height; [3)]Slope; and [4)]Center point

3.2. DRCs of binary mixtures

The DRCs of binary mixtures in Table 1 were experimentally evaluated with high (EC_{50} + EC_{50}) and low (EC_{10} + EC_{10}) exposure levels (Figures 2 and 3). As shown in Table 3, best-fitting curves for all mixture combinations had high regression coefficients (r^2) ranging from 0.817 to 0.997 except for four mixture combinations. The four exceptions are Mixture 14 (trimethoprim with hexaconazole; Mixture 14, r^2 = 0.455), 18 (trimethoprim with isoprothiolane; Mixture 18, r^2 = 0.429) 24 (sulfamethoxazole with isoprothiolane; Mixture 24, r^2 = 0.698) and 28 (hexaconazole with isoprothiolane; Mixture 28, r^2 = 0.257). The probable reason for the high deviation of those two mixtures is that they were the EC_{10} ratio mixture, i.e., an equitoxic mixture based on ratios at 10 % effective concentrations for each component but significantly less toxic than the others so that the ECx values could not be appropriately determined. As tested binary mixtures, the effective concentration data ranged from a low of 2.17 μmol/L (EC_{10} + EC_{10}, tetracycline and hexaconazole) to a high of 779.94 μmol/L (EC_{50} + EC_{50}, trimethoprim and sulfamethoxazole).

Table 3. Parameters of regression models for dose-response curves of 30 binary mixtures of pesticides and pharmaceuticals in Table 1 (the 95 % confidence intervals are provided in the brackets).

Mixture No.	EC_{50} (μM)	EC_{10} (μM)	RM[1)]	r^2	Model parameter		
					A[2)]	B[3)]	Γ[4)]
1	313.95 [313.07-314.82]	16.62 [15.74-17.50]	C	0.987	2528.4458	2.47E-06	0.5477
2	n.a.	7.43 [6.99-7.88]	G	0.968	19.5735	6.4890	4.8497
3	133.58 [132.69-134.46]	2.89 [2.01-3.78]	C	0.989	915.2173	7.38E-06	0.4200
4	n.a.	2.17 [1.75-2.59]	G	0.983	23.9224	2.0367	1.8951
5	129.70 [128.75-130.66]	5.98 [5.02-6.93]	C	0.989	102.0025	0.0025	0.5494
6	n.a.	9.54 [8.83-10.25]	L	0.954	30.2768	-0.8861	21.1859
7	203.46 [202.88-204.04]	36.83 [36.25-37.41]	G	0.996	84.6072	118.9205	127.0557
8	n.a.	11.66 [11.25-12.06]	G	0.874	10.4177	3.3048	1.0944
9	265.16 [264.62-265.69]	15.55 [15.01-16.09]	C	0.996	99.5885	0.0015	0.6049
10	n.a.	8.64 [8.18-9.10]	L	0.970	22.0641	-1.4308	9.8530
11	779.94 [779.31-780.56]	62.99 [62.36-63.61]	C	0.989	83.7765	0.0009	0.7231
12	n.a.	50.31 [49.80-50.81]	G	0.914	19.2041	49.3054	29.2598
13	488.97 [488.44-489.49]	59.282 [58.76-59.81]	H	0.991	131.1544	0.9527	812.9558
14	n.a.	n.a.	G	0.455	4.5523	0.5916	17.0836
15	222.30 [220.95-223.65]	4.56 [3.22-5.91]	H	0.964	63.8649	0.7633	41.4132
16	n.a.	3.91 [3.38-4.44]	C	0.988	33.8541	0.1489	1.4924
17	637.32 [637.01-637.64]	154.31 [153.99-154.63]	G	0.997	60.7316	216.8352	282.2291
18	n.a.	n.a.	G	0.429	8.9924	25.6941	25.7707

19	209.14 [208.45-209.83]	34.75 [34.06-35.44]	G	0.992	78.4915	114.7884	117.7289
20	n.a.	26.94 [26.43-27.44]	G	0.817	17.7472	30.9625	9.7285
21	206.10 [205.57-206.64]	37.41 [36.87-37.95]	G	0.997	96.2390	135.9703	148.5324
22	n.a.	15.85 [15.31-16.38]	G	0.9331	27.4285	34.3506	16.1526
23	339.80 [339.23-340.37]	106.78 [106.22-107.36]	G	0.9951	83.3055	163.6608	229.7587
24	n.a.	45.77 [45.31-46.24]	S	0.6981	1804.3798	51.2073	311.5280
25	119.13 [118.31-119.96]	8.40 [7.57-9.23]	H	0.9884	1.37E+05	0.6069	5.52E+07
26	n.a.	13.89 [13.46-14.33]	C	0.9560	158.6840	9.12E-06	0.3080
27	204.18 [203.53-204.83]	45.75 [45.10-46.40]	G	0.9901	107.4683	139.9025	166.7380
28	n.a.	5.82 [4.61-7.04]	G	0.2571	12.1655	3.7398	-0.2706
29	247.79 [246.98-248.59]	28.44 [27.64-29.24]	H	0.9870	4.73E+05	0.7435	5.52E+07
30	n.a.	4.38 [3.84-4.91]	C	0.9435	18.6241	0.1128	0.6594

Notes. [1)]Regression models (C: Chapman, G: Gompertz, H: Hill, L: Logistic); [2)]Height; [3)]Slope; and [4)]Center point

3.3. Statistical analysis of mixture toxicity to investigate synerism

Figures 2 and 3 illustrate DRCs for the observed bioluminescent inhibitions and the predicted inhibition of *A. fischeri* by the CA model for the binary equitoxic mixtures based on ratios at 50 % and 10 % effective concentrations and following the combinations in Table 1, respectively.

To quantify the toxicity interactions between mixture components, we calculated MDR values as shown in Table 4. Based on the MDR value, we strictly divided the three types of combined effects into synergistic (MDR > 2), additive ($0.5 \leq MDR \leq 2$) and antagonistic (MDR < 0.5) [144].

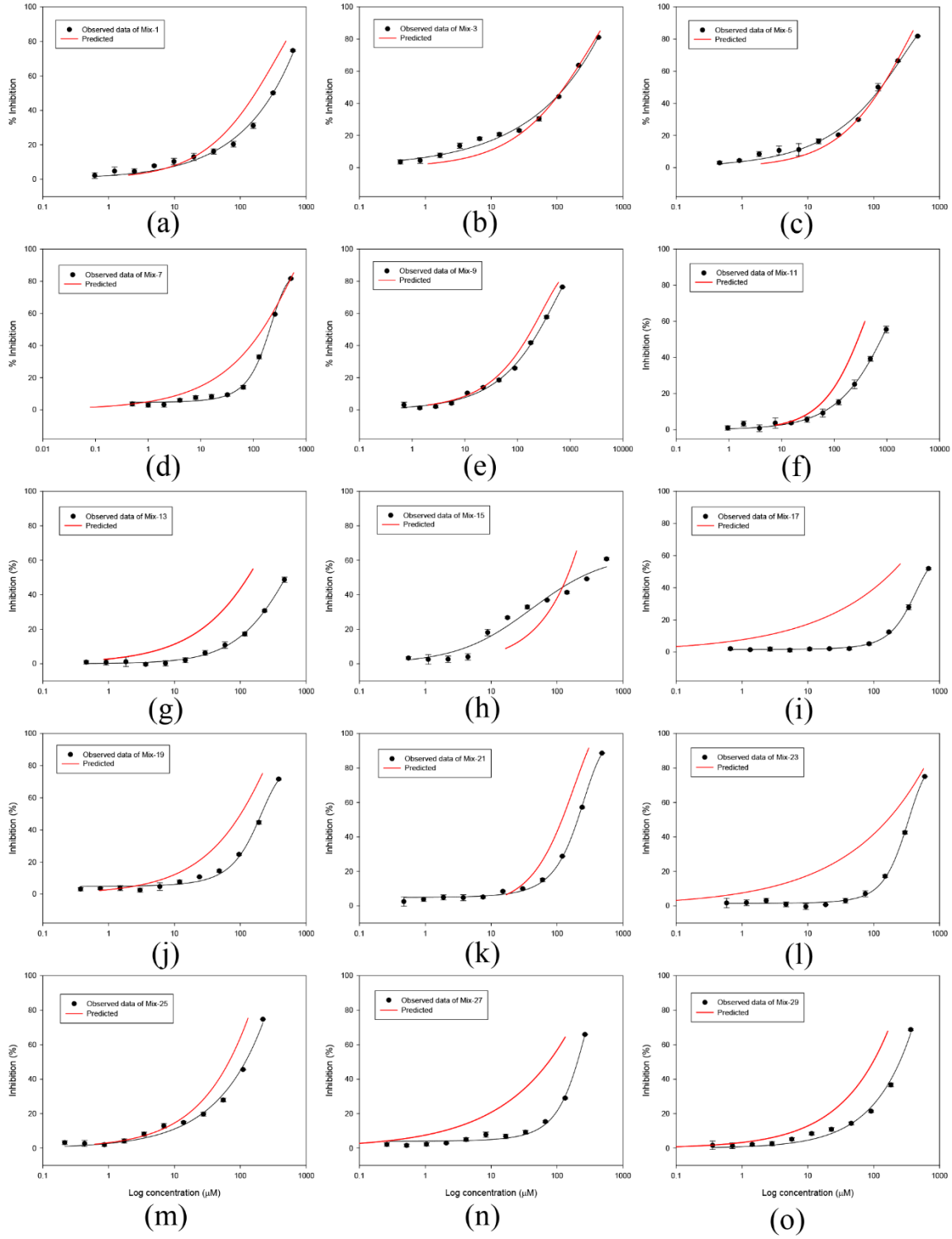

Figure 2. The DRCs for the observed bioluminescent inhibitions and the predicted inhibition [red lines] by the CA model for the binary equitoxic mixtures based on ratios at 50 % effective concentrations for each component (the data points are geometric means ± standard deviation [SD] of experimentally observed data, and statistical best-fits for regression models are summarized in Table 3).

Table 4. Observed and predicted $EC_{x\,mix}$ values of tested mixtures of pharmaceuticals and pesticides in binary combinations, and MDR values to address the interactions between components (the 95 % confidence intervals are provided in the brackets).

Mixture No.	EC_{50mix}[1]				EC_{10mix}			
	Observed (EC_{50}, μM)	Predicted[2]	MDR[3]	Type[4]	Observed (EC_{10}, μM)	Predicted	MDR	Type
EC_{50} ratio mixtures[5]								
1	313.95 [313.07-314.82]	169.63	0.54	Add.[6]	16.62 [15.74-17.50]	13.55	0.82	Add.
3	133.58 [132.69-134.46]	128.47	0.96	Add.	2.89 [2.01-3.78]	8.71	3.01	Syn.
5	129.70 [128.75-130.66]	132.37	1.02	Add.	5.98 [5.02-6.93]	10.92	1.83	Add.
7	203.46 [202.88-204.04]	147.27	0.72	Add.	36.83 [36.25-37.41]	3.84	0.10	Anta.[7]
9	265.16 [264.62-265.69]	189.17	0.71	Add.	15.55 [15.01-16.09]	13.61	0.88	Add.
11	779.94 [779.31-780.56]	281.92	0.36	Anta.	62.99 [62.36-63.61]	36.51	0.58	Add.
13	488.97 [488.44-489.49]	129.65	0.27	Anta.	59.282 [58.76-59.81]	8.20	0.14	Anta.
15	222.30 [220.95-223.65]	139.68	0.63	Add.	4.56 [3.22-5.91]	16.45	3.61	Syn.[8]
17	637.32 [637.01-637.64]	194.16	0.30	Anta.	154.31 [153.99-154.63]	2.00	0.01	Anta.
19	209.14 [208.45-209.83]	101.47	0.49	Anta.	34.75 [34.06-35.44]	7.21	0.21	Anta.
21	206.10 [205.57-206.64]	119.87	0.58	Add.	37.41 [36.87-37.95]	17.01	0.45	Anta.
23	339.80 [339.23-340.37]	167.07	0.49	Anta.	106.78 [106.22-107.36]	1.70	0.02	Anta.
25	119.13 [118.31-119.96]	66.93	0.56	Add.	8.40 [7.57-9.23]	5.04	0.60	Add.
27	204.18 [203.53-204.83]	74.93	0.37	Anta.	45.75 [45.10-46.40]	1.57	0.03	Anta.
29	247.79 [246.98-248.59]	100.21	0.40	Anta.	28.44 [27.64-29.24]	3.18	0.11	Anta.
EC_{10} ratio mixtures								
2	n.a.[9]	n.a.	-	-	7.43 [6.99-7.88]	17.53	2.36	Syn
4	n.a.	n.a.	-	-	2.17 [1.75-2.59]	8.96	4.13	Syn.
6	n.a.	n.a.	-	-	9.54 [8.83-10.25]	12.03	1.26	Add.
8	n.a.	n.a.	-	-	11.66 [11.25-12.06]	8.57	0.73	Add.
10	n.a.	n.a.	-	-	8.64 [8.18-9.10]	13.84	1.60	Add.
12	n.a.	n.a.	-	-	50.31 [49.80-50.81]	41.16	0.82	Add.
14	n.a.	n.a.	-	-	n.a.	n.a.	-	-
16	n.a.	n.a.	-	-	3.91 [3.38-4.44]	15.03	3.84	Syn.
18	n.a.	n.a.	-	-	n.a.	n.a.	-	-
20	n.a.	n.a.	-	-	26.94 [26.43-27.44]	14.00	0.52	Add.
22	n.a.	n.a.	-	-	15.85 [15.31-16.38]	18.52	1.17	Add.
24	n.a.	n.a.	-	-	45.77 [45.31-46.24]	12.98	0.28	Anta.
26	n.a.	n.a.	-	-	13.89 [13.46-14.33]	11.18	0.80	Add.
28	n.a.	n.a.	-	-	5.82 [4.61-7.04]	2.52	0.43	Anta.

30	n.a.	n.a.	-	-	4.38 [3.84-4.91]	10.07	2.30	Syn.

Note. [1)]ECx_{mix}: effective concentrations of a mixture causing x % toxicity effect; [2)]Values predicted by the concentration addition model; [3)]Model deviation ratio; [4)]Type of combined toxic effects; [5)]ECx ratio mixture: an equitoxic mixture based on ratios at x% effective concentrations for each component; [6)]Additivity; [7)]Antagonism; [8)]Synergism; and [9)]Not available.

As shown in Figure 2 and Table 4, ten binaries of the EC_{50} ratio mixtures (i.e., EC_{50mix}) showed the same interactions at two effective concentration values of EC_{10} and EC_{50}. That is, four binaries of the EC_{50mix} (Mixture 1, 5, 9, and 25) showed the additive effects at the EC_{50} and EC_{10} ranges. The antagonistic interaction of six binaries of EC_{50mix} (Mixture 13, 17, 19, 23, 27, and 29) was then detected at the EC_{50} and EC_{10} ranges. Interestingly, five binaries of the mixture combination detected different interactions from the EC_{50} and EC_{10} ranges. Two binaries of the EC_{50mix} (Mixture 3 and 15) found an additive interaction at the EC_{50} ranges and it resulted in a synergistic interaction at the EC_{10} ranges. At similar trend in one binary combination (Mixture 11) was observed for the antagonistic interaction at the EC_{50} ranges and an additive interaction at the EC_{10} ranges. In contrast, the two binaries of the EC_{50mix} (Mixture 7, and 21) resulted in opposite trends in additive interaction at the EC_{50} ranges and antagonistic interaction at the EC_{10} ranges. These observed inversion phenomena of interaction between synergism at low concentrations and additive or antagonism at high concentrations are difficult to explain. As shown in Table 4, similar phenomena have been reported in previous studies [180-183]. Wang et al. [180] tested the spiramycin and ampicillin antibiotics on *Microcystis aeruginosa* at different equitoxic ratios. The study found the equivalent ratio (1:1) of the binary mixture of spiramycin and ampicillin showed a synergistic interaction at low concentrations and an antagonistic interaction at high concentrations. In a similar appearance of research by Nica et al. [181], they tested five veterinary pharmaceuticals for the interaction of synergistic, additive and antagonistic effects on *A. fischeri* by the combination index of the CA and IA models. They found inversion phenomena of antagonism at high concentrations and synergism at low concentrations from six binary combinations and one pentanary mixture with individual predicted no-effect concentrations. The authors assumed that these phenomena seemed to be independent of the mode of action, which are likely complex and mostly unknown in nature. Rodea-Palomares et al. [182] also found interesting results, i.e., opposite interactions between different aquatic organisms of cyanobacteria (*Anabaena* CPB 4337) and *A. fischeri* for three pharmaceuticals. The authors reported a tandemly changing interaction from antagonistic and additive effects at low effective concentration levels to synergistic effects at high effective concentration levels in an *A. fischeri* test for binary and tertiary mixtures. As shown in Table 5, *Anabaena* tests showed a converse pattern against *A. fischeri* toxicity results. Ismael et al. carefully assumed that pharmaceuticals were shared by a common binding motif such as the same target and receptor sites. Because of the structural similarity, these unexpected interactions were shown between different aquatic organisms. Gonzalez-Pleiter et al. [183] also tested cyanobacteria (*Anabaena* CPB 4337)

for levofloxacin and tetracycline. They found synergism at low effective concentration levels and antagonism at high effective concentration levels. Based on these results, we assume that the unexpected interaction was caused by tetracycline. In some cases, the interactions of experimental toxicity screening were different from predictive toxicity results with inversion phenomena of the interaction [180-183]. This observation suggests that the binary components could make the synergistic effects at low concentrations. Wang et al. reported that the reaction mechanism differs between short-term (acute) and long-term (chronic) exposures because of quorum sensing molecules which known as *ain* and *lux* in *A. fischeri* [184]. So that better understanding the accurate synergistic interaction, chronic toxicity tests are required. In this study, the exposure levels of the tested chemicals were less than their environmentally relevant concentrations. Thus, further studies are needed to determine how substances as synergists interact with biomolecules at low concentrations from different model organisms including *A. fischeri*.

Table 5. A summary of the studies related to the interaction of inversion phenomena.

Mixture	Experimental design	Species	Endpoint	Convind effect		Quantification methods	Ref.
				High level	Low level		
Two antibiotics	Binary equitoxic mixture ratio (5:1, 1:1, 1:5)	Bacteria *Microcystis aeruginosa* (MA)	EC50 and EC5 for MA cell from equitoxic ratio SP/Amp (5:1, 1:5, 1:1)	Antagonism 1:1 ratio > 0.7 ug/L	Synergism 1:1 ratio < 0.5 ug/L	Departure from additivity model (CA, IA)	[180]
Five veterinary pharmaceuticals	Binary and multicomponent mixture	Bacteria *A. fischeri*	Applying the combination index method from active pharmaceutical compound interactions for bacteria	Antagonism	Synergism	Departure from combination index (CA, IA)	[181]
			Diclofenac : Sulfamethizole	EC_{50} 1.13	EC_{10} 0.61		
			Acetylsalycilic acid : Sulfamethizole	EC_{50} 2.58	EC_{10} 0.85		
			Chlortetracycline : Amoxicillin	EC_{50} 2.16	EC_{10} 0.08		
			Acetylsalycilic acid : Diclofenac	EC_{50} 1.13	EC_{10} 0.73		
			Sulfamethizole : Amoxicillin	EC_{50} 1.57	EC_{10} 0.41		
			Acetylsalycilic acid : Amoxicillin	EC_{50} 2.17	EC_{10} 0.72		
			Predicted no-effect concentration (five pharmaceutical compound mixture)	EC_{50} 1.36	EC_{10} 0.61		
Three pharmaceuticals	Binary and ternary combinations	Bacteria *A. fischeri* Cyanobacteria *Anabaena* CPB4337	Applying the combination index with isobologram equation methods from pharmaceutical compounds for in vitro and in vivo bioassay	Antagonism	Synergism	Departure from combination index (CA and IA) with isobologram equation	[182]
			Fenofibrate : Bezafibrate	EC_{90} 2.59 EC_{50} 1.19	EC_{10} 0.55		
			Fenofibrate : Gemfibrozil	EC_{90} 12.9 EC_{50} 1.29	EC_{10} 0.13		

				Fenofibrate : Gemfibrozil : Bezafibrate	EC_{90} 3.92	EC_{50} 0.57 EC_{10} 0.09	
Five antibiotics	Binary and multicomponent mixture	Cyanobacteria *Anabaena* CPB4337 Microalgae *Raphidocelis subcapitata*	Applying combination index with isobologram equation methods from pharmaceutical compound for in vitro and in vivo bioassay		Antagonism	Synergism	Departure from combination index (CA and IA) with isobologram equation [183]
				Levofloxacin : Tetracycline	EC_{50} 1.6	EC_{10} 0.37	

2

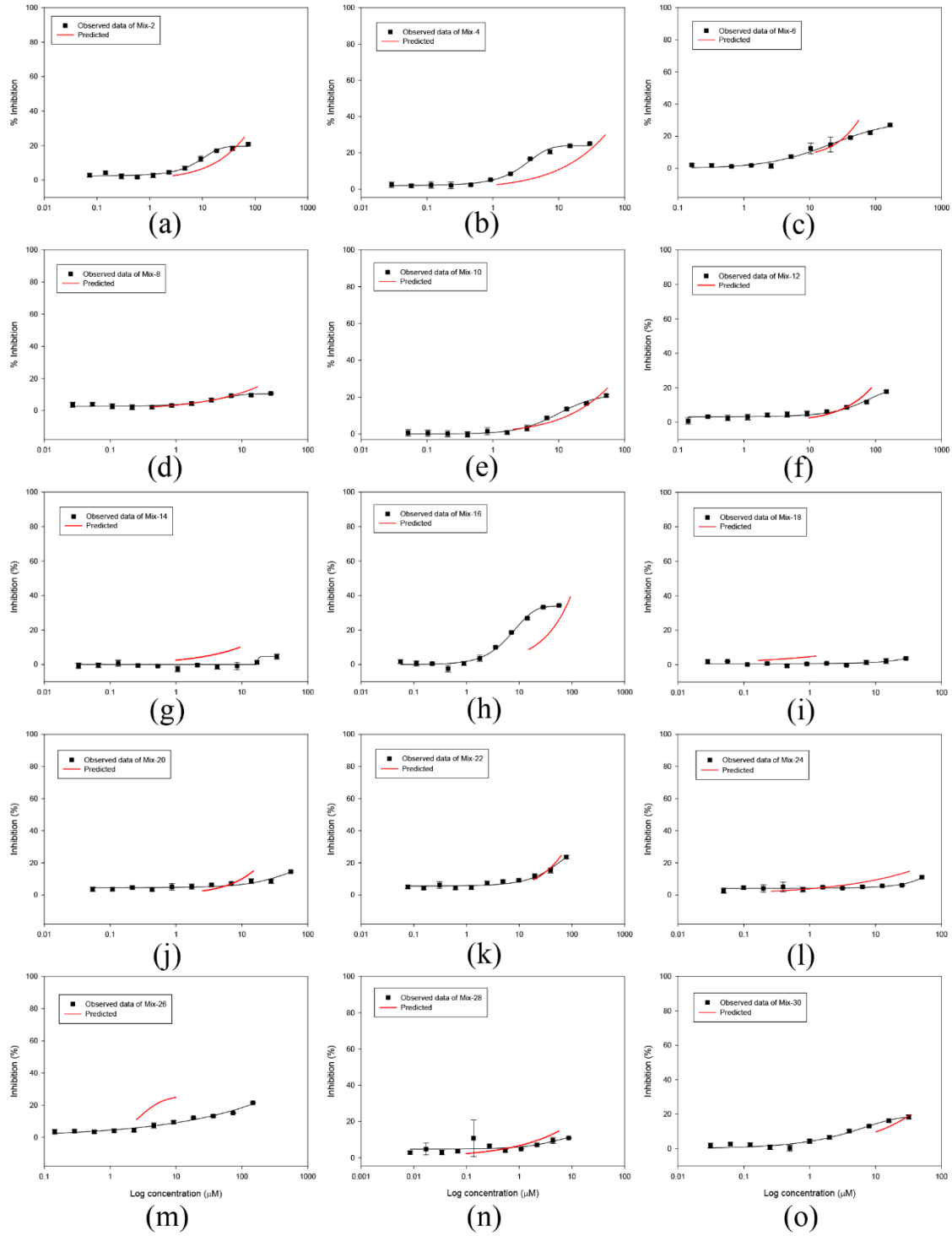

Figure 3. The DRCs for the observed bioluminescent inhibitions and the predicted inhibition [red lines] for the CA model for in the binary equitoxic mixtures and based on ratios at 10 % effective concentrations for each component (the data points are geometric means ± standard deviation [SD] of experimentally observed data, and statistical best-fits for regression models are summarized in Table 3).

As shown in Figure 3 and Table 4, the reason for not available (i.e., n.a.) data indicates that they did not reach the EC_{50} and EC_{10} ranges. Thus, all binaries of the EC_{10} ratio mixtures (i.e., EC_{10mix}) were not calculated for interactions from the binary mixture at EC_{50} ranges. Two binaries of EC_{10mix} (Mixture 14 and 18) did not reach the experimental data at the EC_{10} ranges. Four binaries of the EC_{10mix} (Mixture 2, 4, 16, and 30) showed synergistic interactions at the EC_{10} ranges, whereas seven additive interactions of EC_{10mix} (Mixture 6, 8, 10, 12, 20, 22, and 26) and two antagonistic interactions of EC_{10mix} (Mixture 24, and 28) occurred at EC_{10} ranges.

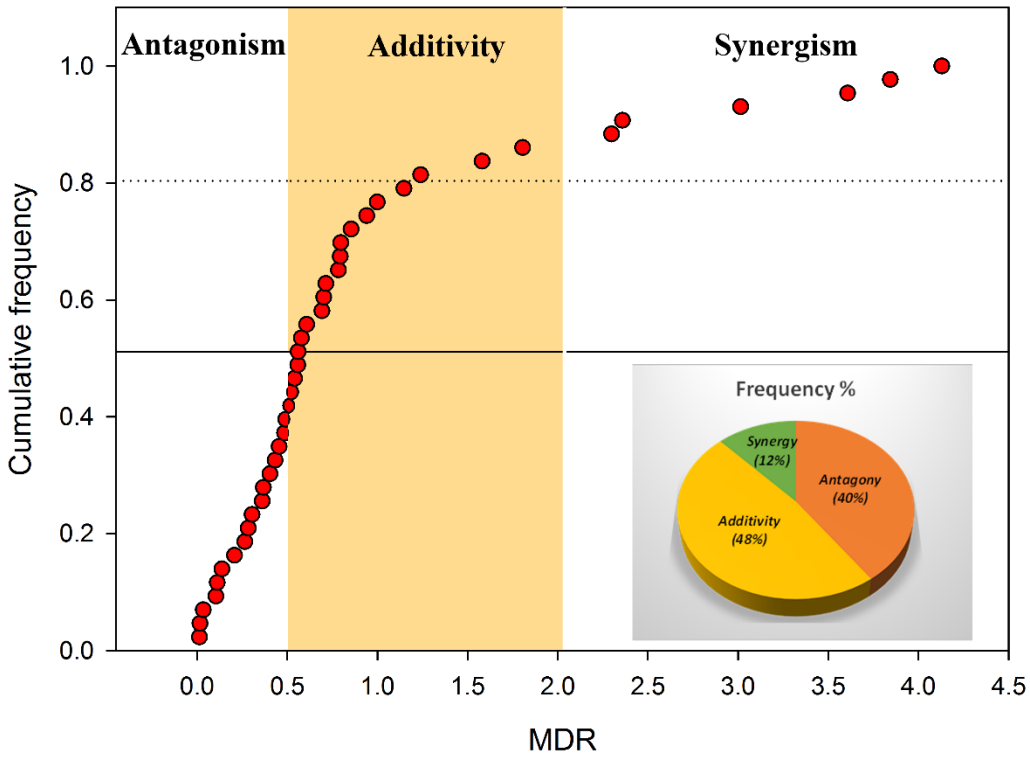

Figure 4. The cumulative distribution of model deviation ratios (MDRs) for quantifying the toxicity interactions of the binary mixtures of pharmaceuticals and pesticides (n = 43 from Table 4, excluding combinations without MDR) for *A. fischeri* (synergism: MDR > 2; additivity: 0.5 ≤ MDR ≤ 2; and antagonism: MDR < 0.5).

Figure 4 illustrates the cumulative distribution of MDRs. In total, the binary combinations of pharmaceuticals and pesticides detected in major river basins in Korea showed 48 %-additive (n = 20 from Table 4 excluding combinations without MDR), 40 %-antagonistic (n = 17), and 12 %-synergistic (n = 6) toxicity effects from 43 binaries on the basis of the MDR values at high [EC_{50}] and low effect [EC_{10}] ranges. In this study, the EC_{10} ratio mixtures were at a low overall effect range and showed a general tendency to have more synergistic effects than EC_{50} ratio mixtures at the high effect range.

4. Conclusions

In this study, the toxicity of the six target compounds (e.g., four pharmaceuticals and two pesticides) detected in major river basins in South Korea and their binary mixtures (30 samples) were tested at high and low effect concentrations (e.g., EC50 and EC10 ratio mixtures) with luminescent bacterium *A. fischeri*. Thus, their toxicological interactions were evaluated at 60 effect concentration data points in total and based on model deviation ratios (MDRs) between predicted and observed toxicity values. The mixture toxicities of these mixtures were also predicted by the CA model to evaluate their toxicological interactions (e.g., additive, synergistic, and antagonistic effects) based on the MDR value. From the 60 data points, MDRs were not possible for 17 points since their toxicities could not be measured. The result showed 48 %-additive (n = 20), 40 %-antagonistic (n = 17), and 12 %-synergistic (n = 6) toxicity effects from 43 binaries (excluding 17 combinations without MDRs). That is, from the mixture toxicity evaluation and modeling, we found twenty combinations of additive effects, seventeen combinations of antagonistic effects and six combinations of synergistic effects. In addition, we found inversion phenomena such as synergism at low concentrations and additive antagonism at high concentrations. The exposure levels of the tested chemicals were less than their environmentally relevant concentrations. Since the environmentally relevant concentrations of pesticides and pharmaceuticals detected in the aquatic environment can be present at low concentrations, further studies with different species need to be conducted to clarify the mechanisms, which can address what creates these inversion phenomena.

5. Acknowledgments

We would like to thank Sungdo Lee for help with the experimental setup. This study was supported by Korea Institute of Science and Technology Europe (KIST-Europe) joint program (Project no. 11805).

6. Author Contributions

YJ Kim, JW Kim and I-H Baek conceived and designed the experiments. I-H Baek performed the experiments. JW Kim analyzed the best-fit curves and modeled the mixture toxicity. SY Baik mass analyzed the stock solution. I-H Baek contributed the reagents/materials/analysis tools. I-H, Baek and JW Kim wrote the paper, and YJ Kim proofread the manuscript.

7. Supplementary tables for:

Investigation of the Synergistic Toxicity of Binary Mixtures of Pesticides and Pharmaceuticals on Aliivibrio fischeri in Major River Basins in South Korea

In-hyuk Baek [1, 2], Youngjun Kim [1, 3], Seungyun Baik [1] and Jongwoon Kim [1, 3, †, *]

[1] Environmental Safety Group, Korea Institute of Science and Technology (KIST) Europe, Campus E 7.1, Saarbruecken, Germany; ih.baek@kist-europe.de @kist-europe.de (I-H.B.); youngjunkim@kist-europe.de (Y.K.); sbaik@kist-europe.de (S.B.); with.jwkim@gmail.com (J.K.)

[2] Center for Bioinformatics, Saarland University, Campus E 2.1, Saarbruecken, Germany

[3] Division of Energy and Environment Technology, KIST School, University of Science and Technology, Hwarang-ro 14-gil, Seoul, Republic of Korea

* Correspondence: with.jwkim@gmail.com

[†] Present address: Chemical Safety Research Center, Korea Research Institute of Chemical Technology (KRICT), 141 Gajeong-ro, Yuseong-gu, Daejeon 34114, Republic of Korea

Table S1. Selected pesticides and pharmaceuticals, which were identified in major river basins in South Korea

Substance	CAS RN	Structure	MW	Type	Use	Reference
Chlortetracycline	57-62-5	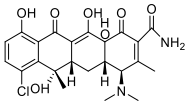	478.88	Pharmaceutical	Veterinary and human medicine	[185-190]
Hexaconazole	79983-71-4	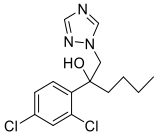	314.21	Pesticide	Fungicide	[191]
Isoprothiolane	50512-35-1	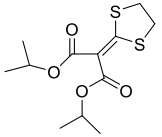	290.40	Pesticide	Fungicide	[191]
Sulfamethoxazole	72-14-0	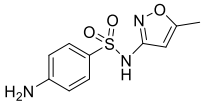	255.32	Pharmaceutical	Human medicine (Antibiotic)	[185, 188-190, 192]
Tetracycline	60-54-8	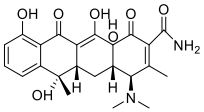	444.43	Pharmaceutical	Veterinary and human medicine	[185, 186, 190, 193]
Trimethoprim	738-70-5	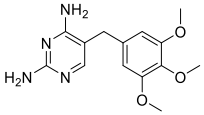	290.32	Pharmaceutical	Human medicine (Antibiotic)	[185, 188-190, 192]

Table S2. The regression models employed in describing the dose-response curves in this study

Regression model	Function
Gompertz (G)	$E(\mathrm{c}) = \alpha\ (\exp\left(-\exp\left(-\left(\frac{-c-\gamma}{\beta}\right)\right)\right))$
Sigmoid (S)	$E(\mathrm{c}) = \frac{\alpha}{1+\exp\left(-\frac{c-\gamma}{\beta}\right)}$
Logistic (L)	$E(\mathrm{c}) = \frac{\alpha}{1+\left(\frac{c}{\gamma}\right)^{\beta}}$
Hill (H)	$E(\mathrm{c}) = \frac{\alpha c^{\beta}}{\gamma^{\beta}+c^{\beta}}$
Chapman (C)	$E(\mathrm{c}) = \alpha\left(1-exp(-\beta c)\right)^{\gamma}$

Notes. E(c): the fractional effect elicited at concentration c; α, β, and γ: parameters of regression models (corresponding statistical estimates)

8. References

1. Kortenkamp, A.; Altenburger, R. Approaches to assessing combination effects of oestrogenic environmental pollutants. *Sci. Total Environ.* **1999**, *233*, 131-140.
2. Junghans, M.; Backhaus, T.; Faust, M.; Scholze, M.; Grimme, L.H. Application and validation of approaches for the predictive hazard assessment of realistic pesticide mixtures. *Aquat Toxicol* **2006**, *76*, 93-110.
3. Plackett, R.L.; Hewlett, P.S. Quantal responses to mixtures of poisons. *Journal of the Royal Statistical Society. Series B (Methodological)* **1952**, *14*, 141-163.
4. German Federal Environment Agency. Ecotoxicological combined effects from chemical mixtures part 1 - relevance and adequate consideration in environmental risk assessment of plant protection products and biocides. Umweltbundesamt: Dessau-Roßlau, Germany, 2014.
5. Kim, J.; Kim, S.; Schaumann, G.E. Reliable predictive computational toxicology methods for mixture toxicity: Toward the development of innovative integrated models for environmental risk assessment. *Reviews in Environmental Science and Bio-Technology* **2013**, *12*, 235-256.
6. European_Commission. *State of the art report on mixture toxicity-final report*; The school of Pharmacy, University of London: London, UK, 2009; pp 1-31.
7. US_EPA. *Guidelines for the health risk assessment of chemical mixtures*; US Environment Protection Agency: Washington DC, USA, 1986; pp 1-29.
8. US_EPA. *Technical support document on health risk assessment of chemical mixtures. Office of research and development*; US Environment Protection Agency: Washington DC, USA, 1990.
9. US_EPA. *Supplementary guidance for conducting health risk assessment of chemical mixtures. Risk assessment forum technical pannel*; US Environment Protection Agency: Washington DC, USA, 2000.
10. Deneer, J.W. Toxicity of mixtures of pesticides in aquatic systems. *Pest Management Science* **2000**, *56*, 516-520.
11. Belden, J.B., Gilliom, R. J., Lydy, M. J. How well can we predict the toxicity of pesticide mixtures to aquatic life? *Integr. Environ. Assess. Manag.* **2007**, *3*, 364-372.
12. Cedergreen, N.; Cristensen, A.M.; Kamper, A.; Kudsk, P.; Mathiassen, S.K.; Streibig, J.C.; Sørensen, H. A rivew of independent action compared to concentration addition as reference models for mixtures of compounds with different molecular target sites. *Environ. Toxicol. Chem.* **2008**, *27*, 1621-1632.
13. Cedergreen, N. Quantifying synergy: A systematic review of mixture toxicity studies within environmental toxicology. *PLoS ONE* **2014**, *9*, e96580.
14. Heys, K.A.; Shore, R.F.; Pereira, M.G.; Jones, K.C.; Martin, F.L. Risk assessment of environmental mixture effects. *RSC Advances* **2016**, *6*, 47844-47857.
15. Kortenkamp, A.; Evans, R.; Faust, M.; Kalberlah, F.; Scholze, M.; Schuhmacher-Wolz, U. Investigation of the state of the science on combined actions of chemicals in food through dissimilar modes of action and proposal for science-based approach for performing related cumulative risk assessment. *EFSA Supporting Publications* **2012**, *9*, 232E-n/a.
16. Smith, J.W.; Seidle, L.G.; Cluff, L.E. Studies on the epideminology of adverse drug reaction (v); clinical factors influencing susceptibility. *Ann. Intern. Med.* **1966**, *65*, 629.
17. Cho, H.Y.; Lee, Y.B. *Mechanism-based drug interactions*. Shinilbooks: Seoul, 2005.
18. Boxall, A.B.A. The environmental side effects of medication. *EMBO Reports* **2004**, *5*, 1110-1116.
19. Ebele, A.J.; Abou-Elwafa Abdallah, M.; Harrad, S. Pharmaceuticals and personal care products (ppcps) in the freshwater aquatic environment. *Emerging Contaminants* **2017**, *3*, 1-16.

20. Jeong, Y.; Schaffer, A.; Smith, K. A comparison of equilibrium and kinetic passive sampling for the monitoring of aquatic organic contaminants in german rivers. *Water Res* **2018**, *145*, 248-258.
21. Battaglin, W.A.; Bradley, P.M.; Iwanowicz, L.; Journey, C.A.; Walsh, H.L.; Blazer, V.S. Pharmaceuticals, hormones, pesticides, and other bioactive contaminants in water, sediment, and tissue from rocky mountain national park, 2012-2013. *Sci Total Environ* **2018**, *643*, 651-673.
22. ISO_11348-3. *Water qualityddetermination of the inhibitory effect of water samples on the light emission of vibrio fischeri (luminescent bacteria test)dpart 3: Method using freeze-dried bacteria.* ; European Committee for Standardization: Brussels, Belgium., **1998**.
23. ASTM_D5660-96. *Standard test method for assessing the microbial detoxification of chemically contaminated water and soil using a toxicity test with a luminescent marine bacterium*; American Society for Testing and Materials: West Conshohocken,Pennsylvania, USA, **2009**.
24. Scholze, M.; Boedeker, W.; Faust, M.; Backhaus, T.; Altenburger, R.; Grimme, L.H. A general best-fit method for concentration-response curves and the estimation of low-effect concentrations. *Environmental Toxicology and Chemistry* **2001**, *20*, 448-457.
25. Kim, M.H.; Park, J.I.; Kim, Y.H.; Choi, K.H. Prioritizing human use antibiotics for environmental health management and estimating their environmental concentrations in korean waterway. *Korean Soc. Environ. Health* **2006**, *10*, 462-468.
26. Korean National Institute of Environmental Research. Development of analytical method and study of exposure of pharmaceuticals and personal care products in environment Seoul, Korea, 2006.
27. Korea Food and Drug Administration. Human exposure assessment for antibiotics in the water environment. Seoul, Korea, 2007.
28. Korean National Institute of Environmental Research. Development of analytical method and study of exposure of pharmaceuticals and personal care products in environment (ii). Seoul, Korea, 2007.
29. Park, J.; Kim, M.-H.; Choi, K.; Kim, Y.; Kim, M.-Y. *Environmental risk assessment of pharmaceutical: Model application for estimating pharmaceutical exposures in the han river basin*; Korea Environment Institute,: Seoul, Korea, 2007.
30. Choi, K.; Kim, Y.; Jung, J.; Kim, M.H.; Kim, C.S.; Kim, N.H.; Park, J. Seasonal variations of several pharmaceutical residues in surface water and sewage treatment plants of han river, korea. *Sci. Total Environ.* **2008**, *405*, 120-128.
31. Kim, J.-H.; Park, C.-K.; Kim, M.-Y.; Ahn, S.-G. Contamination of verterinary antibiotics and antimirobials in han river basin. *J. Korean Soc. Environ. Anal.* **2008**, *11*, 109-118.
32. Korean National Institute of Environmental Research. Environmental risk assessment of pharmaceutical residues. Seoul, Korea, 2008.
33. Lee, J.-H.; Park, B.-J.; Kim, J.-K.; Kim, W.-I.; Hong;, S.-M.; Im, G.-J.; Hong, M.-K. Risk assessment for aquatic organisms of pesticides detected in water phase of six major rivers in korea. *The Korean Journal of Pesticide Science* **2011**, *15*, 48-54.
34. H., K. Fish toxicity tests with mixtures of more than two chemicals: A proposal for a quantitative approach and experimental results. *Toxicology* **1981**, *19*, 229-238.
35. Rolf Altenburger; Thomas Backhaus; Wolfgang Boedeker; Michael Faust; Martin Scholze; Grimme, L.H. Predictability of the toxicity of multiple chemical mixtures to vibrio fischeri: Mixtures composed of similarly acting chemicals. *Environmental toxicology and chemistry* **2000**, *19*, 2341-2347.
36. Thomas Backhaus; Rolf Altenburger; Wolfgang Boedeker; Michael Faust; Martin Scholze; Grim, L.H. Predictability of the toxicity of a multiple mixture of dissimilarly acting chemicals to vibrio fischeri. *Environmental toxicology and chemistry* **2000**, *19*, 2348-2356.

37. Payne, J.; Rajapakse, N.; Wilkins, M.; Kortenkamp, A. Prediction and assessment of the effects of mixtures of four xenoestrogens. *Environ Health Perspect* **2000**, *108*, 983-987.
38. Wang, Z.; Chen, J.; Huang, L.; Wang, Y.; Cai, X.; Qiao, X.; Dong, Y. Integrated fuzzy concentration addition-independent action (ifca-ia) model outperforms two-stage prediction (tsp) for predicting mixture toxicity. *Chemosphere* **2009**, *74*, 735-740.
39. Jongwoon Kim , S.K.G.E.S. Development of a partial least squares–based integrated addition model for predicting mixture toxicity. *Human and Ecological risk Assessment* **2014**, *20*, 174-200.
40. Fang, C.J.; Duan, C.Y.; He, C.; Han, G.; Meng, Q.J. A supramolecular analog of cyclohexane sustained by aromatic c-h center dot center dot center dot pi interactions between ferrocene moieties: Molecular packing of ferrocene-containing thiosemicarbazato metal complexes. *New J Chem* **2000**, *24*, 697-701.
41. Yi-zeng Liang; Kai-tai Fang; Xu, Q.-s. Uniform design and its applications in chemistry and chemical engineering. *Chemometrics and Intelligent Laboratory Systems* **2001**, *58*, 43-57.
42. Zhang, Y.H.; Liu, S.S.; Liu, H.L.; Liu, Z.Z. Evaluation of the combined toxicity of 15 pesticides by uniform design. *Pest management science* **2010**, *66*, 879-887.
43. Kim, J.; Kim, S.; Schaumann, G.E. Development of a partial least squares-based integrated addition model for predicting mixture toxicity. *Human and Ecological Risk Assessment* **2014**, *20*, 174-200.
44. Loewe, S.; Muischnek, H. ber kombinationswirkungen i. Mitteilung: Hilfsmittel der fragestellung. . *Naunyn-Schmiedebergs Arch. Exp. Pathol. Pharmakol.* **1926**, *114*, 313-326.
45. Belden, J.B.; Gilliom, R.J.; Lydy, M.J. How well can we predict the toxicity of pesticide mixtures to aquatic life? *Integrated environmental assessment and management* **2007**, *3*, 364–372.
46. Wieczerzak, M.; Kudłak, B.; Yotova, G.; Nedyalkova, M.; Tsakovski, S.; Simeonov, V.; Namieśnik, J. Modeling of pharmaceuticals mixtures toxicity with deviation ratio and best-fit functions models. *Science of The Total Environment* **2016**, *571*, 259-268.
47. Warne, M.S.J.; Hawker, D.W. The number of components in a mixture determines whether synergistic and antagonistic or additive toxicity predominate: The funnel hypothesis. *Ecotoxicology and Environmental Safety* **1995**, *31*, 23-28.
48. European Commission. Opinion on toxicity and assessment of chemical mixtures. European Commission Brussels, 2012.
49. Wang, Z.; Chen, Q.; Hu, L.; Wang, M. Combined effects of binary antibiotic mixture on growth, microcystin production, and extracellular release of microcystis aeruginosa: Application of response surface methodology. *Environmental science and pollution research international* **2018**, *25*, 736-748.
50. Di Nica, V.; Villa, S.; Finizio, A. Toxicity of individual pharmaceuticals and their mixtures to aliivibrio fischeri: Evidence of toxicological interactions in binary combinations. *Environ Toxicol Chem* **2017**, *36*, 815-822.
51. Rodea-Palomares, I.; Petre, A.L.; Boltes, K.; Leganes, F.; Perdigon-Melon, J.A.; Rosal, R.; Fernandez-Pinas, F. Application of the combination index (ci)-isobologram equation to study the toxicological interactions of lipid regulators in two aquatic bioluminescent organisms. *Water Res* **2010**, *44*, 427-438.
52. Gonzalez-Pleiter, M.; Gonzalo, S.; Rodea-Palomares, I.; Leganes, F.; Rosal, R.; Boltes, K.; Marco, E.; Fernandez-Pinas, F. Toxicity of five antibiotics and their mixtures towards photosynthetic aquatic organisms: Implications for environmental risk assessment. *Water Res* **2013**, *47*, 2050-2064.
53. Wang, T.; Liu, Y.; Wang, D.; Lin, Z.; An, Q.; Yin, C.; Liu, Y. The joint effects of sulfonamides and quorum sensing inhibitors on vibrio fischeri: Differences between the acute and chronic mixed toxicity mechanisms. *J Hazard Mater* **2016**, *310*, 56-67.

Conclusion

This thesis demonstrated the development and application of virus-based molecularly imprinted polymers (MIPs) and bioactive scaffolds using bacteriophages, with potential applications in environmental and biomedical fields. The primary aim was to design a phage-based MIPs system that could selectively detect acidic pharmaceutical compounds such as clofibric acid. The results demonstrated that this system offers enhanced specificity and sensitivity compared to existing detection methods, providing a novel strategy for monitoring and managing pharmaceutical pollution in both environmental and clinical settings. Notably, incorporating bacteriophages into the MIPs enhanced binding affinity through non-covalent interactions between the functionalized phages and target compounds. Particularly, the integration of bacteriophages in the MIPs led to an increase in binding affinity through non-covalent interactions between the functionalized phages and target compounds, and also improving detection limit. Future studies could optimize the mass production and synthesis of phage-based MIPs to create a cost-effective, reusable material that may benefit everyday applications. Additionally, imprinting other pharmaceutical compounds and testing sensitivity and selectivity in complex samples (e.g., wastewater) could expand the practical utility.

The second chapter focuses on developing bioactive scaffolds that promote angiogenesis for tissue engineering and regenerative medicine. The findings showed that bacteriophage-based scaffolds possess the potential to support vascularization and tissue regeneration, suggesting their use as alternative platforms to animal models. This aligns with the 3R principles (Replacement, Reduction, and Refinement) aimed at reducing reliance on animal testing, thereby enhancing experimental efficiency. Moreover, the use of bacteriophages for long-term cell cultures and promoting angiogenesis highlights their potential as innovative biomaterials. Furthermore, this research demonstrated that filamentous bacteriophages functionalized with the growth factor TGF-β1 promote endothelial cell migration, proliferation, and tube formation. The functionalized bacteriophages were shown to maintain biological activity over long-term cell cultures in 3D environments, suggesting their viability as a promising biomaterial for tissue engineering and other biomedical applications. In the future, it will be essential to validate the system's effectiveness not only in controlled settings but also within physiological environments through in vivo experiments. Additionally, expanding the application by incorporating additional growth factors could help address broader regenerative medical challenges

In conclusion, this thesis suggests new applications of filamentous bacteriophages in environmental monitoring and nanomedicine. By integrating phage display technology, molecular imprinting, and nanotechnology, this research contributes to the development of platforms for drug monitoring, detection, and filtration, while also reducing dependency on animal models and enhancing tissue regeneration efficiency. These findings indicate the potential for phage-based systems to serve as innovative

tools in diagnostics and therapeutic applications across nanomedicine and environmental science.

References

1. Adams, M.J., et al., *50 years of the International Committee on Taxonomy of Viruses: progress and prospects.* Arch Virol, 2017. **162**(5): p. 1441-1446.
2. Lefkowitz, E.J., et al., *Virus taxonomy: the database of the International Committee on Taxonomy of Viruses (ICTV).* Nucleic Acids Res, 2018. **46**(D1): p. D708-D717.
3. Knezevic, P., E.M. Adriaenssens, and C. Ictv Report, *ICTV Virus Taxonomy Profile: Inoviridae.* J Gen Virol, 2021. **102**(7).
4. Roux, S., et al., *Cryptic inoviruses revealed as pervasive in bacteria and archaea across Earth's biomes.* Nat Microbiol, 2019. **4**(11): p. 1895-1906.
5. Marvin, D.A., M.F. Symmons, and S.K. Straus, *Structure and assembly of filamentous bacteriophages.* Prog Biophys Mol Biol, 2014. **114**(2): p. 80-122.
6. Wang, Y.A., et al., *The structure of a filamentous bacteriophage.* J Mol Biol, 2006. **361**(2): p. 209-15.
7. van Wezenbeek, P.M., T.J. Hulsebos, and J.G. Schoenmakers, *Nucleotide sequence of the filamentous bacteriophage M13 DNA genome: comparison with phage fd.* Gene, 1980. **11**(1-2): p. 129-48.
8. Hill, D.F. and G.B. Petersen, *Nucleotide sequence of bacteriophage f1 DNA.* J Virol, 1982. **44**(1): p. 32-46.
9. Peeters, B.P., et al., *Nucleotide sequence and genetic organization of the genome of the N-specific filamentous bacteriophage IKe. Comparison with the genome of the F-specific filamentous phages M13, fd and f1.* J Mol Biol, 1985. **181**(1): p. 27-39.
10. Stassen, A.P., et al., *Nucleotide sequence of the genome of the filamentous bacteriophage I2-2: module evolution of the filamentous phage genome.* J Mol Evol, 1992. **34**(2): p. 141-52.
11. Horabin, J.I. and R.E. Webster, *An amino acid sequence which directs membrane insertion causes loss of membrane potential.* J Biol Chem, 1988. **263**(23): p. 11575-83.
12. Zinder, N.D. and K. Horiuchi, *Multiregulatory element of filamentous bacteriophages.* Microbiol Rev, 1985. **49**(2): p. 101-6.
13. Luiten, R.G., et al., *Nucleotide sequence of the genome of Pf3, an IncP-1 plasmid-specific filamentous bacteriophage of Pseudomonas aeruginosa.* J Virol, 1985. **56**(1): p. 268-76.
14. Van, T.T., et al., *Genomic characterization of varphiRS603, a filamentous bacteriophage that is infectious to the phytopathogen Ralstonia solanacearum.* Microbiol Immunol, 2014. **58**(12): p. 697-700.
15. Murugaiyan, S., et al., *Characterization of filamentous bacteriophage PE226 infecting Ralstonia solanacearum strains.* J Appl Microbiol, 2011. **110**(1): p. 296-303.
16. Campos, J., et al., *VEJphi, a novel filamentous phage of Vibrio cholerae able to transduce the cholera toxin genes.* Microbiology (Reading), 2010. **156**(Pt 1): p. 108-115.
17. Nguyen, D.T., et al., *Characterization of Vibrio cholerae O139 of an Aquatic Isolate in Northern Vietnam.* Open Microbiol J, 2012. **6**: p. 14-21.
18. Ikema, M. and Y. Honma, *A novel filamentous phage, fs-2, of Vibrio cholerae O139.*

Microbiology (Reading), 1998. **144 (Pt 7)**: p. 1901-1906.
19. Chan, B., et al., *Isolation and genetic characterization of a novel filamentous bacteriophage, a deleted form of phage f237, from a pandemic Vibrio parahaemolyticus O4:K68 strain.* Microbiol Immunol, 2002. **46**(8): p. 565-9.
20. Chang, B., et al., *Filamentous bacteriophages of Vibrio parahaemolyticus as a possible clue to genetic transmission.* J Bacteriol, 1998. **180**(19): p. 5094-101.
21. Kuo, T.T., et al., *Complete nucleotide sequence of filamentous phage Cf1c from Xanthomonas campestris pv. citri.* Nucleic Acids Res, 1991. **19**(9): p. 2498.
22. Denhardt, D.T., *The single-stranded DNA phages.* CRC Crit Rev Microbiol, 1975. **4**(2): p. 161-223.
23. Ray, D.S., A. Preuss, and P.H. Hofschneider, *Replication of the single-stranded DNA of the male-specific bacteriophage M13: circular forms of the replicative DNA.* J Mol Biol, 1966. **21**(3): p. 485-91.
24. Haigh, N.G. and R.E. Webster, *The pI and pXI assembly proteins serve separate and essential roles in filamentous phage assembly.* J Mol Biol, 1999. **293**(5): p. 1017-27.
25. Henry, T.J. and D. Pratt, *The proteins of bacteriophage M13.* Proc Natl Acad Sci U S A, 1969. **62**(3): p. 800-7.
26. Deng, L.W., P. Malik, and R.N. Perham, *Interaction of the globular domains of pIII protein of filamentous bacteriophage fd with the F-pilus of Escherichia coli.* Virology, 1999. **253**(2): p. 271-7.
27. Gutierrez-Rodarte, M., et al., *The Vibrio cholerae minor pilin TcpB mediates uptake of the cholera toxin phage CTXphi.* J Biol Chem, 2019. **294**(43): p. 15698-15710.
28. Tesar, M., et al., *Monoclonal antibody against pIII of filamentous phage: an immunological tool to study pIII fusion protein expression in phage display systems.* Immunotechnology, 1995. **1**(1): p. 53-64.
29. Li, Q., et al., *Enhanced targeting: Production of filamentous bacteriophage monoclonal antibodies using the major coat protein pVIII as anchor.* Biotechnol J, 2024. **19**(3): p. e2300688.
30. Lee, Y.J., et al., *Fabricating genetically engineered high-power lithium-ion batteries using multiple virus genes.* Science, 2009. **324**(5930): p. 1051-5.
31. Zhou, X., et al., *Advanced detection of cervical cancer biomarkers using engineered filamentous phage nanofibers.* Appl Microbiol Biotechnol, 2024. **108**(1): p. 221.
32. Carrico, Z.M., et al., *N-Terminal labeling of filamentous phage to create cancer marker imaging agents.* ACS Nano, 2012. **6**(8): p. 6675-80.
33. Kim, J.T., et al., *Virus-templated redox nanowire network for enzyme electrode.* Biosens Bioelectron, 2023. **237**: p. 115518.
34. Gavric, D. and P. Knezevic, *Filamentous Pseudomonas Phage Pf4 in the Context of Therapy-Inducibility, Infectivity, Lysogenic Conversion, and Potential Application.* Viruses, 2022. **14**(6).
35. Narancic, J., et al., *First Characterization of Acinetobacter baumannii-Specific Filamentous Phages.* Viruses, 2024. **16**(6).
36. Wang, F., et al., *Bio-mimetic nanostructure self-assembled from Au@Ag heterogeneous*

nanorods and phage fusion proteins for targeted tumor optical detection and photothermal therapy. Sci Rep, 2014. **4**: p. 6808.

37. Dong, X., et al., *Hybrid M13 bacteriophage-based vaccine platform for personalized cancer immunotherapy.* Biomaterials, 2022. **289**: p. 121763.
38. Liu, X., et al., *Highly Effective Stroke Therapy Enabled by Genetically Engineered Viral Nanofibers.* Adv Mater, 2022. **34**(20): p. e2201210.
39. Borg, R.E., et al., *Genetically engineered filamentous phage for bacterial detection using magnetic resonance imaging.* Sens Diagn, 2023. **2**(4): p. 948-955.
40. Szot-Karpinska, K., et al., *Modified Filamentous Bacteriophage as a Scaffold for Carbon Nanofiber.* Bioconjug Chem, 2016. **27**(12): p. 2900-2910.
41. Korkmaz Zirpel, N., T. Arslan, and H. Lee, *Engineering filamentous bacteriophages for enhanced gold binding and metallization properties.* J Colloid Interface Sci, 2015. **454**: p. 80-8.
42. Joung-Il Moon, E.J.C., Younju Joung, Jin-Woo Oh, Sang-Woo Joo, Jaebum Choo, *Development of highly sensitive plasmonic biosensors encoded with gold nanoparticles on M13 bacteriophage networks.* Sensors and Actuators B: Chemical, 2024. **400**(Part B): p. 1.
43. Oh, D., et al., *Graphene sheets stabilized on genetically engineered M13 viral templates as conducting frameworks for hybrid energy-storage materials.* Small, 2012. **8**(7): p. 1006-11.
44. Baek, I.H., et al., *Detection of Acidic Pharmaceutical Compounds Using Virus-Based Molecularly Imprinted Polymers.* Polymers (Basel), 2018. **10**(9).
45. Halling-Sorensen, B., et al., *Occurrence, fate and effects of pharmaceutical substances in the environment--a review.* Chemosphere, 1998. **36**(2): p. 357-93.
46. Sacher, F., et al., *Pharmaceutical residues in the river Rhine--results of a one-decade monitoring programme.* J Environ Monit, 2008. **10**(5): p. 664-70.
47. Jux, U., et al., *Detection of pharmaceutical contaminations of river, pond, and tap water from Cologne (Germany) and surroundings.* Int J Hyg Environ Health, 2002. **205**(5): p. 393-8.
48. Stan, T.H.H.-J., *Determination of Clofibric Acid and N-(Phenylsulfonyl)-Sarcosine in Sewage, River and Drinking Water.* International Journal of Environmental Analytical Chemistry, 1997. **67**: p. 113-124
49. Hans-Rudolf Buser, M.D.M., *Occurrence of the Pharmaceutical Drug Clofibric Acid and the Herbicide Mecoprop in Various Swiss Lakes and in the North Sea.* Environ. Sci. Technol., 1998. **32** ((1)): p. 188–192.
50. Pagano, R.E., et al., *Membrane traffic in sphingolipid storage diseases.* Traffic, 2000. **1**(11): p. 807-815.
51. Esplugas, S., et al., *Ozonation and advanced oxidation technologies to remove endocrine disrupting chemicals (EDCs) and pharmaceuticals and personal care products (PPCPs) in water effluents.* J Hazard Mater, 2007. **149**(3): p. 631-42.
52. Yilmaz, E., K. Mosbach, and K. Haupt, *Influence of functional and cross-linking monomers and the amount of template on the performance of molecularly imprinted polymers in binding assays.* Analytical Communications, 1999. **36**(5): p. 167-170.
53. Lele, B.S., M.G. Kulkarni, and R.A. Mashelkar, *Molecularly imprinted polymer mimics of*

chymotrypsin - 1. Cooperative effects and substrate specificity. Reactive & Functional Polymers, 1999. **39**(1): p. 37-52.

54. Korkmaz, N., Y.J. Kim, and C.H. Nam, *Bacteriophages as templates for manufacturing supramolecular structures.* Macromol Biosci, 2013. **13**(3): p. 376-87.
55. Nezhadali, A., Z. Es'haghi, and A. Khatibi, *Selective extraction of progesterone hormones from environmental and biological samples using a polypyrrole molecularly imprinted polymer and determination by gas chromatography.* Analytical Methods, 2016. **8**(8): p. 1813-1827.
56. Lindqvist, N., T. Tuhkanen, and L. Kronberg, *Occurrence of acidic pharmaceuticals in raw and treated sewages and in receiving waters.* Water Res, 2005. **39**(11): p. 2219-28.
57. Loos, R., et al., *EU-wide survey of polar organic persistent pollutants in European river waters.* Environ Pollut, 2009. **157**(2): p. 561-8.
58. Tan, C.J. and Y.W. Tong, *The effect of protein structural conformation on nanoparticle molecular imprinting of ribonuclease A using miniemulsion polymerization.* Langmuir, 2007. **23**(5): p. 2722-2730.
59. Kanazawa, K.K., et al., *Organic Metals - Polypyrrole, a Stable Synthetic Metallic Polymer.* Journal of the Chemical Society-Chemical Communications, 1979(19): p. 854-855.
60. Niu, Z.W., et al., *Bacteriophage M13 as a Scaffold for Preparing Conductive Polymeric Composite Fibers.* Nano Research, 2008. **1**(3): p. 235-241.
61. Tseng, R.J., et al., *Digital memory device based on tobacco mosaic virus conjugated with nanoparticles.* Nature Nanotechnology, 2006. **1**(1): p. 72-77.
62. Arter, J.A., et al., *Virus-PEDOT nanowires for biosensing.* Nano Lett, 2010. **10**(12): p. 4858-62.
63. Arter, J.A., et al., *Virus-PEDOT Nanowires for Biosensing.* Nano Letters, 2010. **10**(12): p. 4858-4862.
64. Lee, J.W., et al., *Nanoscale bacteriophage biosensors beyond phage display.* International Journal of Nanomedicine, 2013. **8**: p. 3917-3925.
65. Singh, A., et al., *Bacteriophage based probes for pathogen detection.* Analyst, 2012. **137**(15): p. 3405-3421.
66. Chen, J.H., et al., *Detection of Escherichia coli in Drinking Water Using T7 Bacteriophage-Conjugated Magnetic Probe.* Analytical Chemistry, 2015. **87**(17): p. 8977-8984.
67. Sorokulova, I., E. Olsen, and V. Vodyanoy, *Bacteriophage biosensors for antibiotic-resistant bacteria.* Expert Review of Medical Devices, 2014. **11**(2): p. 175-186.
68. Shirale, D.J., et al., *Label-Free Chemiresistive Immunosensors for Viruses.* Environmental Science & Technology, 2010. **44**(23): p. 9030-9035.
69. Lee, S.K., D.S. Yun, and A.M. Belcher, *Cobalt ion mediated self-assembly of genetically engineered bacteriophage for biomimetic Co-Pt hybrid material.* Biomacromolecules, 2006. **7**(1): p. 14-17.
70. Yacoby, I., et al., *Targeting antibacterial agents by using drug-carrying filamentous bacteriophages.* Antimicrobial Agents and Chemotherapy, 2006. **50**(6): p. 2087-2097.
71. Merzlyak, A., S. Indrakanti, and S.W. Lee, *Genetically Engineered Nanofiber-Like Viruses For Tissue Regenerating Materials.* Nano Letters, 2009. **9**(2): p. 846-852.

72. Oh, D.Y., et al., *Graphene Sheets Stabilized on Genetically Engineered M13 Viral Templates as Conducting Frameworks for Hybrid Energy-Storage Materials.* Small, 2012. **8**(7): p. 1006-1011.
73. Huang, D.L., et al., *Application of molecularly imprinted polymers in wastewater treatment: a review.* Environmental Science and Pollution Research, 2015. **22**(2): p. 963-977.
74. Dai, C.M., et al., *Application of Molecularly Imprinted Polymers to Selective Removal of Clofibric Acid from Water.* PLoS One, 2013. **8**(10).
75. Korkmaz, N., Y.J. Kim, and C.H. Nam, *Bacteriophages as Templates for Manufacturing Supramolecular Structures.* Macromolecular Bioscience, 2013. **13**(3): p. 376-387.
76. Warner, C.M., et al., *M13 bacteriophage production for large-scale applications.* Bioprocess and Biosystems Engineering, 2014. **37**(10): p. 2067-2072.
77. Wang, L., et al., *Occurrence and risk assessment of acidic pharmaceuticals in the Yellow River, Hai River and Liao River of north China.* Sci Total Environ, 2010. **408**(16): p. 3139-47.
78. Warner, C.M., et al., *M13 bacteriophage production for large-scale applications.* Bioprocess Biosyst Eng, 2014. **37**(10): p. 2067-72.
79. D.J. Abraham, R.D.R., *The structure elucidation of Rhazinilam, a new class of Alkaloids from the apocynaceae, by X-ray analysis.* Tetrahedron Letters, 1972. **13**(10): p. 909-912.
80. Ghadari, R., *A study on the interactions of amino acids with nitrogen doped graphene; docking, MD simulation, and QM/MM studies.* Phys Chem Chem Phys, 2016. **18**(6): p. 4352-61.
81. Emudianughe, T.S., et al., *Species differences in the metabolic conjugation of clofibric acid and clofibrate in laboratory animals and man.* Drug Metab Dispos, 1983. **11**(2): p. 97-102.
82. Bhattacharjee, S., M.J. Glucksman, and L. Makowski, *Structural Polymorphism Correlated to Surface-Charge in Filamentous Bacteriophages.* Biophysical Journal, 1992. **61**(3): p. 725-735.
83. Hunter, C.A., et al., *Aromatic interactions.* Journal of the Chemical Society-Perkin Transactions 2, 2001(5): p. 651-669.
84. Modin, C., et al., *QCM-D studies of attachment and differential spreading of pre-osteoblastic cells on Ta and Cr surfaces.* Biomaterials, 2006. **27**(8): p. 1346-54.
85. Duner, G., E. Thormann, and A. Dedinaite, *Quartz Crystal Microbalance with Dissipation (QCM-D) studies of the viscoelastic response from a continuously growing grafted polyelectrolyte layer.* J Colloid Interface Sci, 2013. **408**: p. 229-34.
86. Weigel, S., J. Kuhlmann, and H. Huhnerfuss, *Drugs and personal care products as ubiquitous pollutants: occurrence and distribution of clofibric acid, caffeine and DEET in the North Sea.* Sci Total Environ, 2002. **295**(1-3): p. 131-41.
87. Heberer, T., K. Schmidt-Baumler, and H.J. Stan, *Occurrence and distribution of organic contaminants in the aquatic system in Berlin. Part 1: Drug residues and other polar contaminants in Berlin surface and groundwater.* Acta Hydrochimica Et Hydrobiologica, 1998. **26**(5): p. 272-278.
88. Svenson, J., et al., *Spectroscopic studies of the molecular imprinting self-assembly process.* J Mol Recognit, 1998. **11**(1-6): p. 83-6.
89. Schweiger, B., et al., *Electropolymerized molecularly imprinted polypyrrole film for sensing*

of clofibric acid. Sensors (Basel), 2015. **15**(3): p. 4870-89.

90. In-Hyuk Baek, V.H., Youngjun Kim, *Genetically Engineered Filamentous Bacteriophages Displaying TGF-β1 Promote Angiogenesis in 3D Microenvironments.* Journal of Functional Biomaterials, 2024. **15**(11).
91. Gupta, S., et al., *Hemostasis vs. homeostasis: Platelets are essential for preserving vascular barrier function in the absence of injury or inflammation.* Proc Natl Acad Sci U S A, 2020. **117**(39): p. 24316-24325.
92. Ribatti, D., et al., *Surface markers: An identity card of endothelial cells.* Microcirculation, 2020. **27**(1): p. e12587.
93. Annan, D.A., et al., *Tumor Endothelial Cell-A Biological Tool for Translational Cancer Research.* Int J Mol Sci, 2020. **21**(9).
94. Kim, S., et al., *Vasculature-On-A-Chip for In Vitro Disease Models.* Bioengineering (Basel), 2017. **4**(1).
95. Safari, Z., et al., *Promotion of angiogenesis by M13 phage and RGD peptide in vitro and in vivo.* Sci Rep, 2019. **9**(1): p. 11182.
96. Turnbull, G., et al., *3D bioactive composite scaffolds for bone tissue engineering.* Bioact Mater, 2018. **3**(3): p. 278-314.
97. Rybinski, B., J. Franco-Barraza, and E. Cukierman, *The wound healing, chronic fibrosis, and cancer progression triad.* Physiol Genomics, 2014. **46**(7): p. 223-44.
98. Dvorak, H.F., *Tumors: wounds that do not heal. Similarities between tumor stroma generation and wound healing.* N Engl J Med, 1986. **315**(26): p. 1650-9.
99. Chung, J.Y., et al., *TGF-beta Signaling: From Tissue Fibrosis to Tumor Microenvironment.* Int J Mol Sci, 2021. **22**(14).
100. Meulmeester, E. and P. Ten Dijke, *The dynamic roles of TGF-beta in cancer.* J Pathol, 2011. **223**(2): p. 205-18.
101. Kurakazu, I., et al., *TGFbeta1 signaling protects chondrocytes against oxidative stress via FOXO1-autophagy axis.* Osteoarthritis Cartilage, 2021. **29**(11): p. 1600-1613.
102. Zacher, A.N., 3rd, et al., *A new filamentous phage cloning vector: fd-tet.* Gene, 1980. **9**(1-2): p. 127-40.
103. Enshell-Seijffers, D., L. Smelyanski, and J.M. Gershoni, *The rational design of a 'type 88' genetically stable peptide display vector in the filamentous bacteriophage fd.* Nucleic Acids Res, 2001. **29**(10): p. E50-0.
104. Staquicini, D.I., et al., *Design and proof of concept for targeted phage-based COVID-19 vaccination strategies with a streamlined cold-free supply chain.* Proc Natl Acad Sci U S A, 2021. **118**(30).
105. Winton, A.J. and M.A. Allen, *Rational Design of a Bifunctional Peptide Exhibiting Lithium Titanate Oxide and Carbon Nanotube Affinities for Lithium-Ion Battery Applications.* ACS Appl Mater Interfaces, 2023. **15**(6): p. 8579-8589.
106. Xu, P., et al., *Screening of specific binding peptides using phage-display techniques and their biosensing applications.* TrAC Trends in Analytical Chemistry, 2021. **137**(116229).
107. Mairaville, C., et al., *Identification of monoclonal antibodies from naive antibody phage-*

display libraries for protein detection in formalin-fixed paraffin-embedded tissues. J Immunol Methods, 2024. **532**: p. 113730.

108. Sanmukh, S.G., et al., *Bacterial RNA virus MS2 exposure increases the expression of cancer progression genes in the LNCaP prostate cancer cell line.* Oncol Lett, 2023. **25**(2): p. 86.
109. van Houten, N.E., et al., *Filamentous phage as an immunogenic carrier to elicit focused antibody responses against a synthetic peptide.* Vaccine, 2006. **24**(19): p. 4188-200.
110. Samoylova, T.I., et al., *Immunocontraception: Filamentous Bacteriophage as a Platform for Vaccine Development.* Curr Med Chem, 2017. **24**(35): p. 3907-3920.
111. Barbu, E.M., K.C. Cady, and B. Hubby, *Phage Therapy in the Era of Synthetic Biology.* Cold Spring Harb Perspect Biol, 2016. **8**(10).
112. Bhattacharjee, S., M.J. Glucksman, and L. Makowski, *Structural polymorphism correlated to surface charge in filamentous bacteriophages.* Biophys J, 1992. **61**(3): p. 725-35.
113. Cuccia, N.L., et al., *Pore-size dependence and slow relaxation of hydrogel friction on smooth surfaces.* Proc Natl Acad Sci U S A, 2020. **117**(21): p. 11247-11256.
114. Choi, D.S., et al., *Cyclic RGD peptide incorporation on phage major coat proteins for improved internalization by HeLa cells.* Bioconjug Chem, 2014. **25**(2): p. 216-23.
115. Yamamoto, K.R., et al., *Rapid bacteriophage sedimentation in the presence of polyethylene glycol and its application to large-scale virus purification.* Virology, 1970. **40**(3): p. 734-44.
116. Ando, J. and K. Yamamoto, *Effects of shear stress and stretch on endothelial function.* Antioxid Redox Signal, 2011. **15**(5): p. 1389-403.
117. Kocherova, I., et al., *Human Umbilical Vein Endothelial Cells (HUVECs) Co-Culture with Osteogenic Cells: From Molecular Communication to Engineering Prevascularised Bone Grafts.* J Clin Med, 2019. **8**(10).
118. Quintard, C., et al., *A microfluidic platform integrating functional vascularized organoids-on-chip.* Nat Commun, 2024. **15**(1): p. 1452.
119. Hussey, G.S., M.C. Cramer, and S.F. Badylak, *Extracellular Matrix Bioscaffolds for Building Gastrointestinal Tissue.* Cell Mol Gastroenterol Hepatol, 2018. **5**(1): p. 1-13.
120. Abbott, A., *Cell culture: biology's new dimension.* Nature, 2003. **424**(6951): p. 870-2.
121. *National Institute of Allergy and Infectious Diseases (NIAID) A Phase 1b/2 Trial of the Safety and Microbiological Activity of Bacteriophage Therapy in Cystic Fibrosis Subjects Colonized with Pseudomonas Aeruginosa. [(accessed on 28 February 2023)]; Available online: https://clinicaltrials.gov/ct2/show/NCT05453578*.
122. Meixian, L., et al., *Saponin I from Shuitianqi () inhibits metastasis by negatively regulating the transforming growth factor-beta1/Smad7 network and epithelial-mesenchymal transition in the intrahepatic metastasis Bagg's Albino/c mouse model.* J Tradit Chin Med, 2024. **44**(4): p. 642-651.
123. Yoon, J., et al., *Angiogenic Type I Collagen Extracellular Matrix Integrated with Recombinant Bacteriophages Displaying Vascular Endothelial Growth Factors.* Adv Healthc Mater, 2016. **5**(2): p. 205-12.
124. Doub, J.B., *Risk of Bacteriophage Therapeutics to Transfer Genetic Material and Contain Contaminants Beyond Endotoxins with Clinically Relevant Mitigation Strategies.* Infect Drug

Resist, 2021. **14**: p. 5629-5637.
125. Luong, T., et al., *Standardized bacteriophage purification for personalized phage therapy.* Nat Protoc, 2020. **15**(9): p. 2867-2890.
126. Bohle, A.S. and H. Kalthoff, *Molecular mechanisms of tumor metastasis and angiogenesis.* Langenbecks Arch Surg, 1999. **384**(2): p. 133-40.
127. Vajkoczy, P., A. Ullrich, and M.D. Menger, *Intravital fluorescence videomicroscopy to study tumor angiogenesis and microcirculation.* Neoplasia, 2000. **2**(1-2): p. 53-61.
128. Choi, D.H., et al., *Analyzing angiogenesis on a chip using deep learning-based image processing.* Lab Chip, 2023. **23**(3): p. 475-484.
129. Caballero, D., et al., *Tumour-vessel-on-a-chip models for drug delivery.* Lab Chip, 2017. **17**(22): p. 3760-3771.
130. Ko, J., et al., *Tumor spheroid-on-a-chip: a standardized microfluidic culture platform for investigating tumor angiogenesis.* Lab Chip, 2019. **19**(17): p. 2822-2833.
131. Baek, I.H., et al., *Investigation of the Synergistic Toxicity of Binary Mixtures of Pesticides and Pharmaceuticals on Aliivibrio fischeri in Major River Basins in South Korea.* Int J Environ Res Public Health, 2019. **16**(2).
132. Kortenkamp, A. and R. Altenburger, *Approaches to assessing combination effects of oestrogenic environmental pollutants.* Sci. Total Environ., 1999. **233**(1-3): p. 131-140.
133. Junghans, M., et al., *Application and validation of approaches for the predictive hazard assessment of realistic pesticide mixtures.* Aquat Toxicol, 2006. **76**(2): p. 93-110.
134. Plackett, R.L. and P.S. Hewlett, *Quantal responses to mixtures of poisons.* Journal of the Royal Statistical Society. Series B (Methodological), 1952. **14**(2): p. 141-163.
135. German Federal Environment Agency, *Ecotoxicological Combined Effects from Chemical Mixtures Part 1 - Relevance and Adequate Consideration in Environmental Risk Assessment of Plant Protection Products and Biocides*. 2014, Umweltbundesamt: Dessau-Roßlau, Germany.
136. Kim, J., S. Kim, and G.E. Schaumann, *Reliable predictive computational toxicology methods for mixture toxicity: toward the development of innovative integrated models for environmental risk assessment.* Reviews in Environmental Science and Bio-Technology, 2013. **12**(3): p. 235-256.
137. European_Commission, *State of the Art Report on Mixture Toxicity-final report*. 2009, The school of Pharmacy, University of London: London, UK. p. 1-31.
138. US_EPA, *Guidelines for the health risk assessment of chemical mixtures*. 1986, US Environment Protection Agency: Washington DC, USA. p. 1-29.
139. US_EPA, *Technical support document on health risk assessment of chemical mixtures. Office of Research and Development*. 1990, US Environment Protection Agency: Washington DC, USA.
140. US_EPA, *Supplementary guidance for conducting health risk assessment of chemical mixtures. Risk assessment forum technical pannel*. 2000, US Environment Protection Agency: Washington DC, USA.
141. Deneer, J.W., *Toxicity of mixtures of pesticides in aquatic systems.* Pest Management Science,

2000. **56**(6): p. 516-520.

142. Belden, J.B., Gilliom, R. J., Lydy, M. J., *How well can we predict the toxicity of pesticide mixtures to aquatic life?* Integr. Environ. Assess. Manag., 2007. **3**(3): p. 364-372.
143. Cedergreen, N., et al., *A rivew of independent action compared to concentration addition as reference models for mixtures of compounds with different molecular target sites.* Environ. Toxicol. Chem., 2008. **27**(7): p. 1621-1632.
144. Cedergreen, N., *Quantifying Synergy: A Systematic Review of Mixture Toxicity Studies within Environmental Toxicology.* PLoS ONE, 2014. **9**(5): p. e96580.
145. Heys, K.A., et al., *Risk assessment of environmental mixture effects.* RSC Advances, 2016. **6**(53): p. 47844-47857.
146. Kortenkamp, A., et al., *Investigation of the state of the science on combined actions of chemicals in food through dissimilar modes of action and proposal for science-based approach for performing related cumulative risk assessment.* EFSA Supporting Publications, 2012. **9**(1): p. 232E-n/a.
147. Smith, J.W., L.G. Seidle, and L.E. Cluff, *Studies on the epideminology of adverse drug reaction (v); Clinical factors influencing susceptibility.* Ann. Intern. Med., 1966. **65**: p. 629.
148. Cho, H.Y. and Y.B. Lee, *Mechanism-based Drug Interactions*. 2005, Seoul: Shinilbooks.
149. Boxall, A.B.A., *The environmental side effects of medication.* EMBO Reports, 2004. **5**(12): p. 1110-1116.
150. Ebele, A.J., M. Abou-Elwafa Abdallah, and S. Harrad, *Pharmaceuticals and personal care products (PPCPs) in the freshwater aquatic environment.* Emerging Contaminants, 2017. **3**(1): p. 1-16.
151. Jeong, Y., A. Schaffer, and K. Smith, *A comparison of equilibrium and kinetic passive sampling for the monitoring of aquatic organic contaminants in German rivers.* Water Res, 2018. **145**: p. 248-258.
152. Battaglin, W.A., et al., *Pharmaceuticals, hormones, pesticides, and other bioactive contaminants in water, sediment, and tissue from Rocky Mountain National Park, 2012-2013.* Sci Total Environ, 2018. **643**: p. 651-673.
153. ISO_11348-3, *Water QualitydDetermination of the Inhibitory Effect of Water Samples on the Light Emission of Vibrio fischeri (Luminescent Bacteria Test)dPart 3: Method Using Freeze-Dried Bacteria.* , in *International Organization for Standardization*. **1998**, European Committee for Standardization: Brussels, Belgium.
154. ASTM_D5660-96, *Standard Test Method for Assessing the Microbial Detoxification of Chemically Contaminated Water and Soil Using a Toxicity Test with a Luminescent Marine Bacterium*. **2009**, American Society for Testing and Materials: West Conshohocken,Pennsylvania, USA.
155. Scholze, M., et al., *A general best-fit method for concentration-response curves and the estimation of low-effect concentrations.* Environmental Toxicology and Chemistry, 2001. **20**(2): p. 448-457.
156. Kim, M.H., et al., *Prioritizing Human Use Antibiotics for Environmental Health Management and Estimating Their Environmental Concentrations in Korean Waterway.* Korean Soc. Environ.

Health, 2006. **10**: p. 462-468.
157. Korean National Institute of Environmental Research, *Development of Analytical Method and Study of Exposure of Pharmaceuticals and Personal Care Products in Environment* 2006: Seoul, Korea.
158. Korea Food and Drug Administration, *Human exposure assessment for antibiotics in the water environment*. 2007: Seoul, Korea.
159. Korean National Institute of Environmental Research, *Development of Analytical Method and Study of Exposure of Pharmaceuticals and Personal Care Products in Environment (II)*. 2007: Seoul, Korea.
160. Park, J., et al., *Environmental risk assessment of pharmaceutical: Model application for estimating pharmaceutical exposures in the Han River basin*. 2007, Korea Environment Institute,: Seoul, Korea.
161. Choi, K., et al., *Seasonal variations of several pharmaceutical residues in surface water and sewage treatment plants of Han River, Korea.* Sci. Total Environ., 2008. **405**(1-3): p. 120-128.
162. Kim, J.-H., et al., *Contamination of verterinary antibiotics and antimirobials in Han River basin.* J. Korean Soc. Environ. Anal., 2008. **11**(2): p. 109-118.
163. Korean National Institute of Environmental Research, *Environmental Risk Assessment of Pharmaceutical Residues*. 2008: Seoul, Korea.
164. Lee, J.-H., et al., *Risk Assessment for Aquatic Organisms of Pesticides Detected in Water Phase of Six Major Rivers in Korea.* The Korean Journal of Pesticide Science, 2011. **15**(1): p. 48-54.
165. H., K., *Fish toxicity tests with mixtures of more than two chemicals: a proposal for a quantitative approach and experimental results.* Toxicology, 1981. **19**(3): p. 229-38.
166. Rolf Altenburger, et al., *Predictability of the toxicity of multiple chemical mixtures to Vibrio fischeri: Mixtures composed of similarly acting chemicals.* Environmental toxicology and chemistry, 2000. **19**(9): p. 2341-2347.
167. Thomas Backhaus, et al., *Predictability of the toxicity of a multiple mixture of dissimilarly acting chemicals to Vibrio fischeri.* Environmental toxicology and chemistry, 2000. **19**(9): p. 2348-2356.
168. Payne, J., et al., *Prediction and assessment of the effects of mixtures of four xenoestrogens.* Environ Health Perspect, 2000. **108**(10): p. 983-7.
169. Wang, Z., et al., *Integrated fuzzy concentration addition-independent action (IFCA-IA) model outperforms two-stage prediction (TSP) for predicting mixture toxicity.* Chemosphere, 2009. **74**(5): p. 735-40.
170. Jongwoon Kim , S.K.G.E.S., *Development of a Partial Least Squares–Based Integrated Addition Model for Predicting Mixture Toxicity.* Human and Ecological risk Assessment, 2014. **20**(1): p. 174-200.
171. Fang, C.J., et al., *A supramolecular analog of cyclohexane sustained by aromatic C-H center dot center dot center dot pi interactions between ferrocene moieties: molecular packing of ferrocene-containing thiosemicarbazato metal complexes.* New Journal of Chemistry, 2000. **24**(9): p. 697-701.

172. Yi-zeng Liang, Kai-tai Fang, and Q.-s. Xu, *Uniform design and its applications in chemistry and chemical engineering.* Chemometrics and Intelligent Laboratory Systems, 2001. **58**(1): p. 43-57.
173. Zhang, Y.H., et al., *Evaluation of the combined toxicity of 15 pesticides by uniform design.* Pest Manag Sci, 2010. **66**(8): p. 879-87.
174. Kim, J., S. Kim, and G.E. Schaumann, *Development of a Partial Least Squares-Based Integrated Addition Model for Predicting Mixture Toxicity.* Human and Ecological Risk Assessment, 2014. **20**(1): p. 174-200.
175. Loewe, S. and H. Muischnek, *Über Kombinationswirkungen I. Mitteilung: Hilfsmittel der Fragestellung. .* Naunyn-Schmiedebergs Arch. Exp. Pathol. Pharmakol., 1926. **114**: p. 313-326.
176. Belden, J.B., R.J. Gilliom, and M.J. Lydy, *How well can we predict the toxicity of pesticide mixtures to aquatic life?* Integrated environmental assessment and management, 2007. **3**: p. 364–372.
177. Wieczerzak, M., et al., *Modeling of pharmaceuticals mixtures toxicity with deviation ratio and best-fit functions models.* Science of The Total Environment, 2016. **571**: p. 259-268.
178. Warne, M.S.J. and D.W. Hawker, *The Number of Components in a Mixture Determines Whether Synergistic and Antagonistic or Additive Toxicity Predominate: The Funnel Hypothesis.* Ecotoxicology and Environmental Safety, 1995. **31**(1): p. 23-28.
179. European Commission, *Opinion on Toxicity and Assessment of Chemical Mixtures*. 2012, European Commission Brussels.
180. Wang, Z., et al., *Combined effects of binary antibiotic mixture on growth, microcystin production, and extracellular release of Microcystis aeruginosa: application of response surface methodology.* Environ Sci Pollut Res Int, 2018. **25**(1): p. 736-748.
181. Di Nica, V., S. Villa, and A. Finizio, *Toxicity of individual pharmaceuticals and their mixtures to Aliivibrio fischeri: Evidence of toxicological interactions in binary combinations.* Environ Toxicol Chem, 2017. **36**(3): p. 815-822.
182. Rodea-Palomares, I., et al., *Application of the combination index (CI)-isobologram equation to study the toxicological interactions of lipid regulators in two aquatic bioluminescent organisms.* Water Res, 2010. **44**(2): p. 427-38.
183. Gonzalez-Pleiter, M., et al., *Toxicity of five antibiotics and their mixtures towards photosynthetic aquatic organisms: implications for environmental risk assessment.* Water Res, 2013. **47**(6): p. 2050-64.
184. Wang, T., et al., *The joint effects of sulfonamides and quorum sensing inhibitors on Vibrio fischeri: Differences between the acute and chronic mixed toxicity mechanisms.* J Hazard Mater, 2016. **310**: p. 56-67.
185. Kim, J.-H., et al., *Contamination of verterinary antibiotics and antimirobials in han river basin.* J. of the Korean Society for Environmental Analysis, 2008. **11**(2): p. 109-118 (Korean).
186. Kim, M.H., et al., *Prioritizing Human Use Antibiotics for Environmental Health Management and Estimating Their Environmental Concentrations in Korean Waterway.* Korean Journal of Environmental Health, 2006. **32**(5): p. 462-468 (Korean).
187. Park, J.P., et al., *Environmental Risk Assessment of Pharmaceuticals : Model Application for*

Estimating Pharmaceutical Exposures in the Han River Basin. Korea Environment Institute, 2007. **RE-06**: p. 1-178.

188. *Development of analytical method and study of exposure of pharmaceuticals and personal care products in environment*. **2006**, Korean National Institute of Environmental Research: Seoul, Korea. p. 1-308 (Korean).
189. *Residual medical substance environmental risk assessment*. **2008**, Korean National Institute of Environmental Research: Seoul, Korea. p. 1-210 (Korean).
190. *Human exposure assessment for antibiotics in the water environment*. **2007**, Korea Food and Drug Administration: Seoul, Korea. p. 1-149 (Korean).
191. Lee, J.-H., et al., *Risk assessment for aquatic organisms of pesticides detected in water phase of six major rivers in korea.* The Korean Journal of Pesticide Science, 2011. **15**(1): p. 48-54 (Korean).
192. Choi, K., et al., *Seasonal variations of several pharmaceutical residues in surface water and sewage treatment plants of Han River, Korea.* Sci Total Environ, 2008. **405**(1-3): p. 120-8.
193. *Environmental risk assessment of pharmaceutical residues*. **2008**, Korean National Institute of Environmental Research: Seoul, Korea. p. 1-210 (Korean).